# General Disclaimer

One or more of the Following Statements may affect this Document

- This document has been reproduced from the best copy furnished by the organizational source. It is being released in the interest of making available as much information as possible.

- This document may contain data, which exceeds the sheet parameters. It was furnished in this condition by the organizational source and is the best copy available.

- This document may contain tone-on-tone or color graphs, charts and/or pictures, which have been reproduced in black and white.

- This document is paginated as submitted by the original source.

- Portions of this document are not fully legible due to the historical nature of some of the material. However, it is the best reproduction available from the original submission.
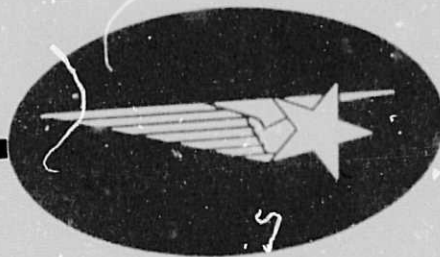
LOCKHEED MISSILES & SPACE COMPANY

HUNTSVILLE RESEARCH & ENGINEERING CENTER

HUNTSVILLE RESEARCH PARK

4800 BRADFORD BLVD., HUNTSVILLE, ALABMA

PREDICTION OF STRUCTURAL DAMPING FOR FUTURE SATURN FLIGHTS

FINAL REPORT

December 1969

Contract NAS8-21446

Prepared for George C. Marshall Space Flight Center
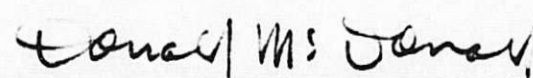National Aeronautics and Space Administration
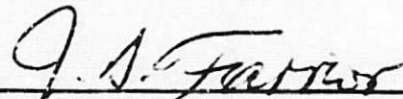
by

W. E. Jones, Jr.

APPROVED BY: _____

A. M. Ellison, Supervisor
Structural Engineering Section

_____

D. McDonald, Manager
Structures & Mechanics Dept.

_____

J. S. Farrior
President Director

FRECEDING PAGE BLANK NOT FILMED.

FOREWORD

This document represents the final report for work performed by Lockheed's Huntsville Research & Engineering Center under Contract NAS8-21446 for the NASA-George C. Marshall Space Flight Center.

The performance period for this study was from 26 June 1968 through 31 December 1969. Mr. Larry A. Kiefling of S&E-AERO-DFS was the MSFC Technical Monitor.

Lockheed/Huntsville contributors to this report were C. S. Chang, A. M. Ellison and G. D. Robinson.

SUMMARY AND INTRODUCTION

A study was made to predict the structural damping of the Apollo Applications Program (AAP) Orbiting Cluster. Structural damping was considered to be the damping due to internal energy dissipations in the material and the energy losses due to joint friction. The results are presented as modal damping coefficients for several low-frequency modes of vibration.

The AAP cluster configuration consists of the S-IVB Orbital Workshop (OWS), Airlock Module (AM) and Multiple Docking Adapter (MDA), with the Command and Service Module (C/SM) docked at the end port of the MDA and the Lunar Module/Apollo Telescope Mount (LM/ATM) docked at a lateral port. The ATM solar panels are deployed. The cluster configuration is shown in Fig. 1. The dynamics analysis of this configuration is being performed at Lockheed/Huntsville under contract NAS8-20082 (Ref. 1).

The mode shapes and frequencies were obtained using the Lockheed-developed Cluster Dynamics Computer Program. In this program, the OWS/AM, C/SM and LM/ATM were modeled as rigid bodies attached to an elastic MDA; the ATM solar panels were modeled as uniform cantilevered beams. The ATM canister was modeled as a rigid body suspended by rotational springs. The OWS solar arrays were also assumed rigid.

Based on the assumed rigid masses for the cluster components in the Cluster Dynamics program, the AAP structural damping is the energy dissipated in the ATM solar panel arrays, ATM canister rings, MDA structure and the docking port joints connecting the C/SM and LM/ATM to the MDA. The material damping occurs in the ATM solar panel structure, MDA structure and ATM canister rings. The joint damping occurs in the ATM solar panel joints and the joints in the MDA longitudinal and radial docking ports.

The cluster modes and natural frequencies used for this study are given in Table 1 with a brief description of the deformation mode shapes. These eight modes were selected as being representative of the expected response. These values, with the exception of Modes 7 and 8, were obtained from Ref. 1. Modes 7 and 8 were taken from a separate Cluster Dynamics program analysis by Dr. E. L. Bernstein of Lockheed/Huntsville.

This report is divided into four sections. The first section presents the total structural damping and the resultant modal damping coefficients for the cluster. Section 2 is the material damping study and Section 3, the joint damping test and results. Descriptions of the instrumentation and test procedure for the joint damping tests are given in Section 4.

CONTENTS

LIST OF TABLES

LIST OF TABLES (Continued)

LMSC/HREC D149346

LIST OF ILLUSTRATIONS

LIST OF ILLUSTRATIONS (Continued)

Section 1
STRUCTURAL DAMPING

Structural damping is considered to be the total of the material damping and the joint friction damping. For the Apollo Applications cluster configuration the material damping occurs in the ATM solar panel framework, the ATM canister rings and the MDA structure. The joint damping is the friction losses in the ATM solar panel joints and the MDA docking port joints. The other structures in the AAP cluster were assumed to be rigid bodies for the AAP Cluster Dynamics Analysis (Ref. 1) and, hence, were assumed to be non-dissipative.

Structural damping coefficients for the AAP cluster obtained from this study are given in Tables 2, 3 and 4 for temperatures of $72^{\circ}F$, $-50^{\circ}F$, and $150^{\circ}F$, respectively. The damping values are presented as energy dissipated per cycle of vibration in a normal mode and also as a percentage of critical damping for the mode. The damping coefficient is computed from the expression

$$\zeta = \frac{DE}{4\pi SE} \times 100\% \qquad (1.1)$$

where: DE is energy dissipated in the structure per cycle
SE is peak strain energy in a normal mode.

Damping values are presented for eight modal participation factors for each normal mode. The modes are normalized so that the generalized mass of each mode is equal to 1.0 lb-in-sec^2.

The contribution to total damping of the MDA docking port joints and the ATM solar panel joints is included in the tables. The material damping

energy values determined by analysis were judged to be invalid and were not included in the tabulated structural damping. A discussion of this problem is given in Section 2.

The peak strain energy during a cycle of vibration was determined by equating the peak strain energy to the peak kinetic energy:

$$SE = KE = \frac{1}{2} \int^{mass} v^2 \, dm \qquad (1.2)$$

where

v = velocity

Let

ω_i = natural frequency of ith mode, rad/sec.

η = modal participation factor, dimensionless

ϕ_i = eigenvector of the ith mode

Then

$$SE = \frac{1}{2} \eta^2 \omega_i^2 \int^{mass} \phi_i^2 \, dm \qquad (1.3)$$

In Eq. (1.3) the integral term is equal to the generalized mass, and, since the eigenvector is normalized to give a generalized mass of 1.0, the strain energy in the ith mode is

$$SE = \frac{1}{2} \eta^2 \omega_i^2 = \eta^2 \cdot 2\pi^2 f_{ni}^2 \qquad (1.4)$$

where f_{ni} is the natural frequency of the mode measured in Hertz.

Equation (1.4) was used to determine the strain energies for each of the eight normal modes as a function of modal participation factor. Eigenvalues and eigenvectors for the modes were determined from the Cluster Dynamics Analysis of Ref. 1.

Room temperature data for MDA joint damping were used to calculate the modal damping values of the cluster because this portion of the structure is protected by a radiation shield and the structural thermal environment ranged from -43°F to 68°F (Ref. 2). The ATM solar panel joint friction values for the "normal" joint tightness were used in the tables.

Results and Conclusions

Values for the AAP cluster modal damping coefficient ranged from 14.973% to 0.13365% discounting the coefficient for Modes 7 and 8. These two modes are predominately ATM canister bending. Without any values for the joint damping for the roll-and-gimbal-ring structure, the damping predicted for these modes is negligible. The canister ring locks and pivot joints are of such complexity that no meaningful estimate of the dissipated energy is possible without test data for the actual hardware.

The highest coefficient was for Mode 2, participation factor 0.25 and -50°F temperature. The lowest value was for Mode 5, participation factor 2.0 and temperature of 72°F. The average coefficient value was approximately 1% damping for the unit participation factor, 72°F temperature mode cases. The structural damping for the 150°F cases was approximately the same as for the 72°F cases. The average low temperature modal damping coefficient was around 2% for the unit participation factor.

Figure 2 is a chart of the variation of the modal damping coefficients for the three temperature values for Mode 1. The modal damping coefficient is seen to decrease with increasing amplitude. This decrease is due to the strain energy increasing as the square of the amplitude while the damping energy increases approximately linearly.

The results of this study indicate that a detailed investigation of the damping mechanism is required to predict modal damping coefficients for a complex structure if something better than "rule of thumb" values are required.

The computation of the energy dissipated in material damping was not satisfactory in this study. In the case of the MDA this was probably due to the use of a framework mathematical model which gave a distorted picture of the internal stress distribution even when the stiffness and deflection results were sufficiently accurate. In the case of the material damping in the solar arrays, the mode shapes computed by the Cluster Dynamics Analysis program was based on a uniform cantilever beam representation for the solar arrays. These mode shapes were not compatible with the actual structure of the deployable solar arrays and resulted in high stresses and strain energies in the solar arrays. These high stresses naturally caused the computed energy dissipated in material damping to be excessive.

Although the values for energy dissipated in material damping are not valid, a comparison of the energy dissipated with the peak strain energy computed for the model of the deflected structure indicates that material damping is small compared to joint damping. For this reason the results presented in Tables 2 through 4 are believed to represent a good estimate of the modal damping coefficient even though they are based only on joint damping values.

The computed values of the energy dissipated in joint damping appear reasonable although a comparison of results with full-scale tests could not be made. These joint damping values were based on tests of typical joint specimens, and the instrumentation and test techniques reported in Sections 3 and 4 give repeatable results and the accuracy of measurement is excellent.

Further investigation should cover additional components of the AAP cluster such as the airlock, workshop and the workshop solar panel arrays.

These components were considered as rigid bodies in the present Cluster Dynamics Analysis (Ref. 1). Joint damping tests of actual flight hardware, such as the ATM canister ring pivot joints and locks, would supply data that cannot be obtained from simplified test specimens. Also, ATM solar panel joints should be tested in a space environment to determine the effect, if any, of vacuum conditions. The inclusion of the above items in the study would increase the amount of predicted structural damping and provide a more accurate prediction of the cluster modal damping coefficient.

In this study techniques were developed for making a rational estimate of the modal damping coefficients of a complex structure by summing the energy dissipated due to the various damping mechanisms throughout the structure. If further study indicates good correlation with results obtained from full-scale structural damping tests, a significant advance has been made in the art of predicting structural damping. Complex and expensive full-scale testing will no longer be required, and damping predictions can be made on structures for which a full scale ground test is impractical. The deployed solar arrays are a good example of this last type of structure, since they are extremely flexible and designed to operate in a very low gravity environment.

Section 2
AAP MATERIAL DAMPING STUDY

2.1 MATERIAL DAMPING

Material damping, or energy dissipated due to internal friction, can be determined by the following relationship (Ref. 3):

$$D = J\sigma^n \qquad (2.1)$$

where

D = specific material damping energy in a part under uniform stress (in-lb/in^3-cycle)

σ = peak stress (lb/in^2)

J, n = material damping constants

The specific damping energy is representative of the area within the stress-strain hysteresis loop of the material. Specific damping energy, D, depends only on the material and is not a function of shape, stress distribution, or volume, Ref. 3.

The total damping of a specimen can be determined by integrating over the volume if D is known,

$$D_o = \int^V D dV \qquad (2.2)$$

where

D_o = total damping energy dissipated by specimen (in-lb/cycle).

V = volume, in.^{3}

6

The total material damping for a structure is the sum of the material damping of its parts.

For the general rectangular section with the loads shown in Fig. 3, the material damping can be determined by integrating between the limits shown in Fig. 4.

Note that the Y and Z axes are the principal bending axes and the sides of the rectangle are parallel to these axes. Eq. (2.3) will be valid only for cross-sections which can be broken up into rectangles with the sides parallel to the principal bending axes.

From Eqs. (2.1) and (2.2):

$$D_o = J \int_o^L \int_{Y_1}^{Y_2} \int_{Z_1}^{Z_2} \left\{ ABS \left[(A_1 + B_1 X)Y + (A_2 + B_2 X)Z + C \right] \right\}^n dZ\,dY\,dX \qquad (2.3)$$

where

$$A_1 = M_z/I_z, \; (lb/in^3)$$

$$B_1 = V_y/I_z, \; (lb/in^4)$$

$$A_2 = M_y/I_y, \; (lb/in^3)$$

$$B_2 = V_z/I_y, \; (lb/in^4)$$

$$C = V_x/A \; (lb/in^2)$$

ABS = absolute value

Figure 3 shows the orientation of the member and the loads. The cross-sectional moments of inertia about the principal axes Y and Z are I_y and I_z, respectively; A is the cross-sectional area. Performing the double integration on Y and Z, Eq. (2.3) gives

$$D_o = \int_0^L \frac{J}{(n+2)(n+1)ABS\left[(A_1+B_1X)(A_2+B_2X)\right]} \left\{ ABS\left[(A_1+B_1X)Y_2 + (A_2+B_2X)Z_2+C\right]^{n+2} \right.$$

$$+ABS\left[(A_1+B_1X)Y_1 + (A_2+B_2X)Z_1+C\right]^{n+2}$$

$$-ABS\left[(A_1+B_1X)Y_2+(A_2+B_2X)Z_1+C\right]^{n+2}$$

$$\left. -ABS\left[(A_1+B_1X)Y_1+(A_2+B_2X)Z_2+C\right]^{n+2} \right\} dX \qquad (2.4)$$

Equation (2.4) is indeterminate when the bending moment in a plane is zero, i.e., $(A_i + B_iX) = 0$. For the case of zero moment in the Y plane; Eq. (2.3) becomes

$$D_o = JY \int_0^L \int_{Z_1}^{Z_2} \left\{ ABS\left[(A_2+B_2X)Z + C\right] \right\}^n dZ\,dX \qquad (2.5)$$

where

$$Y = Y_2 - Y_1$$

Integrating Eq.(2.5) on Z

$$D_o = \int_0^L \frac{JY}{(n+1)ABS(A_2+B_2X)} \left\{ ABS\left[(A_2+B_2X)Z_2 + C\right]^{n+1} \right.$$

$$\left. -ABS\left[(A_2+B_2X)Z_1 + C\right]^{n+1} \right\} dX \qquad (2.6)$$

Similarly for zero loads in the Z-plane

$$D_o = \int_0^L \frac{JZ}{(n+1)ABS(A_1+B_1X)} \left\{ ABS\left[(A_1+B_1X)Y_2 + C\right]^{n+1} \right.$$

$$\left. -ABS\left[(A_1+B_1X)Y_1 + C\right]^{n+1} \right\} dX \qquad (2.7)$$

The total damping energy per cycle for the specimen can be determined by numerical integration of Eqs. (2.4), (2.6) or (2.7), depending on the load condition.

For the "axial load only" case, Eq. (2.3) reduces to

$$D_o = \int_0^L JYZ \left| C \right|^n dX \qquad (2.8)$$

where

$$Y = Y_2 - Y_1$$
$$Z = Z_2 - Z_1$$

Integrating over the length gives

$$D_o = JYZL \left| C \right|^n = JV \left| C \right|^n \qquad (2.9)$$

The material damping per cycle for a composite rectangular cross section can be determined by addition of the energy dissipated by the individual segments.

The above equations have been programmed for the digital computer to automatically determine the material damping for a specified specimen cross section and loading. The ATM solar panel structural frame and the ATM canister roll and gimbal rings are constructed of rectangular tubing. The MDA structure was modeled as a space frame by use of the Yettram/Husain plane-framework method, Ref. 4. This method replaces shear panels by a framework having the same shear resistance properties. This framework can be represented by rectangular cross sections.

9

2.2 MATERIAL PROPERTIES

The structural frame of the ATM solar panels is constructed of 6061-T6 aluminum alloy tubing and 4130 steel tubing. The ATM canister roll and gimbal rings are constructed from 6061-T6 aluminum tubing. The following values were used for the material damping constants:

6061-T6 Aluminum Alloy (Ref. 5)

$\sigma < 15.5$ ksi
$$J = 4.41 \times 10^{-11}$$
$$n = 1.942$$

$\sigma > 15.5$ ksi
$$J = 5.13 \times 10^{-15}$$
$$n = 2.881$$

4130 Steel (Ref. 6)

9 ksi $< \sigma <$ 45 ksi
$$J = 4.3 \times 10^{-14}$$
$$n = 3.0$$

A literature survey failed to find any material damping properties for the MDA structural material, 2219-T87 aluminum alloy. A plot of log decrement vs nominal bending stress for several materials including several aluminum alloys was found, Ref. 7. The aluminum data were grouped together and presented as a wide band indicating wide scatter in the test results for all of these alloys. Based on this observation, the damping constants for 2024-T4 were substituted in the MDA analysis since its chemical composition comes closest to matching 2219 aluminum alloy.

The damping properties are:

2024-T4 Aluminum Alloy (Ref. 5)

$\sigma < 14$ ksi
$$J = 3.82 \times 10^{-11}$$
$$n = 2.01$$

2.3 ATM SOLAR PANEL ARRAYS

The cluster mode shape for each ATM solar panel is a linear combination of the first two classical cantilever beam mode shapes plus a torsional mode shape. The eigenvectors used to determine the deflected shapes were obtained from Table A.2 of Ref. 1.

The resultant mode shapes were input into the Lockheed FRAME program ATM solar panel mathematical model (Ref. 8) to obtain the loads for each member. The FRAME program output was used as input data for the Material Damping program. The Material Damping program integrates over each member to determine the energy dissipated for the internal member loads.

A summation of the total energy dissipated for all the structural members was computed for each mode. This summation for the four solar panel arrays is given in Table 5 for each cluster mode.

2.4 MULTIPLE DOCKING ADAPTER

The internal member loads for the MDA structure were determined by a FRAME mathematical model, Ref. 1. The Yettram-Husain plane-framework method of Ref. 4 was used to model the structure as a frame.

The eigenvectors from the cluster dynamics analysis for the eight modes were used as input to the FRAME model. The internal member loads determined by the FRAME analysis were input in the Material Damping program to compute the damping energy for each mode.

The results of this analysis are presented in Table 5.

2.5 ATM CANISTER ROLL AND GIMBAL RINGS

The procedure of paragraph 2.4 was used to determine the material damping in the canister roll ring and gimbal ring. The internal loads were determined by a FRAME mathematical model and damping energy computed by the material damping program. Table 5 lists the results for the eight computed modes.

2.6 RESULTS AND CONCLUSIONS

The total material damping energy for the MDA structure, ATM canister rings and ATM solar panel structure is summed in Table 5. The eight cluster modes analyzed are representative of the expected orbital vibration response and cover several frequencies in the range from 0.186 Hz to 5.624 Hz. The value of the total material damping is seen to vary over a range from 0.037511 to 27.349 (in-lb/cycle). Most of the values appear to be several times larger than normally expected and are not consistent from mode to mode. Based on these values the modal damping coefficient would be around 32% for the highest damped case, Mode 2, and approximately 15% for Modes 3 and 4. Damping ratios of this magnitude are not probable for a structural system similar to the AAP cluster.

The validity of the material damping energy as determined in this analysis appears to be questionable. The values do not appear to follow any trend, and they fluctuate greatly from mode to mode.

The mathematical simulation of the MDA structure by the Yettram-Husain method does not present an accurate load distribution from which to determine the material damping. This model was originally formulated to determine the MDA stiffness matrix for the Cluster Dynamics Analysis (Ref. 1) and was not intended to be used for a detail stress analysis. A finite element model would be more applicable and accurate for this task.

In the Cluster Dynamics Analysis, the ATM solar panel arrays were modeled as uniform cantilevered beams (Ref. 1). The mode shapes were

assumed to be a combination of the first two cantilever bending modes plus the first torsional mode. Difficulties were encountered in trying to obtain the the resultant cluster dynamic mode shapes with the solar panel FRAME program mathematical model. To obtain the cantilever deflected mode shapes, unrealistically high load values were required, especically for panels close to the restrained end of the array. This resulted in high stress values, hence high material damping for the modes where the cluster natural frequency was the panel response value. For a more accurate analysis the panel arrays should be modeled in the cluster dynamic analysis as a structure more accurately describing the response of the panel array instead of the cantilevered beam of equivalent stiffness.

The excessively high values for the material damping discussed in the first paragraph of this section are based on the peak strain energy expected in each mode, Equation 1.4. Since the solar panels require unrealistically high loads to conform to the modal displacements computed by the Cluster Dynamics program, the solar panel strain energy as computed by the FRAME program is generally much higher than the strain energy characteristic of the mode, Eq. 1.4. By using the strain energy computed by the FRAME program, the material damping is found to be small compared to the joint damping. Since energy dissipated in material damping and strain energy in the solar arrays are based on the same mathematical model, it can be concluded that the effect of neglecting material damping is small.

Section 3

AAP JOINT DAMPING

The objective of this test program was to determine basic joint damping properties for the various types of joints in the AAP cluster. Representative joint types were made and tested under varying loads, temperatures and frequencies. Two specimens simulated portions of the MDA docking ports, and a third specimen simulated a typical joint of the ATM solar panels. Test data from the docking port specimens were reduced to yield damping energy and load per unit length of joint circumference. Test data from the solar panel specimen yielded friction torque and the bearing coefficient of friction. Test results were tabulated and applied to the Joint Damping program (Ref. 2).

3.1 MDA DOCKING PORT JOINTS

The docking port specimens (Fig. 5) were tension-bolted joints based on NASA Dwgs. 30M14230, 30M14300, 30M14388 and shear-bolted joints based on NASA Dwgs. 30M14392, 30M14401. These specimens were similar to the full-scale structure in material (2219-T87), finish tolerances and cross section, but they covered only a two- or three-bolt segment of the circumference. A coating of room-temperature vulcanizing sealing compound (RTV 90) was applied to the faying surfaces of the test specimens, after which the bolts were "torqued" to drawing specifications. The test fixture was a torsion pendulum, having a load beam and two driving shakers at the top and a crank and angle plate at the base to hold the specimen. Figures 6a, 6b and 6c show the specimen in the test fixture.

Figure 7 shows circuitry of the test instrument. The torsional pendulum design was chosen so that high loads could be applied to the specimens using small shakers. Pye-Ling shakers were tuned with the Monsanto oscillator to

14

drive the pendulum at the system resonant frequency. Large changes in the natural frequency were possible by moving the weights on the load beam. A crank and link transformed the pendulum torque to axial load on the specimen axial load and relative deflection across the specimen joint were measured, thereby excluding material damping and friction losses in the pendulum system. The specimen load was measured by th ' Kistler quartz load washer, which had a preload compression of 2200 lb applied by the specimen attach bolt. The change in force was read on the oscilloscope. The sensitivity of the load washer-charge amplifier system was 0.392 mV/lb. The load level was controlled by the power amplifier and adjustments of the exciting frequency with respect to the natural frequency of the test system.

To measure the specimen deflection, a Pickering linear variable differential transformer (LVDT) was cemented in place and adjusted or nulled to a minimum signal on the Tektronics oscilloscope. The sensitivity of the system was 10 V/0.001 in., with the attenuator of the displacement carrier preamplifier set on 1.0. (Example displacement: The oscilloscope vertical channel was set at 5 V/cm, attenuator on 2: Deflection = 5 V/cm (2) $\div$ 10 V/ 0.001 in. = 0.001 in./cm.)

A more detailed description of the test instrumentation is given in Section 4. Test specimen temperature was monitored with thermocouples attached to each end of the specimen. Temperature was controlled with an insulated box fitted around the base of the torsional pendulum. Dry ice was used for coolant on low temperature tests. Two heat guns circulated air inside the box to provide a uniform temperature.

Data taken during testing were as follows: The first photograph (Fig. 8) is a hysteresis curve of force versus deflection. The applied force and deflection are scaled and calculated according to the sensitivity examples described previously. To obtain a measurable area within the hysteresis

15

curve, the function dial of the oscilloscope was switched to Channel A — Channel B and the curve was expanded as much as possible. The attenuator was used to decrease the deflection signal whenever the amplifier became saturated. Saturation was indicated by a sharp bend in the hysteresis curve at peak load. The second photograph (representing the tensile loading) and the third (compressive loading) were each measured with a planimeter for damping energy calculations.

The test envelope was determined from the following design and enviromental conditions:

Load: Design bending moment at docking port, M = 300,000 in-lb

$$o.d. = 33.375 \text{ in.} \quad t = 0.25 \text{ in.}$$

$$I = 3568 \text{ in}^4$$

$$f_b = Mc/I$$

$$= \frac{300,000}{3568} \times \frac{33.375}{2}$$

$$= 1400 \text{ psi} \tag{3.1}$$

For a 2-in. segment the design load is $(0.25 \times 2) \text{ in}^2 \times 1400 \text{ psi} = 700 \text{ lb}$. For a 3-in. segment 0.2 in. thick, the design load is $0.2 \times 3 \times 1400 = 840 \text{ lb}$.

Temperature: The largest temperature range occurs at the MDA radial port: $-43°F$ to $68°F$, MDA Mission Cold Case, Radiators $-45°F$ (Ref. 2).

Frequency: 0.1 to 5.0 Hz (Ref. 1).

Data Tabulation:

Reference: Table 6, Test No. 12

Load: Tensile and compressive loads were assumed to be equal in magnitude.

Reference Fig. 8: Load = 2 cm (127.5 lb/cm)

= 255 lb

where

2 cm = load amplitude

127.5 lb/cm = oscilloscope setting

Deflection: Zero deflection was taken as the midpoint of the hysteresis curve where the load line bisector passes through. Tension was measured above this level, and compression below.

Reference Fig. 8:

Compressive deflection δ_c = 0.85 cm x 0.001 in./cm

$= 0.85 \times 10^{-3}$ in.

Tensile deflection δ_t = 2.0 cm x 0.001 in./cm

$= 2.0 \times 10^{-3}$ in.

Damping Energy:

$$DE = \frac{C_a}{0.392} \frac{C_v A_t A_r}{S W_s} \quad \text{in.-lb/in.} \quad (3.2)$$

where

C_a = channel A setting mV/cm

0.392 = sensitivity of load washer mV/lb

$$\frac{C_a}{0.392} = \frac{mV}{cm} \div \frac{mV}{lb} = lb/cm \quad \text{load factor} \quad (3.3)$$

C_v = vertical channel setting V/cm

S = sensitivity of LVDT = 10V/.001 in.

$$\frac{C_v}{S} = \frac{v}{cm} \div \frac{10V}{.001 \text{ in.}} = \frac{in.}{cm} \times 10^{-4} \quad \text{deflection factor} \quad (3.4)$$

A_t = attenuator setting - multiplier of C_v/S

A_r = area of hysteresis curve - cm^2

W_s = specimen width - in.

Joint Stiffness, Tensile (per inch of docking port circumference):

$$\text{Joint Stiffness} = \frac{a_1 F_a}{b_1 F_b} / W_s \qquad (3.5)$$

$$= \frac{2.0\,(127.5)}{2.1\,(10^{-3})} / 2.0$$

$$= 6.05 \times 10^4 \text{ lb/in./in.}$$

where

a_1 = tensile load (cm)

F_a = load multiplier (lb/cm)

b_1 = tensile deflection (cm)

F_b = deflection multiplier (in./cm)

W_s = specimen width (in.)

Circumferential Joint Stiffness, Compressive:

$$\text{Joint Stiffness} = \frac{a_2 F_a}{b_2 F_b} / W_s \qquad (3.6)$$

$$= \frac{3.0\,(127.5)}{0.5\,(10^{-3})} / 2.0$$

$$= 38.25 \times 10^4 \text{ lb/in./in.}$$

where

$\dfrac{a_2}{b_2}$ = slope of hysteresis curve at maximum compression load.

The distance between the zero deflection line and the point at which the rate of change of slope on the hysteresis curve is maximum, factored by F_b is designated as δ_i.

$$\delta_i = -0.3 \text{ cm} \times 0.001 \text{ in./cm}$$
$$= -0.3 \times 10^{-3} \text{ in.}$$

The tabulated data (Tables 6 and 7) are plotted on Figs. 10 and 11 as Damping Energy vs Deflection.

Test Observations and Conclusions

Some factors in joint damping are:

Gasket Material: RTV 90, a stiff paste consistency material, was used in the test piece. "Torquing" pressure squeezed it to a film of about 2 mils thickness.

Bonding Primer: The test articles did not use bonding primer (nor does the full-scale vehicle) but the shear-bolted specimen showed some abraded areas, and a bonded gasket could have an increased damping effect.

Bolt Tension: The bolts (1/4 - 28) in the tension-bolted specimen were torqued to 70 in.-lb which gives a stress of 40,000 psi or a tension load of approximately 1360 lb. The maximum applied loads were approximately half of this, so for two bolts the load/bolt = 340 lb and no additional bolt elongation would occur.

Specimen Bending: The tension-bolted specimen had relatively high bending under tensile loads (Fig. 8). In turn, this caused some bending along the longitudinal axis.

Bolt Hole Clearance: In the shear-bolted specimen the bolts were fitted with clearance in accordance with the drawing. Some sliding occurred which

19

can be seen as "kicks" near the zero deflection line in the force-deflection photograph (Fig. 9b).

4-Deg Ramp: The 4-deg ramp (on the shear-bolted joint) gives increased resistance to sliding under compressive load, and the effect can be seen as smaller compressive deflections than the tensile deflections.

Temperature: There appears to be little effect on damping energy due to temperature variations (Figs. 10 and 11). The high temperature results shown on Fig. 11 are for information only (beyond the test envelope).

Vacuum: Gas pumping in structural joints can occur if there is sufficient joint deflection to "pump" gas in and out, and if the frequency is relatively high — 250 to 32,000 Hz (Ref. 3). The test piece had little gas space because of the sealant in each joint, and the frequency was so low that no viscous gas damping would occur.

3.2 MDA DOCKING PORT JOINT DAMPING

The joint damping for the MDA docking ports was determined using the test values obtained for the joint segments and numerically integrating around the port circumference. The results are presented as joint damping versus bending moment for the tension joint and shear-bolted joint.

The joint force-displacement relation is shown in Fig. 12, where k is the variation of the line load with deflection. The term δ_i represents the deflection value at which the relationship between line load and deflection change slope.

Figure 13 shows the load and deflection distribution for the docking port for an applied moment, m.

The line load can be determined for any deflection, δ, from the following equations.

$$N_x = k_1 \delta + (k_2 - k_1) \delta_i \qquad \delta \geq \delta_i \tag{3.7}$$

$$N_x = k_2 \delta \qquad \delta \leq \delta_i \tag{3.8}$$

From symmetry the damping energy need only be determined for half the docking port, $\phi = \pi/2$ to $-\pi/2$.

Summing forces and moments over the interval ϕ

$$\sum F = 0$$

$$\int_{-\pi/2}^{\pi/2} N_x R \, d\phi = 0 \tag{3.9}$$

$$\sum M_x = M_x/2$$

$$\int_{-\pi/2}^{\pi/2} N_x R^2 \sin\phi \, d\phi = M_x/2 \tag{3.10}$$

The deflection δ can be expressed as

$$\delta = \delta_1 - \left[R(1 - \sin\phi) \right] \theta$$

$$= \delta_1 - R\theta + R\theta \sin\phi \tag{3.11}$$

where $\theta = (\delta_1 - \delta_2)/2R$

Substituting Eqs. (3.7) and (3.8) into (3.9) and integrating

$$\int k\,\delta R\,d\phi = 0$$

$$R\int_{\phi_e}^{\pi/2}\left[k_1\,\delta + (k_2 - k_1)\,\delta_i\right]\,d\phi + R\int_{-\pi/2}^{\phi_e}k_2\,\delta\,d\phi = 0$$

$$(k_1 + k_2)\left[\delta_1 - R\theta\right](\pi/2) + (k_2 - k_1)\left[(\delta_1 - R\theta)\,\phi_e - R\theta\,\cos\phi_e\right]$$

$$+ (k_2 - k_1)\,\delta_i\,(\pi/2 - \phi_e) = 0$$

Dividing by θR

$$(k_1 + k_2)\left[\frac{\delta_1}{\theta R} - 1\right]\left\{(k_1 + k_2)\,(\pi/2) + (k_2 - k_1)\,\phi_e\right\}$$

$$+ (k_2 - k_1)\left\{\frac{\delta_i}{R\theta}\,(\pi/2 - \phi_e) - \cos\phi_e\right\} = 0$$

$$\left[\frac{\delta_1}{R\theta} - 1\right] = \frac{(-\Delta k)\left\{\dfrac{\delta_i}{R\theta}\,(\pi/2 - \phi_e) - \cos\phi_e\right\}}{(\sum k)\,(\pi/2) + (\Delta k)\,\phi_e} \tag{3.12}$$

where

$$\Delta k = k_2 - k_1$$
$$\sum k = k_1 + k_2$$

Substituting Eqs. (3.7) and (3.8) into (3.10)

$$M/2 = R^2\int_{\phi_e}^{\pi/2}\left[k_1\,\delta + (k_2 - k_1)\,\delta_i\right]\sin\phi\,d\phi$$

$$+ R^2\int_{-\pi/2}^{\phi_e}k_2\,\delta\,\sin\phi\,d\phi$$

Substituting Eq. (3.11) and integrating

$$M = 2R^2 \left\{ (-\Delta k)(\delta_1 - R\theta) \cos \phi_e + (-\Delta k) R\theta \left(\frac{\sin 2\phi_e}{4} - \phi_e/2 \right) \right.$$

$$\left. + R\theta \left(\sum k\right) (\pi/4) + (\Delta k) \delta_i \cos \phi_e \right\} \qquad (3.13)$$

Divide by θR

$$M/\theta R = 2R^2 \left\{ (-\Delta k)\left(\frac{\delta_1}{\theta R} - 1\right) \cos \phi_e + (-\Delta k)\left(\frac{\sin 2\phi_e}{4} - \phi_e/2 \right) \right.$$

$$\left. + \left(\sum k\right)(\pi/4) + \frac{(\Delta k)\,\delta_i}{\theta R} \cos \phi_e \right\}$$

Substituting Eq. (3.12)

$$M/\theta R = 2R^2 \left\{ (-\Delta k) \left[\frac{(-\Delta k)\,\dfrac{\delta_i}{\theta R}\,(\pi/2 - \phi_e) - \cos \phi_e}{\left(\sum k\right)(\pi/2) + \Delta k\,\phi_e} \right] \cos \phi_e \right.$$

$$+ (-\Delta k) \left(\frac{\sin 2\phi_e}{4} - \phi_e/2 \right) + \sum k\,(\pi/4)$$

$$\left. + \Delta k\,\frac{\delta_i}{\theta R} \cos \phi_e \right\} \qquad (3.14)$$

From Eq. (3.11)

$$\delta = \delta_1 - R\theta + R\theta \sin \phi$$

at $\phi = \phi_e$, $\delta = \delta_i$

$$\frac{\delta_i}{\theta R} = \left[\frac{\delta_1}{\theta R} - 1 \right] + \sin \phi_e$$

Substituting Eq. (3.12) and multiplying through

$$\frac{\delta_i}{\theta R} (\pi k_2) = \Delta k \cos \phi_e + \left(\sum k (\pi/2) + \Delta k \phi_e \right) \sin \phi_e$$

Solving for θR

$$\theta R = \frac{\delta_i \, \pi k_2}{\Delta k \cos \phi_e + \left[(\sum k) (\pi/2) + \Delta k \phi_e \right] \sin \phi_e} \tag{3.15}$$

For the case where the force-deflection slope changes at zero deflec-tion, $\delta_i = 0.0$, the following derivation is valid.

Summing forces

$$\int_{-\pi/2}^{\pi/2} N_x R \, d\phi = 0 \tag{3.16}$$

The line load can be expressed

$$N_x = k_1 \delta \qquad\qquad \delta \geq 0 \tag{3.17}$$

$$N_x = k_2 \delta \qquad\qquad \delta \leq 0$$

$$\delta = R\theta (\sin \phi - \sin \phi_e) \tag{3.18}$$

Substituting Eqs. (3.17) and (3.18) into Eq. (3.16) and integrating

$$\int_{\phi_e}^{\pi/2} k_1 \, \theta R (\sin \phi - \sin \phi_e) \, d\phi$$

$$+ \int_{-\pi/2}^{\phi_e} k_2 \, \theta R (\sin \phi - \sin \phi_e) \, d\phi = 0$$

$$\theta R \left[(-\Delta k)(\cos \phi_e + \phi_e \sin \phi_e) - (\textstyle\sum k)(\pi/2) \sin \phi_e \right] = 0$$

$$\cot \phi_e + \phi_e = (-\pi/2) \frac{\sum k}{\Delta k} \qquad (3.19)$$

The above equations were digitally programmed to determine the docking port joint damping.

For the docking port geometry and k_1 and k_2 test values, the above equations were solved for a range of ϕ_e values from $-\pi/2$ to $\pi/2$ in five-degree intervals. For the case where $\delta_i = 0.0$ there is only one ϕ_e value as determined by Eq. (3.19) above.

The docking port rotation θ was determined by Eq. (3.15) and the resultant bending moment from Eq. (3.14) for the particular ϕ_e, θ, k_1 and k_2 values. Integrating numerically around the docking port circumference, the deflections were determined and the corresponding damping values obtained from the joint test data. The results of this study are presented in Figs. 14 through 15 as charts of docking port joint damping vs bending moment for the two types of joints. These charts are presented for the different temperature values.

The eigenvectors from the AAP Cluster dynamics analysis were multiplied by the MDA stiffness matrix to obtain the docking port bending moments for the eight cluster modes. These bending moments for the radial and longitudinal docking ports are given in Table 8. These values and the charts in Figs. 14 and 15 were used to obtain the joint damping values listed in Tables 9 and 10 for eight normalizing factors. Each of the docking ports was constructed with two shear-bolted joints and one tension joint.

3.3 ATM SOLAR PANEL JOINTS

The solar panel joint specimen (Fig. 16) is representative of a scissors joint of the ATM solar array (NASA Dwg. GC700315). The test joint was designed into the pivot point of a simple pendulum. The nut on the pivot bolt was used to adjust the tightness of the "scissors joint" from the drawing specified "finger tight" to 1/6-turn tighter and 1/6-turn looser. Pendulum frequency was varied by moving the weight tray through four positions on the pendulum tube. Shear load on the joint was varied with lead weights on the tray. Tests were run at -50, 72 and 150°F with the specimen enclosed in the insulated box. Thermocouples were attached to the specimen to measure and monitor the temperature.

Figure 17 is a typical data sheet from the X-Y recorder. The output of the LVDT was adjusted to read as the offset of the lower end of the pendulum tube. For each test the pendulum rod was manually displaced through the same angle and then released. The feed rate of the x-y plotter was set to accommodate one set of loadings on a sheet.

$$\text{Frequency} = \text{cycles/in.} \div \text{sec/in.}$$
$$= \text{cycles/sec}$$

The test envelope was determined by the following:

Load: Shear load at joint is 275 lb, which is factored for equivalent loading on a 1/2-in. diameter bearing. Factored shear load: $Ps = 183$ lb; joint rotation = ± 1.56 deg.

Temperature: The range for the S-IVB solar panel structure was -60 to 167°F and for the ATM solar panel, 35 to 154°F (Ref. 2).

Frequency: 0.1 to 5.0, Ref. (1).

Data Tabulation — Solar Panel Specimen:

Reference: Table 11 and Fig. 17

Decay: The change in amplitude from the initial offset of 3.0 in. was measured over several cycles and then averaged.

C.G. Distance: This is a calculated value for the c.g. of the pendulum tube, tray and weights.

Friction Torque Derivation: Friction torque was derived as follows:

For a pendulum having a distributed mass:
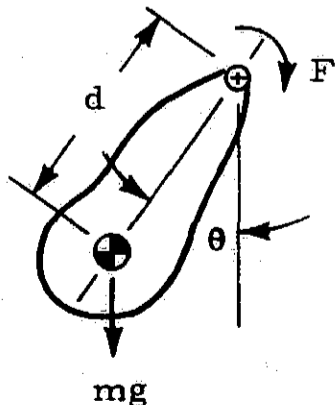
d = distance of centroid from pivot
ρ = radius of gyration about pivot
m = total mass
F = friction torque at pivot

Over a one-half cycle, measured from maximum positive displacement to negative displacement, the change in kinetic energy is zero. Equating the change in kinetic energy to the work:

$$\tfrac{1}{2} \, mgd \, (\theta_o^2 - (\theta_o - \Delta\theta)^2) - F \, (2\theta_o - \Delta\theta) = 0$$

$$\tfrac{1}{2} \, mgd \, (2\theta_o \Delta\theta - \Delta\theta^2) - F(2\theta_o - \Delta\theta) = 0$$

$$\Delta\theta = \frac{2F}{mgd} \quad \text{for one-half cycle.} \tag{3.22}$$

The change in amplitude for a full cycle is:

$$2\,\Delta\theta = \frac{4F}{mgd}$$

$$F = 2\,\Delta\theta \, \frac{(mgd)}{4} \tag{3.23}$$

$$2\,\Delta\theta = \frac{b}{R} \quad \text{in./cycle/in.} = \text{rad/cycle}$$

$$F = \frac{bmgd}{4R} \quad \text{in-lb} \tag{3.24}$$

where

b = deflection of tip of pendulum arm, in.

R = length of pendulum arm, in.

The tabulated data from Tables 11, 12 and 13 is plotted on Figs. 18, 19 and 20 as friction torque vs load.

If F has the form:

$$F = mg\mu + c\mu \tag{3.25}$$

where μ is the product of the coefficient of friction and the radius of the friction circle:

$$\mu = fr \tag{3.26}$$

Equation of Motion: Equation of motion, with friction damping at pivot is

$$m \rho^2 \ddot{\theta} + mg \, d\theta = \pm F \qquad (3.20)$$

where $\theta = \theta(t)$ is the angular displacement of the pendulum from vertical and

$$f_n = \frac{1}{2\pi} \sqrt{\frac{gd}{\rho^2}} \qquad (3.21)$$

then

$$F = mg \, fr_1 + c \, fr_2$$

r_1 = radius of cylindrical part of bearing

= 0.25 in.

r_2 = radius of center of pressure of the disc portion of bearing

= 0.395 in.

Coefficient of friction $f = \mu/r$

$$\text{e.g., (Fig. 18)} = \frac{\Delta F}{\Delta mg} = \frac{1.35}{125} = 0.0108$$

$$c = 1.20$$

$$f = \frac{0.0108}{0.25} = 0.0432$$

The calculated values of f are given in Table 14.

Test Observation and Conclusions

Solar panel joint damping is expressed as friction torque, and from this a coefficient of friction was calculated. The effect of low temperature on the scissors joint is very large: friction torque increases about 3 times when the temperature changes from 72 to -50°F. This effect is probably

caused by the large contraction of the aluminum block tightening onto the steel pivot bolt. The high temperature case (150°F) decreased friction torque about 10%.

Joint tightness was varied through three positions to allow for variations in assembly to "finger tight." As expected the "tight" condition increased the friction torque (approximately 35% for -50 and 72°F, and 15% for 150°F).

Frequency increases brought increases in friction torque of 15 to 25% over the range of 0.34 to 0.75 Hz.

3.4 ATM SOLAR PANEL JOINT DAMPING

The joint damping for the ATM solar panel arrays was determined using the results of the test program. The panel joint rotations and loads, for the eight cluster modes, were obtained from the Lockheed FRAME program analysis.

The joint damping can be determined by integrating the torsional friction force.

$$D = \int F \, d\theta \qquad (3.27)$$

where

$$F = c + \mu P$$
$$P = k\theta$$

Substituting into Eq. (3.27) and integrating

$$D = \int \left[c + \mu k\theta \right] \, d\theta$$

$$D = c\theta + \frac{1}{2} \mu k \theta^2 \qquad (3.28)$$

30

·since

$$\theta = \eta\,\theta^j$$

$$k = P^j/\theta^j$$

where P^j and θ^j are the force and displacement for the unit modal amplitude. Eq. (3.28) becomes

$$D = c\,\eta\,\theta^j + \frac{1}{2}\,\mu\,\eta^2 P^j\,\theta^j \qquad (3.29)$$

For the one complete cycle

$$D = 4c\,\eta\,\theta^j + \frac{1}{2}\,\mu\,\eta^2 P^j\,\theta^j \qquad (3.30)$$

The total joint damping for the solar panel array was determined by summing the rotations and forces for all the panel joints.

$$D = 4c\,\eta\,\sum \theta^j + 2\,\mu\,\eta^2 \sum P^j\,\theta^j \qquad (3.31)$$

Equation (3.31) was digitally programmed to automatically determine the total joint damping for the four solar panel arrays for all eight cluster modes. The constants c and μ were taken from the table of test results, Table 14. Eight normalizing factors, η, were used in the analysis.

Tables 15, 16 and 17 are the results of this analysis for the three temperature values for the three joint tightnesses.

3.5 ATM CANISTER RING JOINT DAMPING

The ATM canister roll and gimbal rings were interconnected and attached to the ATM structure by four pivot joints and two locks. Due to the complexity of these connections no simple simulation could be made to adequately determine the damping in these joints. Actual joints and locks would be required for any sort of meaningful test program.

Section 4
INSTRUMENTATION

To determine the net work being done on a subject by a cyclic load, the area enclosed by the hysteresis loop representing the force-displacement relationship may be used. For most structural joints, this area is expected to be extremely small in comparison with that representing the peak level of stored (recoverable) energy reached during a cycle.

4.1 MEASUREMENT METHOD

Referring to the hypothetical hysteresis loop in Fig. 21, the work done by the force per cycle is

$$D_o = \int_{-x_o}^{x_o} [F_1(x) - F_2(x)]\ dx \tag{4.1}$$

where $F_1[x(t)]$ is the loading branch of the hysteresis loop during a cycle and $F_2[x(t)]$ is the unloading branch. The force and displacement amplitudes are F_o and x_o, respectively. If damping is low, the maximum difference

$$\max \left| F_1(x) - F_2(x) \right| << F_o = \max \left| F_1(x) \right| = \max \left| F_2(x) \right|$$

i.e., the force signal is much greater than the bracketed integrand in Eq. (4.1) so that the integrand is difficult to measure with accuracy from records of the force and displacement signals. The degree of amplication of the force signal to obtain the desirable resolution is limited by the dynamic range of the amplifier and/or the recording equipment which must handle F_o without reaching saturation. This limitation may be overcome, however, by first subtracting

the quantity $\left(F_o/x_o\right)x\,(t)$ from $F\,\left[x(t)\right]$. The resulting signal is never greater than the integrand, so that amplication to obtain the necessary resolution is possible.* Damping is determined by evaluating the integral

$$D_o = \int_{-x_o}^{x_o} \left\{ \left[F_1(x) - \frac{F_o}{x_o}x\right] - \left[F_2(x) - \frac{F_o}{x_o}x\right] \right\} dx \qquad (4.2)$$

from the plot $\left[F(x) - \dfrac{F_o}{x_o}x(t)\right]$ vs. $x(t)$, as shown in Fig. 22.

Published damping data for, say, 6061 aluminum in the T6 condition are that

$$D_o = 4.41 \times 10^{-11}\ \sigma_o^{1.942}, \text{in-lb/in}^3/\text{cycle}$$

for

$$\sigma_o \le 15,500\ \text{lb/in}^2$$

where D_o is the specific damping capacity of the material and σ_o the stress amplitude. Young's modulus for the material is approximately $10^7\ \text{lb/in}^2$. For a stress amplitude

$$\sigma_o = 10^4\ \text{psi}$$

The corresponding strain amplitude is

$$\epsilon_o = 10^{-3}$$

---

*Assuming sufficient signal-to-noise ratio.

and, referring to Fig. 21, the width of the hysteresis opening (a strain) at zero stress is

$$\epsilon_h \cong \frac{D_o}{2\sigma_o} \cong 10^{-7}.$$

In other words, ϵ_h is approximately 0.01% of ϵ_o. In a previous dynamic experiment with a specimen with very little structural damping the actual width of the hysteresis was some 30 times greater than the predicted value based on material damping alone. For a joint specimen where frictional losses are definitely present (as in the present case), a hysteresis loop width of 1% may be assumed as a working figure for instrumentation design purposes. If both force and displacement are sinusoidal in time, a hysteresis loop of 1% width is equivalent to a phase difference of 1 deg between these signals. The damping measurement instrumentation must, therefore, be capable of resolving very small strains (or displacements) while maintaining almost zero-phase relationship during low frequency dynamic tests.

4.2 TRANSDUCERS AND ASSOCIATED INSTRUMENTATION

A piezoelectric force transducer was selected for measuring the force applied to the test specimen. The selection of the piezoelectric type over a strain-gage type was based on considerations of signal-to-noise ratio, linearity, repeatability, accuracy, temperature insensitivity, and general ruggedness and simplicity. With a high-grade charge amplifier, a good piezoelectric transducer can preserve amplitude and phase responses to well below 1 Hz. The characteristics of a recommended transducer-amplifier combination will subsequently be discussed in detail.

A Linear Variable Differential Transformer (LVDT) is selected for measuring specimen deformations.

4.2.1 Force Transducer and Charge Amplifier

The recommended force measuring instrumentation consists of a Kistler Model 903A quartz force transducer and a Kistler Model 503 charge amplifier. The specifications for the 903A are:

Range (compression) .... lb		12,000
Resolution (limited by amplifier noise) .... lb		0.01
Sensitivity (nominal) .... picocoulomb/lb		20
Resonant frequency, no load (nominal) .... kHz		50
Compliance .... in./lb		4×10^{-8}
Capacitance (nominal) .... picofarads		70
Height .... in.		0.5
Outer diameter (max.) .... in.		1.10
Inner diameter .... in.		0.41
Temperature range .... °F		-320 to +500
Vibration and shock .... g		10,000
Weight (approximate) .... oz.		1.3
Linearity .... % of full scale		1
Repeatability .... % of full scale		0.5
Insulation resistance .... ohms		1012 (min)
Temperature sensitivity .... %/°F		0.01

Outstanding features of this make and model are the low capacitance and high insulation resistance, which are essential qualities for low noise and flat response in the subaudio frequency range.

The performance of the Kistler Model 503 charge amplifier is greatly dependent on the transducer characteristics and the mode of operation. A full description of the anticipated performance of the force measuring system is given in the following.

4.2.2 Frequency Response Limits

The frequency response of the piezoelectric transducer-charge amplifier combination is determined by the following parameters: transducer capacitance and insulating resistance, cable capacitance, amplifier feedback capacitance and shunting resistance. If the feedback capacitance is greater than 1% of the total input capacitance (transducer plus cable), the upper frequency limit (-3 dB point) of the system is approximately 100 kHz. For the present application, therefore, the high frequency limit of the system introduces no measurement error so long as the feedback capacitance is not less than 3 pF which is, in fact, less than the smallest selectable capacitance in the amplifier.

The low frequency limit of the system is most critically measured in terms of the phase relationship between the physical input and the voltage output of the charge amplifier, and is governed by: (1) the transducer capacitance and insulating resistance, and (2) the time constant of the feedback circuit in the charge amplifier.

Referring to the specifications, the Kistler Model 903 A force transducer is seen to have a nominal capacitance of 70 pF and a nominal insulation resistance greater than 10^{12} ohms. This transducer, therefore, has a time constant greater than $70 \times 10^{-12} \times 10^{12} = 70$ sec. The phase shift at 1 Hz is then less than 0.1 deg, so that the low frequency response characteristics of the system is not limited by the transducer.

For normal operations, the Short Time Constant is selected on the Kistler 503 charge amplifier, in which case, a 10^9-ohm resistor is connected between the input and output terminals. This resistance shunts the feedback capacitor and limits the low frequency response of the charge amplifier. The phase shift at 1 Hz is approximately 0.2 deg if a feedback capacitance of 50,000 pF is used in parallel with the shunting resistance of 10^9 ohms. Using the system in the indicated mode, therefore, the predicted maximum phase error is 0.3 deg at 1 Hz. The accompanying amplitude response is completely flat.

4.2.3 Sensitivity and Noise

The nominal voltage sensitivity of the transducer-charge amplifier system is given by the expression

$$S(v/lb) = \frac{\text{transducer sensitivity } (pCb/lb))}{\text{feedback capacitance } (pF)} \tag{4.3}$$

with a 50,000 pF feedback

$$S = \frac{20}{50,000} = 0.4 \times 10^{-3} \ v/lb$$

The noise output of the system is determined by the total input capacitance, and is approximately equivalent to one picocoulomb per 10,000 pF of input capacitance. With a 600 pF input, the noise is, therefore, approximately 0.06 pCb (rms), or 0.0030 lb. The noise of the force measuring system, therefore, does not limit the resolution of measurement for all practical purposes.

4.2.4 Zero Drift and Time Constant Check

The piezoelectric force transducer used in the experiments was a Kistler Model 903A Load Washer (LW, Serial No. 32219). It has a certified sensitivity of 19.6 pCb/lb, and a capacitance of 51.0 pF. The charge amplifier (CA) used for the LW signal was a Kistler Model 503 (serial No. 731). A teflon insulated coaxial cable was used. The length of this cable is 15 ft, with a total capacitance of 550 pF. The total input capacitance to the CA input is, therefore,

$$550 + 51 = 601 \ pF.$$

The CA output drift was measured with the LW connected but without a load. Results are shown in Fig. 23. It is seen that in the long time constant mode, with the range setting on 5K that the CA no-load output drift is

less than ± 0.2 mv in 270 sec. Since the overall sensitivity in this condition is 0.392 mv/lb, the above voltage drift corresponded to approximately a range of drift of ± 1 lb, which is quite satisfactory for the tests in this project.

The time constant of the force measuring system was investigated by applying a constant force to the LW and recording the decay of the CA output. Results of three tests are also shown in Fig. 23 corresponding to three CA range settings. It is noted that in the Long TC mode, the time constant for either the 5K range setting or the 2K range setting was greater than 270 sec.

The force measuring system therefore, introduced a phase shift significantly less than 1 deg during tests.

4.2.3 Displacement Sensor and Carrier Preamplifier

As indicated previously, a LVDT was selected for measuring the relative displacement between the two segments of the bolted test specimen. The LVDT used was a Pickering Model No. 7234 (Serial No. 1) with the following nominal properties:

Displacement range:	± 0.020 in.
Linearity:	$< 0.1\%$
Excitation requirement:	2.0 v at 2400 Hz
Null voltage:	0.07 mv
Temperature range:	-20 to $160^\circ F$

Beyond this range nonlinearity is $1\%/100^\circ F$

Uncorrected phase shift: ± 5 deg (approx.)

(between carrier output at 2400 Hz)

The carrier preamplifier (CP) used was a Hewlett-Packard/Sanborn Model 350-1100B (serial No. 2409) with the following nominal characteristics

Carrier Voltage:	5.0 v (approx.)
Carrier Frequency:	2400 Hz (approx.)
Frequency Response:	-3 dB at 480 Hz
Gain Stability:	better than 2%
Linearity:	$\pm 0.2\%$
Noise and Ripple:	2% of signal
Drift:	<2 mv/hr.

Figure 24 shows a schematic diagram of the displacement sensing instrumentation. A stepdown transformer was used to match the carrier voltage output of the CP to the LVDT.

The maximum sensitivity of the system is 10^4 v/in. The noise at this sensitivity is equivalent to 0.6×10^{-4} in., peak to peak.

4.3 DATA RECORDS

Docking port joint specimen damping data were obtained by photographing the force-deflection relationship in the steady-state, as it was displayed on the CRT of an oscilloscope (Fig. 25).

After the specimen response had reached a steady-state condition the force-deflection relationship was first obtained by switching the horizontal amplifier to the "channel A only" mode of operation. The horizontal amplifier is then switched into operation in the differential ("A-B") mode. The 300K ohm potentiometer is adjusted until an optimum value of K is determined to obtain the maximum possible expansion of the horizontal display of (F-kd). A photographic record of the resulting "expanded hysteresis loop" was then made. The measurement accuracy of the area enclosed by the

hysteresis loop (proportional to the energy dissipated per cycle) was, of course, greatly improved by this technique. Figures 8 and 9 represent typical photographic records taken during docking port joint tests.

REFERENCES

1. Bernstein, E. L., "Free-Free Modes and Frequencies for the AAP Cluster Including ATM Canister Motion," LMSC/HREC A791771, Lockheed Missiles & Space Company, Huntsville, Ala., September 1968.

2. Robinson, G. D., "Investigation of Joint Damping for AAP Cluster," LMSC/HREC D149176, Lockheed Missiles & Space Company, Huntsville, Ala., 25 August 1969.

3. Maidanik, G., and E. E. Ungar, "Panel Loss Factors Due to Gas Pumping at Structural Joints," NASA CR-954, (1967).

4. Lazan, B. J., "Energy Dissipation Mechanisms in Structures with Particular Reference to Material Damping," in Structural Damping, from papers at Colloquium on Structural Damping at ASME annual meeting, Atlantic City, New Jersey, 1959.

5. Yettram, A. L., and H. M. Husain, "Plane-Framework Methods for Plates in Extension," J. Engineering Mechanics, ASCE, Vol. 92, No. EM1, February 1966, pp. 157-168.

6. Lazan, B. J., Damping of Materials and Members in Structural Mechanics, Pergamon Press, 1968.

7. Robertson, J. M. and A. J. Yorgiadis, "Internal Friction in Engineering Materials," J. of Applied Mechanics, September 1946.

8. Kaufman, J. G., "Damping of Light Metals," Materials in Design Engineering, August 1962.

9. Bernstein, E. L., and W. E. Jones, "Flexural and Torsional Stiffnesses of ATM Solar Panels," LMSC/HREC A791390, Lockheed Missiles & Space Company, Huntsville, Ala., 26 April 1968.

Table 1

MODES AND FREQUENCIES FOR AAP CLUSTER

Mode	Frequency (Hz)	Description of Mode Shape
1	0.186	ATM Solar Panel First Bending Mode
2	0.590	LM/ATM Coupled with Solar Panel Motion
3	0.668	ATM Solar Panel Twisting
4	0.670	LM/ATM Bending Coupled with Solar Panel Motion
5	1.154	ATM Solar Panel Second Bending Mode
6	2.193	C/SM Bending
7	3.662	Canister Bending
8	5.624	Canister Bending

PRECEDING PAGE BLANK NOT FILMED.

Table 2

STRUCTURAL DAMPING – AAP CLUSTER (72°F)

MODE 1

Modal Partici-pation	Docking Port Joint Damping (in-lb/cycle)	ATM Solar Panel Joint Damping (in-lb/cycle)	Total Damping (in-lb/cycle)	Strain Energy (in-lb)	Damping Coefficient (Percentage)
.25	.12115-2*	.20843-1	.22055-1	.42681-1	.41132+1
.50	.24231-2	.42483-1	.44906-1	.17072+0	.20938+1
.75	.36347-2	.64920-1	.68555-1	.38413+0	.14103+1
1.0	.48461-2	.88154-1	.93000-1	.68289+0	.10841+1
1.25	.60577-2	.11218+0	.11824+0	.10670+1	.88213+0
1.50	.72692-2	.13701+0	..14428+0	.15365+1	.74746+0
1.75	.84808-2	.16264+0	.17112+0	.20914+1	.65130+0
2.0	.96922-2	.18906+0	.19875+0	.27316+1	.57917+0

MODE 2

Modal Partici-pation	Docking Port Joint Damping (in-lb/cycle)	ATM Solar Panel Joint Damping (in-lb/cycle)	Total Damping (in-lb/cycle)	Strain Energy (in-lb)	Damping Coefficient (Percentage)
.25	.35348+0	.38727-1	.39221+0	.42944+0	.71270+1
.50	.80430+0	.77987-1	.84303+0	.17178+1	.39064+1
.75	.13541+1	.11778+0	.14719+1	.38650+1	.30314+1
1.0	.21223+1	.15810+0	.22804+1	.68711+1	.26418+1
1.25	.31424+1	.19896+0	.33414+1	.10736+2	.24774+1
1.50	.43814+1	.24035+0	.46218+1	.15460+2	.23796+1
1.75	.58571+1	.28227+0	.61394+1	.21043+2	.23223+1
2.0	.75049+1	.32472+0	.78296+1	.27484+2	.22676+1

*.12115-2 = .12115 x 10^{-2}

Table 2 (Continued)

MODE 3

Modal Participation	Docking Port Joint Damping (in-lb/cycle)	ATM Solar Panel Joint Damping (in-lb/cycle)	Total Damping (in-lb/cycle)	Strain Energy (in-lb)	Damping Coefficient (Percentage)
.25	Small	.13175+0	.13175+0	.55049+0	.19051+1
.50	Small	.29166+0	.29166+0	.22020+1	.10543+1
.75	Small	.47973+0	.47973+0	.49544+1	.77076+0
1.0	Small	.69595+0	.69595+0	.88079+1	.62895+0
1.25	Small	.94034+0	.94034+0	.13762+2	.54390+0
1.50	Small	.12129+1	.12129+1	.19818+2	.48717+0
1.75	Small	.15136+1	.15136+1	.26974+2	.44666+0
2.0	Small	.18425+1	.18425+1	.35232+2	.41628+0

MODE 4

.25	.69653-1	.17759+0	.24724+0	.55380+0	.35537+1
.50	.13930+0	.38299+0	.52229+0	.22152+1	.18768+1
.75	.20896+0	.61620+0	.82516+0	.49842+1	.13178+1
1.0	.27861+0	.87722+0	.11558+1	.88608+1	.10383+1
1.25	.34826+0	.11661+1	.15144+1	.13845+1	.87066+0
1.50	.41792+0	.14827+1	.19006+1	.19937+1	.75883+0
1.75	.48757+0	.18272+1	.23148+1	.27136+2	.67902+0
2.0	.57094+0	.21995+1	.27704+1	.35443+2	.62219+0

Table 2 (Continued)

MODE 5

Modal Partici- pation	Docking Port Joint Damping (in-lb/cycle)	ATM Solar Panel Joint Damping (in-lb/cycle)	Total Damping (in-lb/cycle)	Strain Energy (in-lb)	Damping Coefficient (Percentage)
.25	Small	.23362+0	.23362+0	.16429+1	.11319+1
.50	Small	.48708+0	.48708+0	.65715+1	.59000+0
.75	Small	.76038+0	.76038+0	.14786+2	.40935+0
1.0	Small	.10535+1	.10535+1	.26286+2	.31902+0
1.25	Small	.13665+1	.13665+1	.41072+2	.26484+0
1.50	Small	.16993+1	.16993+1	.59144+2	.22869+0
1.75	Small	.20520+1	.20520+1	.80501+2	.20290+0
2.0	Small	.24245+1	.24245+1	.10514+3	.18356+0

MODE 6

Modal Partici- pation	Docking Port Joint Damping (in-lb/cycle)	ATM Solar Panel Joint Damping (in-lb/cycle)	Total Damping (in-lb/cycle)	Strain Energy (in-lb)	Damping Coefficient (Percentage)
.25	.98310+0	.48625-1	.10317+1	.59330+1	.13842+1
.50	.29795+1	.98538-1	.30780+1	.23732+2	.10324+1
.75	.63164+1	.14971+0	.64661+1	.53398+2	.96387+0
1.0	.10972+2	.20217+0	.11174+2	.94929+2	.93697+0
1.25	.16684+2	.25591+0	.16940+2	.14833+3	.90903+0
1.50	.23505+2	.31093+0	.23816+2	.21359+3	.88754+0
1.75	.31381+2	.36722+0	.31748+2	.29072+3	.86923+0
2.0	.39627+2	.42480+0	.40052+2	.37972+3	.83962+0

Table 2 (Continued)

MODE 7

Modal Partici- pation	Docking Port Joint Damping (in-lb/cycle)	ATM Solar Panel Joint Damping (in-lb/cycle)	Total Damping (in-lb/cycle)	Strain Energy (in-lb)	Damping Coefficient (Percentage)
.25	.12489-1	.49037-2	.17393-1	.16544+2	.83683-2
.50	.24978-1	.98395-2	.34818-1	.66175+2	.41882-2
.75	.37466-1	.14807-1	.52273-1	.14889+3	.27946-2
1.0	.49955-1	.19807-1	.69762-1	.26470+3	.20979-2
1.25	.62444-1	.24839-1	.87283-1	.41359+3	.16799-2
1.50	.74933-1	.29904-1	.10484+0	.59558+3	.14012-2
1.75	.87422-1	.35000-1	.12242+0	.81064+3	.1202-2
2.0	.99911-1	.40128-1	.14004+0	.10588+4	.10528-2

MODE 8

Modal Partici- pation	Docking Port Joint Damping (in-lb/cycle)	ATM Solar Panel Joint Damping (in-lb/cycle)	Total Damping (in-lb/cycle)	Strain Energy (in-lb)	Damping Coefficient (Percentage)
.25	.18635-1	.62968-2	.24932-1	.39020+2	.50860-2
.50	.37271-1	.12637-1	.49908-1	.15608+3	.25453-2
.75	.55906-1	.19022-1	.74928-1	.35118+3	.16983-2
1.0	.74542-1	.25450-1	.99992-1	.62432+3	.12749-2
1.25	.93177-1	.31923-1	.12510+0	.97550+3	.10208-2
1.50	.11181+0	.38439-1	.15025+0	.14047+4	.85140-3
1.75	.13045+0	.44999-1	.17545+0	.19120+4	.73043-3
2.0	.14908+0	.51603-1	.20068+0	.24973+4	.63966-3

Table 3

STRUCTURAL DAMPING — AAP CLUSTER (-50°F)

MODE 1

Modal Partici-pation	Docking Port Joint Damping (in-lb/cycle)	ATM Solar Panel Joint Damping (in-lb/cycle)	Total Damping (in-lb/cycle)	Strain Energy (in-lb)	Damping Coefficient (Percentage)
.25	.25575-2*	.33731-1	.36287-1	.42681-1	.67675+1
.50	.51153-2	.70491-1	.75606-1	.17072+0	.35252+1
.75	.76727-2	.11028+0	.11795+0	.38413+0	.24442+1
1.0	.10230-1	.15310+0	.16333+0	.68289+0	.19038+1
1.25	.12788-1	.19895+0	.21174+0	.10670+1	.15796+1
1.50	.15346-1	.24783+0	.26318+0	.15365+1	.13634+1
1.75	.17903-1	.29973+0	.31763+0	.20913+1	.12089+1
2.0	.20461-1	.35467+0	.37513+0	.27316+1	.10931+1

MODE 2

.25	.74619+0	.61617-1	.80781+0	.42944+0	.14973+2
.50	.16494+1	.12526+0	.17747+1	.17178+1	.82237+1
.75	.28287+1	.19092+0	.30196+1	.38650+1	.62189+1
1.0	.43137+1	.25861+0	.45723+1	.68711+1	.52969+1
1.25	.60915+1	.32832+0	.64198+1	.10736+2	.47598+1
1.50	.81679+1	.40005+0	.85680+1	.15460+2	.44115+1
1.75	.10495+2	.47381+0	.10969+2	.21043+2	.41493+1
2.0	.13072+2	.54959+0	.13622+2	.37484+2	.39452+1

*.25575-2 = .25575 x 10^{-2}

Table 3 (Continued)

MODE 3

Modal Partici- pation	Docking Port Joint Damping (in-lb/cycle)	ATM Solar Panel Joint Damping (in-lb/cycle)	Total Damping (in-lb/cycle)	Strain Energy (in-lb)	Damping Coefficient (Percentage)
.25	Small	.23894+0	.23894+0	.55049+0	.34550+1
.50	Small	.58494+0	.58494+0	.22020+1	.21145+1
.75	Small	.10380+1	.10380+1	.49544+1	.16677+1
1.0	Small	.15981+1	.15981+1	.88079+1	.14443+1
1.25	Small	.22652+1	.22652+1	.13762+2	.13102+1
1.50	Small	.30395+1	.30395+1	.19818+2	.12208+1
1.75	Small	.39207+1	.39207+1	.26974+2	.11570+1
2.0	Small	.49090+1	.40909+1	.35232+2	.92426+0

MODE 4

.25	.14704+0	.31079+0	.45793+0	.55380+0	.65806+1
.50	.29408+0	.72731+0	.10214+1	.22152+1	.36703+1
.75	.44112+0	.12496+1	.16907+1	.49842+1	.27001+1
1.0	.58816+0	.18776+1	.24658+1	.88608+1	.22151+1
1.25	.73519+0	.26113+1	.33465+1	.13845+2	.19240+1
1.50	.89988+0	.34508+1	.43507+1	.19937+2	.17371+1
1.75	.10665+1	.43960+1	.54625+1	.27136+2	.16023+0
2.0	.12414+1	.54469+1	.66883+1	.35443+2	.15021+0

Table 3 (Continued)

MODE 5

Modal Partici-pation	Docking Port Joint Damping (in-lb/cycle)	ATM Solar Panel Joint Damping (in-lb/cycle)	Total Damping (in-lb/cycle)	Strain Energy (in-lb)	Damping Coefficient (Percentage)
.25	Small	.39021+0	.39021+0	.16429+1	.18906+1
.50	Small	.85585+0	.85585+0	.65715+1	.10367+1
.75	Small	.13969+1	.13969+1	.14786+2	.75202+0
1.0	Small	.20134+1	.20134+1	.26286+2	.60970+0
1.25	Small	.27053+1	.27053+1	.41072+2	.52430+0
1.50	Small	.34727+1	.34727+1	.59144+2	.46738+0
1.75	Small	.43154+1	.43154+1	.80501+2	.42671+0
2.0	Small	.52336+1	.52336+1	.10514+3	.39623+0

MODE 6

.25	.21133+1	.78044-1	.21913+1	.59330+1	.29400+1
.50	.57980+1	.16095+0	.59490+1	.23732+2	.19987+1
.75	.11206+2	.24871+0	.11455+2	.53398+2	.17076+1
1.0	.17785+2	.34134+0	.18126+2	.94929+2	.15199+1
1.25	.25705+2	.43882+0	.26144+2	.14833+3	.14030+1
1.50	.34985+2	.54117+0	.35526+2	.21359+3	.13240+1
1.75	.44930+2	.64837+0	.45578+2	.29072+3	.12479+1
2.0	.55276+2	.76044+0	.56036+2	.37972+3	.11747+1

Table 3 (Continued)

MODE 7

Modal Partici-pation	Docking Port Joint Damping (in-lb/cycle)	ATM Solar Panel Joint Damping (in-lb/cycle)	Total Damping (in-lb/cycle)	Strain Energy (in-lb)	Damping Coefficient (Percentage)
.25	.16435+0	.77627-2	.17211+0	.16544+2	.82809-1
.50	.32850+0	.15648-1	.34415+0	.65175+2	.41397-1
.75	.49282+0	.23654-1	.51647+0	.14889+3	.27612-1
1.0	.65909+0	.31783-1	.69087+0	.26470+3	.20776-1
1.25	.82136+0	.40034-1	.86139+0	.41359+3	.16578-1
1.50	.98563+0	.48407-1	.10340+1	.59558+3	.13820-1
1.75	.11499+1	.56902-1	.12068+1	.81064+3	.11850-1
2.0	.13142+1	.65519-1	.13797+1	.10588+4	.10373-1

MODE 8

.25	.21965+0	.99710-2	.30647+0	.39020+2	.62519-1
.50	.43930+0	.20109-1	.45941+0	.15608+3	.23430-1
.75	.65894+0	.30414-1	.68935+0	.35118+3	.15625-1
1.0	.87860+0	.40885-1	.91949+0	.62432+3	.11723-1
1.25	.10983+1	.51524-1	.11498+1	.97550+3	.93823-2
1.50	.13297+1	.62330-1	.13920+1	.14047+4	.78880-2
1.75	.15696+1	.73302-1	.16419+1	.19120+4	.68355-2
2.0	.18212+1	.84441-1	.19056+1	.24973+4	.60740-2

Table 4

STRUCTURAL DAMPING — AAP CLUSTER (150°F)

MODE 1

Modal Partici-pation	Docking Port Joint Damping (in-lb/cycle)	ATM Solar Panel Joint Damping (in-lb/cycle)	Total Damping (in-lb/cycle)	Strain Energy (in-lb)	Damping Coefficient (Percentage)
.25	.12115-2*	.26904-1	.28116-1	.42681-1	.52437+1
.50	.24231-2	.54334-1	.56757-1	.17072+0	.26464+1
.75	.36347-2	.82291-1	.85926-1	.38413+0	.17806+1
1.0	.48461-2	.11078+0	.11563+0	.68289+0	.13478+1
1.25	.60577-2	.13979+0	.14585+0	.10670+1	.10881+1
1.50	.72692-2	.16932+0	.17659+0	.15365+1	.91484+0
1.75	.84808-2	.19939+0	.20787+0	.20914+1	.79117+0
2.0	.96922-2	.22998+0	.23967+0	.27316+1	.69841+0

MODE 2

.25	.35348+0	.50292-1	.40377+0	.42944+0	.7484+1
.50	.80430+0	.10094+0	.90524+0	.17178+1	.41948+1
.75	.13541+1	.15193+0	.15060+1	.38650+1	.31016+1
1.0	.21223+1	.20328+0	.23256+1	.68711+1	.26941+1
1.25	.31424+1	.25498+0	.33974+1	.10736+2	.25189+1
1.50	.43814+1	.30703+0	.46884+1	.15460+2	.24139+1
1.75	.58571+1	.35943+0	.62165+1	.21043+2	.23515+1
2.0	.75049+1	.41219+0	.79171+1	.27484+2	.22930+1

*.12115-2 = .12115 x 10^{-2}

55

Table 4 (Continued)

MODE 3

Modal Partici-pation	Docking Port Joint Damping (in-lb/cycle)	ATM Solar Panel Joint Damping (in-lb/cycle)	Total Damping (in-lb/cycle)	Strain Energy (in-lb)	Damping Coefficient (Percentage)
.25	Small	.16264+0	.16264+0	.55049+0	.23518+1
.50	Small	.34389+0	.34389+0	.22020+1	.12431+1
.75	Small	.54376+0	.54376+0	.54376+0	.87361+0
1.0	Small	.76225+0	.76225+0	.88079+1	.68887+0
1.25	Small	.99936+0	.99936+0	.13762+2	.57803+0
1.50	Small	.12551+1	.12551+1	.19818+2	.50411+0
1.75	Small	.15294+1	.15294+1	.26974+2	.45133+0
2.0	Small	.18224+1	.18224+1	.35232+2	.41173+0

MODE 4

.25	.69653-1	.22247+0	.29212+0	.55380+0	.41987+1
.50	.13930+0	.46334+0	.60264+0	.22152+1	.21655+1
.75	.20896+0	.72259+0	.93155+0	.49842+1	.14877+1
1.0	.27861+0	.10002+1	.12788+1	.88608+1	.94557+0
1.25	.34826+0	.12963+1	.16446+1	.13845+1	.94557+0
1.50	.41792+0	.16107+1	.20286+1	.19937+1	.81001+0
1.75	.48757+0	.19435+1	.24311+1	.27136+2	.71313+0
2.0	.57094+0	.22947+1	.28656+1	.35443+2	.64357+0

Table 4 (Continued)

MODE 5

Modal Partici-pation	Docking Port Joint Damping (in-lb/cycle)	ATM Solar Panel Joint Damping (in-lb/cycle)	Total Damping (in-lb/cycle)	Strain Energy (in-lb)	Damping Coefficient (Percentage)
.25	Small	.29805+0	.29805+0	.16429+1	.14441+1
.50	Small	.60921+0	.60921+0	.65715+1	.73793+0
.75	Small	.93349+0	.93349+0	.14786+2	.50254+0
1.0	Small	.12709+1	.12709+1	.26286+2	.38486+0
1.25	Small	.16214+1	.16214+1	.41072+2	.31424+0
1.50	Small	.19850+1	.19850+1	.59144+2	.26715+0
1.75	Small	.23618+1	.23618+1	.80501+2	.23354+0
2.0	Small	.27517+1	.27517+1	.10514+3	.20833+0

MODE 6

.25	.98310+0	.62949-1	.10460+1	.59330+1	.14034+1
.50	.29795+1	.12674+0	.31062+1	.34732+2	.10419+1
.75	.63164+1	.19138+0	.65078+1	.53398+2	.97011+0
1.0	.10972+2	.25687+0	.11240+2	.94929+2	.94250+0
1.25	.16684+2	.32320+0	.17007+2	.14833+3	.91267+0
1.50	.23505+2	.39038+0	.23895+2	.21359+3	.89051+0
1.75	.31381+2	.45840+0	.31839+2	.29072+3	.87176+0
2.0	.39627+2	.52726+0	.40154+2	.37972+3	.84174+0

Table 4 (Continued)

MODE 7

Modal Partici- pation	Docking Port Joint Damping (in-lb/cycle)	ATM Solar Panel Joint Damping (in-lb/cycle)	Total Damping (in-lb/cycle)	Strain Energy (in-lb)	Damping Coefficient (Percentage)
.25	.12489-1	.63793-2	.18868-1	.16544+2	.90784-2
.50	.24978-1	.12780-1	.37758-1	.66175+2	.45418-2
.75	.37466-1	.19202-1	.56668-1	.14889+3	.30296-2
1.0	.49955-1	.25645-1	.75600-1	.26470+3	.22735-2
1.25	.62444-1	.32109-1	.94553-1	.41359+3	.18198-2
1.50	.74933-1	.38594-1	.11353+0	.59558+3	.15173-2
1.75	.87422-1	.45101-1	.13252+0	.81064+3	.13013-2
2.0	.99911-1	.51629-1	.15154+0	.10588+4	.11392-2

MODE 8

.25	.18635-1	.81908-2	.26826-1	.39020+2	.54724-2
.50	.37271-1	.16411-1	.53682-1	.15608+3	.27378-2
.75	.55906-1	.24659-1	.80565-1	.35118+3	.18261-2
1.0	.74542-1	.32937-1	.10748+0	.62432+3	.13704-2
1.25	.93177-1	.41244-1	.13442+0	.97550+3	.10969-2
1.50	.11181+0	.49580-1	.16139+0	.14047+4	.91452-3
1.75	.13045+0	.57945-1	.18840+0	.19120+4	.78435-3
2.0	.14908+0	.66339-1	.21542+0	.24973+4	.68664-3

Table 5

MATERIAL DAMPING – AAP CLUSTER

Mode	MDA	ATM Solar Panels	ATM Canister Rings	Total Damping (in-lb/cycle)
1	.11345 - 1[*]	.26153 - 1	.13346 - 4	.37511 - 1
2	.27097 + 2	.23961 + 0	.12522 - 1	.27349 + 2
3	.13812 - 11	.16842 + 2	.27802 - 14	.16842 + 2
4	.65279 + 0	.15673 + 2	.37068 - 3	.16326 + 2
5	.81236 - 13	.16961 + 1	.15731 - 15	.16961 + 1
6	.26243 + 1	.42942 - 1	.11094 - 3	.26674 + 1
7	.20927 + 0	.11786 - 2	.58363 + 0	.79408 + 0
8	.61672 + 0	.16636 - 2	.68719 + 0	.13056 + 1

[*].11345-1 = .11345 x 10^{-1}

59

Table 6

AAP CLUSTER — CSM — MDA — DOCKING PORT — TENSION-BOLTED SPECIMEN

Test Data

Test No.	Load (lb)	Freq. (Hz)	Temp. (°F)	Compr. Defln. (in)	Tensile Defln. (in)	Damping Energy/Cycle		Unit Joint Stiffness		δ_i (in)
						Compr. (in-lb/in)	Tensile (in-lb/in)	Compr. (lb/in/in)	Tensile (lb/in/in)	
1	34	1.75	73	0.1×10^{-3}	0.14×10^{-3}	0.48×10^{-3}	0.40×10^{-3}	16.5×10^{4}	11.45×10^{4}	0
2	65	1.73	73	0.17	0.38	0.83	1.40	19.15	8.75	0
3	472	1.71	73	0.65	4.1	6.0	36.3	39.35	4.67	0.2×10^{-3}
4	688	1.72	73	0.75	7.0	8.3	83.0	51.0	4.08	0.5
5	34	1.50	74	0.12	0.19	0.38	0.74	14.05	8.62	0
6	68	1.47	74	0.22	0.5	0.95	1.78	18.45	6.8	0
7	408	1.45	74	0.9	3.4	5.9	35.15	31.9	5.98	-0.3
8	600	1.47	74	1.25	5.15	8.8	48.2	39.3	5.45	-0.4
9	35	0.92	75	0.2	0.22	2.2	2.81	7.05	7.95	0
10	75	0.92	75	0.4	0.55	4.22	6.25	11.95	7.3	0
11	171	0.93	75	0.673	1.25	8.1	14.2	19.2	6.9	-0.3
12	255	0.94	75	0.85	2.0	8.62	21.9	38.25	6.05	-0.3

LMSC/HREC D149346

Table 6 (Continued)

Test No.	Load (lb)	Freq. (Hz)	Temp. (°F)	Compr. Defln. (in)	Tensile Defln. (in)	Damping Energy/Cycle Compr. (in-lb/in)	Tensile (in-lb/in)	Unit Joint Stiffness Compr. (lb/in/in)	Tensile (lb/in/in)	δ_i (in.)
13	153	0.91	-20	1.25×10^{-3}	1.55×10^{-3}	15.25×10^{-3}	19.7×10^{-3}	6.55×10^{4}	4.64×10^{4}	0
14	268	0.93	-18	1.55	2.9	24.8	41.0	17.05	4.46	-1.0×10^{-3}
15	421	0.94	-18	1.6	4.1	36.3	44.7	19.15	5.05	-1.0
16	163	0.91	-45	1.5	1.75	17.05	19.0	5.0	4.65	0
17	242	0.93	-45	1.9	2.9	21.1	29.3	14.6	4.49	-1.6
18	447	0.95	-45	2.38	5.5	32.5	60.0	36.9	10.15	-0.6
19	153	2.42	-45	1.5	1.75	12.8	15.8	5.35	4.25	0
20	255	2.46	-45	1.9	3.0	16.6	25.5	11.25	4.35	-1.6
21	427	2.52	-40	2.0	5.25	21.1	44.9	25.5	4.35	-1.5
22	173	1.64	-30	1.52	1.85	15.5	15.7	4.95	5.4	0
23	242	1.66	-26	1.7	2.85	15.9	22.35	12.2	5.2	-1.0
24	402	1.69	-25	2.0	4.7	26.7	53.8	27.0	4.95	-1.5
25	274	0.94	73	0.8	2.2	9.15	22.2	17.5	6.25	-0.4
26	396	0.94	73	1.0	3.2	12.85	35.15	33.5	6.2	-0.4
27	575	0.96	73	1.1	4.75	18.9	61.5	35.7	6.0	-0.3

Table 7

AAP CLUSTER – CSM – MDA – DOCKING PORT – SHEAR-BOLTED SPECIMEN

Test Data

Test No	Load (lb)	Freq. (Hz)	Temp. (°F)	Compr. Defln. (in)	Tensile Defln. (in)	Damping Energy/Cycle		Unit Joint Stiffness		δ_i (in)
						Compr. (in-lb/in)	Tensile (in-lb/in)	Compr. (lb/in/in)	Tensile (lb/in/in).	
28	59	0.84	73	0.18×10^{-3}	0.19×10^{-3}	0.43×10^{-3}	0.48×10^{-3}	10.2×10^{4}	11.2×10^{4}	0
29	153	0.91	73	0.56	0.88	1.59	4.65	8.7	5.6	0
30	223	0.93	73	0.92	1.72	11.3	19.9	8.1	4.0	0
31	421	0.95	73	1.9	3.5	65.7	100	6.2	3.9	0
32	447	0.95	73	2.0	3.7	78.7	113	6.5	4.4	0
33	638	0.95	73	3.3	5.5	237.3	268	6.1	4.3	0
34	81	1.30	76	0.31	0.34	1.2	1.15	7.6	9.1	0
35	153	1.36	76	0.6	0.72	4.3	4.7	7.7	7.5	0
36	243	1.40	76	1.15	1.75	39.0	63.3	6.8	4.2	0
37	370	1.43	76	1.8	3.5	128.0	205.3	6.7	3.6	0
38	562	1.45	76	2.9	5.0	206.7	253	6.6	3.4	0
39	59	2.15	76	0.21	0.21	0.48	0.51	9.8	8.5	0
40	145	2.35	76	0.55	0.62	3.38	3.62	8.8	8.8	0
41	249	2.43	76	1.16	1.32	20.4	30.9	7.3	5.6	0
42	383	2.49	76	1.8	3.55	76.3	140.7	6.9	3.6	0

(Continued)

Table 7 (Continued)

Test Data

Test No	Load (lb)	Freq (Hz)	Temp (°F)	Compr Defln. (in)	Tensile Defln. (in)	Damping Energy/Cycle		Unit Joint Stiffness		δ_i (in)
						Compr. (in-lb/in)	Tensile (in-lb/in)	Compr. (lb/in/in)	Tensile (lb/in/in)	
43	68	2.10	-50	0.29×10^{-3}	0.275×10^{-3}	0.89×10^{-3}	1.03×10^{-3}	8.2×10^4	8.2×10^4	0
44	148	2.31	-50	0.64	0.71	2.93	4.7	7.5	7.3	0
45	255	2.42	-50	1.3	1.45	13.8	16.4	6.5	5.9	0
46	433	2.49	-48	2.35	5.35	79.8	241.1	6.0	2.6	0
47	80	1.28	-40	0.365	0.4	1.13	1.2	7.4	7.0	0
48	151	1.34	-38	0.72	0.79	3.8	4.3	7.3	6.4	0
49	249	1.39	-38	1.425	2.1	27.3	75.47	5.7	3.8	0
50	408	1.43	-38	2.25	5.55	70.3	236.7	5.9	2.4	0
51	102	0.84	-30	0.47	0.48	1.3	1.41	7.4	6.8	0
52	168	0.89	-30	0.8	0.94	4.97	5.7	6.4	6.3	0
53	389	0.93	-30	2.25	5.3	70.3	216.0	5.6	2.4	0
54	75	0.84	150	0.225	0.235	0.53	0.48	11.0	10.7	0
55	107	0.85	150	0.21	0.33	1.05	1.03	11.2	10.3	0
56	209	0.90	150	0.65	0.80	9.1	10.6	10.0	8.2	0
57	344	0.93	150	1.35	1.375	47.7	52.7	8.5	7.9	0

Table 7 (Continued)

Test Data

Test No	Load (lb)	Freq. (Hz)	Temp. (°F)	Compr. Defln. (in)	Tensile Defln. (in)	Damping Energy/Cycle		Unit Joint Stiffness		δ_i (in)
						Compr. (in-lb/in)	Tensile (in-lb/in)	Compr. (lb/in/in)	Tensile (lb/in/in)	
58	535	0.95	150	2.4×10^{-3}	3.65×10^{-3}	168.3×10^{-3}	217.7×10^{-3}	7.7×10^4	4.9×10^4	0
59	57	1.20	150	0.175	0.2	0.27	0.29	10.4	9.7	0
60	107	1.30	150	0.35	0.4	1.10	1.22	10.5	9.3	0
61	186	1.36	150	0.58	0.73	4.56	5.3	10.2	8.0	0
62	236	1.39	150	0.9	1.25	18.8	27.3	8.5	6.5	0
63	351	1.42	150	1.35	2.35	59.7	88.0	8.8	5.0	0
64	48	1.96	150	0.15	0.16	0.205	0.235	10.8	10.1	0
65	105	2.23	150	0.3	0.36	0.87	1.13	10.6	9.4	0
66	204	2.37	150	0.65	0.8	8.6	8.1	10.2	8.1	0
67	255	2.42	150	1.04	1.364	21.8	32.0	8.6	5.2	0

Table 8

MDA DOCKING PORT BENDING MOMENTS

Description of Mode Shape	Bending Moment (in.-lb)	
	Longitudinal Docking Port	Radial Docking Port
ATM Solar Panel First Bending Mode	Small	153.70
LM/ATM Coupled with Solar Panel Motion	5106.94	39736.30
ATM Solar Panel Twisting	Small	Small
LM/ATM Bending Coupled with Solar Panel Motion	993.77	7842.69
ATM Solar Panel Second Bending Mode	Small	Small
C/SM Bending	96863.30	10892.70
Canister Bending	4995.53	4876.60
Canister Bending	7454.15	5745.90

Table 9

MDA DOCKING PORT JOINT DAMPING (72°F)

MODE 1

Modal Partici- pation	Longitudinal Port		Radial Port		Total Damping (in.-lb/cycle)
	Shear Joint	Tension Joint	Shear Joint	Tension Joint	
0.25	Small	Small	.38425-3*	.44303-3	.12115-2
0.50	Small	Small	.76850-3	.88606-3	.24231-2
0.75	Small	Small	.11528-2	.13291-2	.36347-2
1.0	Small	Small	.15370-2	.17721-2	.48461-2
1.25	Small	Small	.10213-2	.22151-2	.60577-2
1.50	Small	Small	.23055-2	.26582-2	.72692-2
1.75	Small	Small	.26898-2	.31012-2	.84808-2
2.0	Small	Small	.30740-2	.35442-2	.96922-2

MODE 2

Modal Partici- pation	Longitudinal Port		Radial Port		Total Damping (in.-lb/cycle)
	Shear Joint	Tension Joint	Shear Joint	Tension Joint	
0.25	.12767-1	.14720-1	.99341-1	.11454+0	.35348+0
0.50	.25535-1	.29441-1	.24736+0	.22907+0	.80430+0
0.75	.38302-1	.44161-1	.44486+0	.34361+0	.13541+1
1.0	.51069-1	.58881-1	.75156+0	.45814+0	.21223+1
1.25	.63837-1	.73602-1	.11842+1	.57268+0	.31424+1
1.50	.76604-1	.88322-1	.17263+1	.68722+0	.43814+1
1.75	.89371-1	.10304+0	.23868+1	.80176+0	.58571+1
2.0	.10214+0	.11776+0	.31333+1	.91630+0	.75049+1

*.38425-3 = .38425 x 10^{-3}

Table 9 (Continued)

MODE 4

Modal Participation	Longitudinal Port		Radial Port		Total Damping (in.-lb/cycle)
	Shear Joint	Tension Joint	Shear Joint	Tension Joint	
0.25	.24844-2	.28645-2	.19607-1	.22606-1	.69653-1
0.50	.49688-2	.57289-2	.39213-1	.45212-1	.13930+0
0.75	.74533-2	.85934-2	.58820-1	.67818-1	.20896+0
1.0	.99377-2	.11458-1	.78427-1	.90424-1	.27861+0
1.25	.12422-1	.14322-1	.98034-1	.11303+0	.34826+0
1.50	.14907-1	.17187-1	.11764+0	.13564+0	.41792+0
1.75	.17391-1	.20051-1	.13725+0	.15824+0	.48757+0
2.0	.19875-1	.22916-1	.17371+0	.18085+0	.57094+0

MODE 6

Modal Participation	Longitudinal Port		Radial Port		Total Damping (in.-lb/cycle)
	Shear Joint	Tension Joint	Shear Joint	Tension Joint	
0.25	.30902+0	.27920+0	.27232-1	.31397-1	.98310+0
0.50	.11247+1	.55840+0	.54463-1	.62795-1	.29795+1
0.75	.26106+1	.83760+0	.81695-1	.94192-1	.63164+1
1.0	.47557+1	.11168+1	.10893+0	.12559+0	.10972+2
1.25	.74295+1	.13960+1	.13616+0	.15699+0	.16684+2
1.50	.10644+2	.16752+1	.17678+0	.18838+0	.23505+2
1.75	.14372+2	.19544+1	.23124+0	.21978+0	.31381+2
2.0	.18296+2	.22336+1	.27500+0	.25118+0	.39627+2

70

Table 9 (Continued)

MODE 7

Modal Participation	Longitudinal Port		Radial Port		Total Damping (in.-lb/cycle)
	Shear Joint	Tension Joint	Shear Joint	Tension Joint	
0.25	.12489-1	.14399-1	.12192-1	.14056-1	.77817-1
0.50	.24978-1	.28798-1	.24383-1	.28113-1	.15563+0
0.75	.37466-1	.43198-1	.36574-1	.42169-1	.23345+0
1.0	.49955-1	.57597-1	.48766-`	.56226-1	.31127+0
1.25	.62444-1	.71996-1	.60957-1	.70282-1	.38908+0
1.50	.74933-1	.86395-1	.73149-1	.84339-1	.46690+0
1.75	.87422-1	.10079+0	.85340-1	.98395-1	.54471+0
2.0	.99911-1	.11519+0	.97532-1	.11245+0	.62253+0

MODE 8

Modal Participation	Longitudinal Port		Radial Port		Total Damping (in.-lb/cycle)
	Shear Joint	Tension Joint	Shear Joint	Tension Joint	
0.25	.18635-1	.21486-1	.14365-1	.16562-1	.10450+0
0.50	.37271-1	.42972-1	.28730-1	.33124-1	.20810+0
0.75	.55906-1	.64458-1	.43094-1	.49686-1	.31214+0
1.0	.74542-1	.85944-1	.57459-1	.66248-1	.41619+0
1.25	.93177-1	.10743+0	.71824-1	.82811-1	.52024+0
1.50	.11181+0	.12892+0	.86188-1	.99373-1	.62429+0
1.75	.13045+0	.15040+0	.10055+0	.11593+0	.72833+0
2.0	.14903+0	.17189+0	.11492+0	.13250+0	.83239+0

Table 10

MDA DOCKING PORT DAMPING (-50°F)

MODE 1

Modal Partici- pation	Longitudinal Port		Radial Port		Total Damping (in.-lb/cycle)
	Shear Joint	Tension Joint	Shear Joint	Tension Joint	
0.25	Small	Small	.57638-3*	.14048-2	.25575-2
0.50	Small	Small	.11528-2	.28097-2	.51153-2
0.75	Small	Small	.17291-2	.42145-2	.76727-2
1.0	Small	Small	.23055-2	.56193-2	.10230-1
1.25	Small	Small	.28819-2	.70241-2	.12788-1
1.50	Small	Small	.34583-2	.84290-2	.15346-1
1.75	Small	Small	.40346-2	.98338-2	.17903-1
2.0	Small	Small	.46110-2	.11239-1	.20461-1

MODE 2

Modal Partici- pation	Longitudinal Port		Radial Port		Total Damping (in.-lb/cycle)
	Shear Joint	Tension Joint	Shear Joint	Tension Joint	
0.25	.19151-1	.46678-1	.14901+0	.36319+0	.74619+0
0.50	.38302-1	.93356-1	.37657+0	.72639+0	.16494+1
0.75	.57453-1	.14003+0	.74209+0	.10896+1	.28287+1
1.0	.76604-1	.18671+0	.12605+1	.14528+1	.43137+1
1.25	.95755-1	.23339+0	.19253+1	.18160+1	.60915+1
1.50	.11491+0	.28007+0	.27394+1	.21792+1	.81679+1
1.75	.13406+0	.32674+0	.36789+1	.25423+1	.10495+2
2.0	.15428+0	.37342+0	.47420+1	.29055+1	.13071+2

*.57638-3 = .57638 x 10^{-3}

73

Table 10 (Continued)

MODE 4

Modal Partici- pation	Longitudinal Port		Radial Port		Total Damping (in.-lb/cycle)
	Shear Joint	Tension Joint	Shear Joint	Tension Joint	
0.25	.37266-2	.90831-2	.29410-1	.71683-1	.14704+0
0.50	.74533-2	.18166-1	.58820-1	.14337+0	.29408+0
0.75	.11180-1	.27249-1	.88230-1	.21505+0	.44112+0
1.0	.14907-1	.36333-1	.11764+0	.28673+0	.58816+0
1.25	.18633-1	.45416-1	.14705+0	.35841+0	.73519+0
1.50	.22360-1	.54499-1	.18528+0	.43010+0	.89988+0
1.75	.26086-1	.63582-1	.22449+0	.50178+0	.10665+1
2.0	.29813-1	.72665-1	.26782+0	.57346+0	.12414+1

MODE 6

Modal Partici- pation	Longitudinal Port		Radial Port		Total Damping (in.-lb/cycle)
	Shear Joint	Tension Joint	Shear Joint	Tension Joint	
0.25	.52334+0	.88534+0	.40848-1	.99560-1	.21133+1
0.50	.18324+1	.17707+1	.81695-1	.19912+0	.57980+1
0.75	.40030+1	.26560+1	.12254+0	.29868+0	.11206+2
1.0	.67550+1	.35414+1	.16785+0	.39824+0	.17785+2
1.25	.10168+2	.44267+1	.2223 +0	.49780+0	.25705+2
1.50	.14253+2	.53120+1	.28482+0	.59736+0	.34985+2
1.75	.18662+2	.61974+1	.35562+0	.69692+0	.44930+2
2.0	.23258+2	.70823+1	.44070+0	.79648+0	.55276+2

Table 10 (Continued)

MODE 7

Modal Participation	Longitudinal Port		Radial Port		Total Damping (in.-lb/cycle)
	Shear Joint	Tension Joint	Shear Joint	Tension Joint	
0.25	.18733-1	.45660-1	.18287-1	.44572-1	.16435+0
0.50	.37466-1	.91319-1	.36574-1	.89145-1	.32850+0
0.75	.56200-1	.13698+0	.54862-1	.13372+0	.49282+0
1.0	.74933-1	.18264+0	.73149-1	.17829+0	.65909+0
1.25	.93666-1	.22830+0	.91436-1	.22286+0	.82136+0
1.50	.11240+0	.27396+0	.10972+0	.26743+0	.98563+0
1.75	.13113+0	.31962+0	.12801+0	.31201+0	.11499+1
2.0	.14987+0	.36523+0	.14730+0	.35658+0	.13142+1

MODE 8

Modal Participation	Longitudinal Port		Radial Port		Total Damping (in.-lb/cycle)
	Shear Joint	Tension Joint	Shear Joint	Tension Joint	
0.25	.27953-1	.68131-1	.21547-1	.52518-1	.21965+0
0.50	.55906-1	.13626+0	.43094-1	.10504+0	.43930+0
0.75	.83859-1	.20439+0	.64641-1	.15755+0	.65894+0
1.0	.11181+0	.27253+0	.86189-1	.21007+0	.87860+0
1.25	.13977+0	.34066+0	.10774+0	.26259+0	.10983+1
1.50	.17362+0	.40879+0	.12928+0	.31511+0	.13297+1
1.75	.21090+0	.47692+0	.15111+0	.36763+0	.15686+1
2.0	.24817+0	.54505+0	.17984+0	.42014+0	.18212+1

Table 11a
SOLAR PANEL SCISSORS JOINT DATA (72°F)

Nut: Normal (finger tight)

Test Date: 4-22-69   PM   R = 99.06

Position of Weights	Freq. (cps)	Decay b in/cycle	Weight $W = mg$ lb.	C.G.Distance d in.	$F = \dfrac{bmgd}{4 \cdot R}$ in-lb
Lower	.34	0.07	254.5	92.7	4.17
		0.09	143.5	93.1	3.03
		0.11	98.5	92.7	2.54
		0.475	9.5	84.7	0.97
2nd	.42	0.12	254.5	57.8	4.45
		0.15	143.5	58.25	3.16
		0.187	98.5	58.2	2.71
		0.663	9.5	58.2	0.93
3rd	.50	0.22	254.5	37.9	5.36
		0.25	143.5	38.6	3.50
		0.30	98.5	38.75	2.89
		0.85	9.5	43.3	0.88
Top	.71	0.46	254.5	17.2	5.1
		0.56	143.5	18.0	3.64
		0.65	98.5	18.26	2.80
		1.33	9.5	27.75	0.89

Table 11b

SOLAR PANEL SCISSORS JOINT DATA (72°F)

Nut: Tight

Test Date: 4-22-69   R = 99.06

Position of Weights	Freq. (cps)	Decay b in/cycle	Weight $W = mg$ lb.	C.G.Distance d in.	$F = \dfrac{bmgd}{4R}$ in-lb
Lower	.34	0.11	254.5	92.7	6.51
		0.13	143.5	93.1	4.39
		0.16	98.5	92.7	3.68
		0.94	9.5	84.7	1.91
2nd	.43	0.18	254.5	57.8	6.21
		0.26	143.5	58.25	5.49
		0.325	98.5	58.2	4.76
		1.5	9.5	58.2	2.09
3rd	.52	0.28	254.5	37.9	6.83
		0.45	143.5	38.6	6.29
		0.52	98.5	38.75	5.02
			9.5	43.3	
Top	.75	0.80	254.5	17.2	8.90
		0.95	143.5	18.0	6.18
		1.2	98.5	18.26	5.46
			9.5	27.75	

Table 11c

SOLAR PANEL SCISSORS JOINT DATA (72°F)

Nut: Loose

Test Date: 4-22-69   R = 99.06

Position of Weights	Freq. (cps)	Decay b in/cycle	Weight W = mg lb.	C.G.Distance d in.	$F = \dfrac{bmgd}{4R}$ in-lb
Lower	.34	.050	254.5	92.7	2.98
		.070	143.5	93.1	2.36
		.078	98.5	92.7	1.76
		.20	9.5	84.7	0.41
2nd	.43	.11	254.5	57.8	4.09
		.13	143.5	58.25	2.74
		.153	98.5	58.2	2.21
		.31	9.5	58.2	0.43
3rd	.5	.156	254.5	37.9	3.8
		.186	143.5	38.6	2.6
		.21	98.5	38.75	2.02
		.39	9.5	43.3	0.405
Top	.71	.39	254.5	17.2	4.33
		.47	143.5	18.0	3.06
		.55	98.5	18.26	2.5
		.61	9.5	27.75	0.407

Table 12a

SOLAR PANEL SCISSORS JOINT DATA (150°F)

Nut: Normal (finger tight)

Test Date: 4-24-69 AM   R = 99.06

Position of Weights	Freq. (cps)	Decay b in/cycle	Weight W = mg lb.	C.G. Distance d in.	$F = \dfrac{bmgd}{4R}$ in-lb
Lower	.34	0.065	254.5	92.7	3.88
		0.093	143.5	93.1	3.14
		0.113	98.5	92.7	2.61
		0.70	9.5	84.7	1.42
2nd	.40	0.109	254.5	57.8	4.05
		0.151	143.5	58.25	3.19
		0.20	98.5	58.2	2.89
		1.05	9.5	58.2	1.46
3rd	.50	0.165	254.5	37.9	4.02
		0.218	143.5	38.6	3.25
		0.281	98.5	38.75	2.71
		1.35	9.5	43.3	1.40
Top	.66	0.34	254.5	17.2	3.78
		0.50	143.5	18.0	3.26
		0.60	98.5	18.26	2.58
		2.8	9.5	27.75	1.87

Table 12b

SOLAR PANEL SCISSORS JOINT DATA (150°F)

Nut: Tight

Test Date: 4-24-69 AM   R = 99.06

Position of Weights	Freq. (cps)	Decay b in/cycle	Weight W = mg lb.	C.G.Distance d in.	$F = \dfrac{bmgd}{4R}$ in-lb
Lower	.34	0.067	254.5	92.7	3.99
		0.092	143.5	93.1	3.10
		0.13	98.5	92.7	2.99
		0.63	9.5	84.7	1.28
2nd	.42	0.12	254.5	57.8	4.47
		0.17	143.5	58.25	3.59
		0.22	98.5	58.2	3.17
		0.96	9.5	58.2	1.34
3rd	.50	0.19	254.5	37.9	4.62
		0.27	143.5	38.6	3.77
		0.36	98.5	38.75	3.46
		1.5	9.5	43.3	1.56
Top	.75	0.50	254.5	17.2	5.55
		0.60	143.5	18.0	3.91
		0.68	98.5	18.26	2.93
		2.3	9.5	27.75	1.53

Table 12c

SOLAR PANEL SCISSORS JOINT DATA (150°F)

Nut: Loose

Test Date: 4-24-69

R = 99.06

Position of Weights	Freq. (cps)	Decay b in/cycle	Weight W = mg lb.	C.G.Distance d in.	$F = \dfrac{bmgd}{4\,R}$ in-lb
Lower	.34	,032	254.5	92.7	1.91
		.042	143.5	93.1	1.42
		.053	98.5	92.7	1.22
		.205	9.5	84.7	.416
2nd	.44	.055	254.5	57.8	2.04
		.075	143.5	58.25	1.58
		.095	98.5	58.2	1.37
		.34	9.5	58.2	.47
3rd	.50	.08	254.5	37.9	1.95
		.12	143.5	38.6	1.68
		.15	98.5	38.75	1.45
		.42	9.5	43.3	.44
Top	.70	.225	254.5	17.2	2.50
		.30	143.5	18.0	1.95
		.36	98.5	18.26	1.55
		.70	9.5	27.75	.47

Table 13a

SOLAR PANEL SCISSORS JOINT DATA (-50°F)

Nut: Normal

Test Date: 4-24-69   R = 99.06

Position of Weights	Freq. (cps)	Decay b in/cycle	Weight W = mg lb.	C.G. Distance d in.	$F = \dfrac{bmgd}{4R}$ in-lb
Lower	.33	0.21	254.5	92.7	12.5
		0.25	143.5	93.1	8.43
		0.27	98.5	92.7	6.22
		0.61	9.5	84.7	1.24
2nd	.43	0.35	254.5	57.8	13.0
		0.41	143.5	58.25	8.65
		0.45	98.5	58.2	6.50
		0.91	9.5	58.2	1.27
3rd	.52	0.56	254.5	37.9	13.64
		0.68	143.5	38.6	9.52
		0.71	98.5	38.75	6.84
		1.24	9.5	43.3	1.29
Top	.7	1.47	254.5	17.2	16.3
		1.55	143.5	18.0	10.1
		1.61	98.5	18.26	7.32
		2.0	9.5	27.75	1.33

Table 13b

SOLAR PANEL SCISSORS JOINT DATA (-50°F)

Nut: Tight

Test Date: 4-23-69   R = 99.06

Position of Weights	Freq. (cps)	Decay b in/cycle	Weight W = mg lb.	C.G.Distance d in.	$F = \dfrac{bmgd}{4R}$ in-lb
Lower	.34	0.31	254.5	92.7	18.5
		0.39	143.5	93.1	13.15
		0.5	98.5	92.7	11.5
		2.7	9.5	84.7	5.98
2nd	.42	0.5	254.5	57.8	18.6
		0.65	143.5	58.25	13.7
		0.8	98.5	58.2	11.56
			9.5	58.2	
3rd	.54	0.85	254.5	37.9	20.65
		1.1	143.5	38.6	15.4
		1.22	98.5	38.75	11.75
			9.5	43.3	
Top	.71	1.67	254.5	17.2	18.56
		2.1	143.5	18.0	13.70
		2.5	98.5	18.26	11.38
			9.5	27.75	

Table 13c

SOLAR PANEL SCISSORS JOINT DATA (-50°F)

Nut: Loose

Test Date: 4-24-69   R = 99.06

Position of Weights	Freq. (cps)	Decay b in/cycle	Weight W = mg lb.	C.G.Distance d in.	$F = \dfrac{bmgd}{4R}$ in-lb
Lower	.34	0.22	254.5	92.7	13.1
		0.24	143.5	93.1	8.1
		0.27	98.5	92.7	6.22
		0.63	9.5	84.7	1.28
2nd	.43	0.37	254.5	57.8	13.74
		0.44	143.5	58.25	9.3
		0.50	98.5	58.2	7.22
		0.95	9.5	58.2	1.32
3rd	.52	0.61	254.5	37.9	14.84
		0.72	143.5	38.6	10.1
		0.75	98.5	38.75	7.23
		1.26	9.5	43.3	1.31
Top	.83	1.39	254.5	17.2	15.45
		1.6	143.5	18.0	10.40
		1.7	98.5	18.26	7.73
		1.9	9.5	27.75	1.27

Table 14

SOLAR PANEL SCISSORS JOINT COEFFICIENT OF FRICTION

Design Load	Temp $^{\circ}F$	Tightness	Slope μ	Intercept c	Coeff. f
183	72	Normal	0.0121	1.65	0.0484
183	72	Tight	0.0128	3.6	0.0512
183	72	Loose	0.0108	1.2	0.0432
183	-50	Normal	0.046	2.6	0.184
183	-50	Tight	0.048	7.5	0.192
183	-50	Loose	0.044	3.1	0.176
183	150	Normal	0.008	2.15	0.032
183	150	Tight	0.008	2.55	0.032
183	150	Loose	0.006	1.0	0.024

Table 15

ATM SOLAR PANEL ARRAY JOINT DAMPING —
ROOM TEMPERATURE (72°F)

Norm.	MODE 1			MODE 2		
Factor	Loose Fit	Normal Fit	Tight Fit	Loose Fit	Normal Fit	Tight Fit
0.25	.15525-1*	.20843-1	.45028-1	.28209-1	.38727-1	.84197-1
0.50	.31160-1	.42483-1	.90899-1	.56894-1	.77987-1	.16896+0
0.75	.47807-1	.64920-1	.13761+0	.86053-1	.11778+0	.25428+0
1.0	.65166-1	.88154-1	.18517+0	.11569+0	.15810+0	.34017+0
1.25	.83235-1	.11218+0	.23357+0	.14580+0	.19896+0	.42661+0
1.50	.10202+0	.13701+0	.28281+0	.17638+0	.24035+0	.51363+0
1.75	.12151+0	.16264+0	.33290+0	.20744+0	.28227+0	.60120+0
2.0	.14171+0	.18906+0	.38383+0	.23897+0	.32472+0	.68934+0

Norm.	MODE 3			MODE 4		
Factor	Loose Fit	Normal Fit	Tight Fit	Loose Fit	Normal Fit	Tight Fit
0.25	.98145-1	.13175+0	.27163+0	.13145+0	.17759+0	.37183+0
0.50	.22142+0	.29166+0	.57304+0	.28773+0	.38299+0	.77308+0
0.75	.36984+0	.47973+0	.90425+0	.46883+0	.61620+0	.12038+1
1.0	.54338+0	.69595+0	.12652+1	.67476+0	.87722+0	.16639+1
1.25	.74206+0	.94034+0	.16560+1	.90551+0	.11661+1	.21534+1
1.50	.96588+0	.12129+1	.20766+1	.11611+1	.14827+1	.26723+1
1.75	.12148+1	.15136+1	.25270+1	.14415+1	.18272+1	.32207+1
2.0	.14889+1	.18425+1	.30071+1	.17467+1	.21995+1	.37985+1

*.15525-1 = .15525 x 10^{-1}

Table 15 (Continued)

Norm.	MODE 5			MODE 6		
Factor	Loose Fit	Normal Fit	Tight Fit	Loose Fit	Normal Fit	Tight Fit
0.25	.17115+0	.23362+0	.49857+0	.35469-1	.48625-1	.10537+0
0.50	.36080+0	.48708+0	.10181+1	.72080-1	.98538-1	.21210+0
0.75	.56776+0	.76038+0	.15587+1	.10983+0	.14971+0	.32017+0
1.0	.79243+0	.10535+1	.21202+1	.14872+0	.20217+0	.42960+0
1.25	.10348+1	.13665+1	.27027+1	.18876+0	.25591+0	.54039+0
1.50	.12949+1	.16993+1	.33062+1	.22993+0	.31093+0	.65252+0
1.75	.15727+1	.20520+1	.39307+1	.27225+0	.36722+0	.76601+0
2.0	.18682+1	.24245+1	.45762+1	.31570+0	.42480+0	.88084+0

Norm.	MODE 7			MODE 8		
Factor	Loose Fit	Normal Fit	Tight Fit	Loose Fit	Normal Fit	Tight Fit
0.25	.35690-2	.49037-2	.10681-1	.45821-2	.62968-2	.13714-1
0.50	.71666-2	.98395-2	.21396-1	.92054-2	.12637-1	.27474-1
0.75	.10793-1	.14807-1	.32145-1	.13867-1	.19022-1	.41280-1
1.0	.14448-1	.19807-1	.42927-1	.18567-1	.25450-1	.55133-1
1.25	.18131-1	.24839-1	.53744-1	.23307-1	.31923-1	.69033-1
1.50	.21844-1	.29904-1	.64595-1	.28086-1	.38439-1	.82979-1
1.75	.25584-1	.35000-1	.75479-1	.32904-1	.44999-1	.96971-1
2.0	.29354-1	.40128-1	.86398-1	.37762-1	.51603-1	.11101+0

Table 16

ATM SOLAR PANEL ARRAY JOINT DAMPING –
LOW TEMPERATURE (-50°F)

Norm.	MODE 1			MODE 2		
Factor	Loose Fit	Normal Fit	Tight Fit	Loose Fit	Normal Fit	Tight Fit
0.25	.39860-1*	.33731-1	.94511-1	.73228-1	.61617-1	.17588+0
0.50	.82618-1	.70491-1	.19218+0	.14839+0	.12526+0	.35387+0
0.75	.12827+0	.11028+0	.29302+0	.22549+0	.19092+0	.53397+0
1.0	.17683+0	.15310+0	.39701+0	.30452+0	.25861+0	.71619+0
1.25	.22828+0	.19895+0	.50417+0	.38549+0	.32832+0	.90051+0
1.50	.28263+0	.24783+0	.61448+0	.46840+0	.40005+0	.10869+1
1.75	.33987+0	.29973+0	.72796+0	.55324+0	.47381+0	.12755+1
2.0	.40002+0	.35467+0	.84460+0	.64001+0	.54959+0	.14661+1

Norm.	MODE 3			MODE 4		
Factor	Loose Fit	Normal Fit	Tight Fit	Loose Fit	Normal Fit	Tight Fit
0.25	.27227+0	.23894+0	.59071+0	.35809+0	.31079+0	.79916+0
0.50	.64695+0	.58494+0	.12931+1	.81732+0	.72731+0	.17087+1
0.75	.11240+1	.10380+1	.21073+1	.13777+1	.12496+1	.27285+1
1.0	.17035+1	.15981+1	.30331+1	.20392+1	.18776+1	.38587+1
1.25	.23853+1	.22652+1	.40706+1	.28018+1	.26113+1	.50992+1
1.50	.31696+1	.30395+1	.52199+1	.36656+1	.34508+1	.64500+1
1.75	.40563+1	.39207+1	.64808+1	.46305+1	.43960+1	.79111+1
2.0	.50453+1	.49090+1	.78535+1	.56966+1	.54469+1	.94826+1

*.39860-1 = .39860 x 10^{-1}

Table 16 (Continued)

Norm.	MODE 5			MODE 6		
Factor	Loose Fit	Normal Fit	Tight Fit	Loose Fit	Normal Fit	Tight Fit
0.25	.45636+0	.39021+0	.10562+1	.92479-1	.78044-1	.22065+0
0.50	.98486+0	.85585+0	.21910+1	.18961+0	.16095+0	.44638+0
0.75	.15855+1	.13969+1	.34046+1	.29138+0	.24871+0	.67717+0
1.0	.25583+1	.20134+1	.46969+1	.39781+0	.34134+0	.91304+0
1.25	.30033+1	.27053+1	.60679+1	.50889+0	.43882+0	.11540+0
1.50	.38204+1	.34727+1	.75176+1	.62461+0	.54117+0	.14000+1
1.75	.47096+1	.43154+1	.90460+1	.74498+0	.64837+0	.16511+1
2.0	.56710+1	.52336+1	.10653+2	.87000+0	.76044+0	.19072+1

Norm.	MODE 7			MODE 8		
Factor	Loose Fit	Normal Fit	Tight Fit	Loose Fit	Normal Fit	Tight Fit
0.25	.92412-2	.77627-2	.22280-1	.11869-1	.99710-2	.28609-1
0.50	.18599-1	.15648-1	.44688-1	.23897-1	.20109-1	.57392-1
0.75	.28074-1	.23654-1	.67223-1	.36085-1	.30414-1	.86349-1
1.0	.37665-1	.31783-1	.89885-1	.48433-1	.40885-1	.11548+0
1.25	.47373-1	.40034-1	.11267+0	.60941-1	.51524-1	.14479+0
1.50	.57198-1	.48407-1	.13559+0	.73608-1	.62330-1	.17427+0
1.75	.67140-1	.56902-1	.15864+0	.86434-1	.73302-1	.20392+0
2.0	.77198-1	.65519-1	.18181+0	.99421-1	.84441-1	.23375+0

94

Table 17

ATM SOLAR PANEL ARRAY JOINT DAMPING —
HIGH TEMPERATURE (150°F)

Norm.	MODE 1			MODE 2		
Factor	Loose Fit	Normal Fit	Tight Fit	Loose Fit	Normal Fit	Tight Fit
0.25	.12588-1*	.26904-1	.31860-1	.23442-1	.50292-1	.59616-1
0.50	.25572-1	.54334-1	.64247-1	.47148-1	.10094+0	.11958+0
0.75	.38950-1	.82291-1	.97160-1	.7117-1	.15193+0	.17990+0
1.0	.5274-1	.11078+0	.13060+0	.95351-1	.20323+0	.24058+0
1.25	.66893-1	.13979+0	.16457+0	.11984+0	.25498+0	.30160+0
1.50	.81457-1	.16932+0	.19906+0	.14461+0	.30703+0	.36297+0
1.75	.96416-1	.19939+0	.23408+0	.16963+0	.35943+0	.42470+0
2.0	.11177+0	.22998+0	.26963+0	.19492+0	.41212+0	.48678+0

Norm.	MODE 3			MODE 4		
Factor	Loose Fit	Normal Fit	Tight Fit	Loose Fit	Normal Fit	Tight Fit
0.25	.78296-1	.16264+0	.19116+0	.10710+0	.22247+0	.26215+0
0.50	.17056+0	.34389+0	.40094+0	.22598+0	.46334+0	.54270+0
0.75	.27678+0	.54376+0	.62934+0	.35966+0	.72259+0	.84162+0
1.0	.39697+0	.76225+0	.87635+0	.50712+0	.10002+1	.11589+1
1.25	.53112+0	.99936+9	.11420+1	.66839+0	.12963+1	.14947+1
1.50	.67923+0	.12551+1	.14263+1	.84345+0	.16107+1	.18488+1
1.75	.84131+0	.15294+1	.17291+1	.10323+1	.19435+1	.22212+1
2.0	.10173+1	.18224+1	.20506+1	.12349+1	.22947+1	.26121+1

*.12588-1 = .12588 x 10^{-1}

95

Table 17 (Continued)

Norm.	MODE 5			MODE 6		
Factor	Loose Fit	Normal Fit	Tight Fit	Loose Fit	Normal Fit	Tight Fit
0.25	.14049+0	.29805+0	.35228+0	.29399-1	.62949-1	.74582-1
0.50	.29083+0	.60921+0	.71767+0	.59432-1	.12674+0	.15001+0
0.75	.45100+0	.93349+0	.10962+1	.90099-1	.19138+0	.22628+0
1.0	.62101+0	.12709+1	.14878+1	.12140+0	.25687+0	.30340+0
1.25	.80086+0	.16214+1	.18926+1	.15334+0	.32320+0	.38136+0
1.50	.99054+0	.19850+1	.23104+1	.18590+0	.39038+0	.46017+0
1.75	.11901+1	.23618+1	.27414+1	.21911+0	.45840+0	.53983+0
2.0	.13994+1	.27517+1	.31855+1	.25294+0	.52726+0	.62033+0

Norm.	MODE 7			MODE 8		
Factor	Loose Fit	Normal Fit	Tight Fit	Loose Fit	Normal Fit	Tight Fit
0.25	.29702-2	.63793-2	.75642-2	.38138-2	.81908-2	.97119-2
0.50	.59562-2	.12780-1	.15150-1	.76494-2	.16411-1	.19453-1
0.75	.89582-2	.19202-1	.22756-1	.11507-1	.24659-1	.29223-1
1.0	.11976-1	.25645-1	.30384-1	.15386-1	.32937-1	.39022-1
1.25	.15010-1	.32109-1	.38033-1	.19287-1	.41244-1	.48850-1
1.50	.18060-1	.38594-1	.45704-1	.23209-1	.49580-1	.58707-1
1.75	.21125-1	.45101-1	.53395-1	.27154-1	.57945-1	.68593-1
2.0	.24207-1	.51629-1	.61108-1	.31120-1	.66339-1	.78508-1

ILLUSTRATIONS

LMSC/HREC D149346

Fig. 1a - AAP Cluster Configuration

OWS Solar Panels 8, 9, 10

ATM Canister

ATM Solar Panels 3 and 4

ATM Solar Panels 1 and 2

OWS

LM/ATM

MDA

C/SM
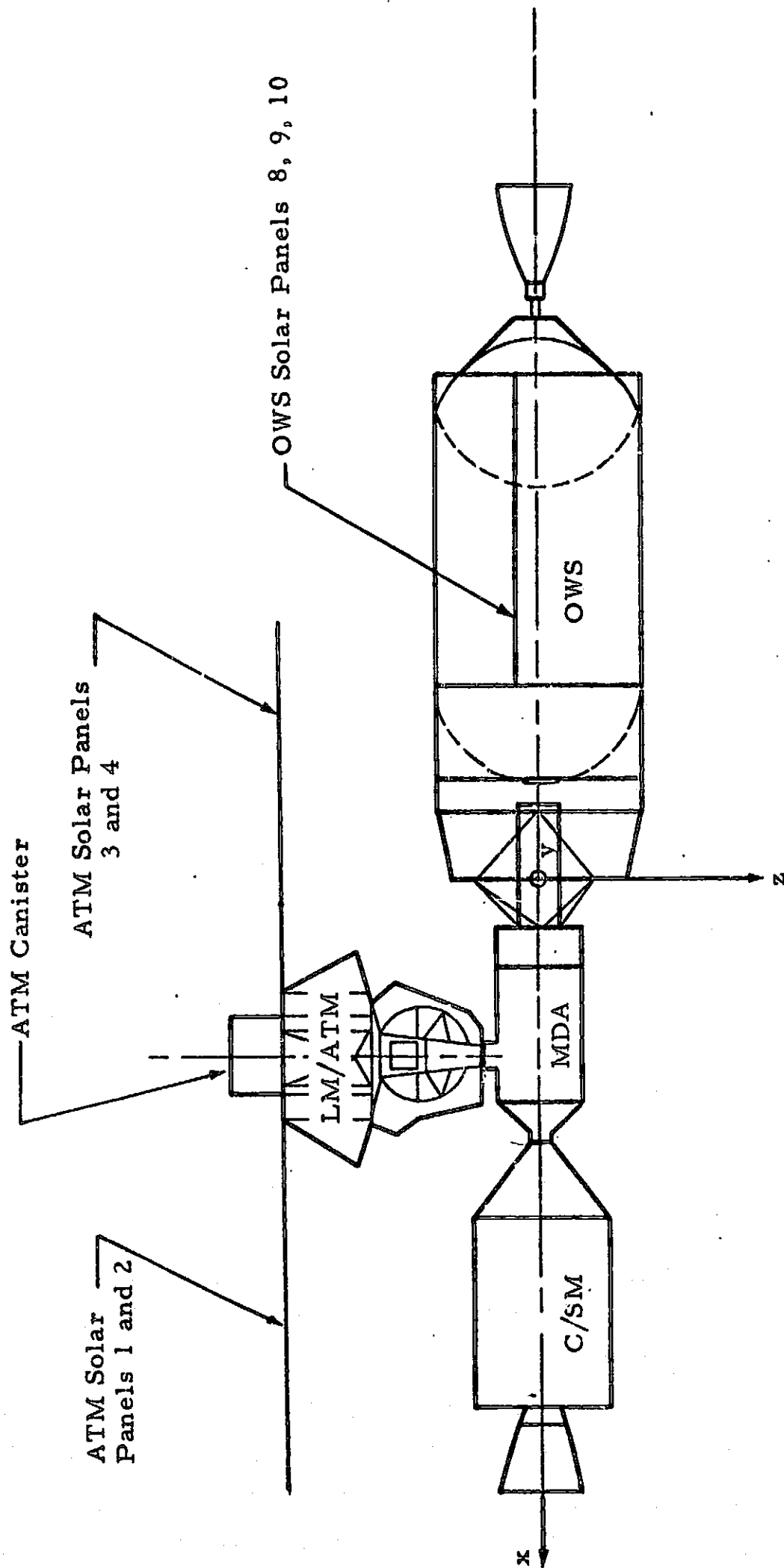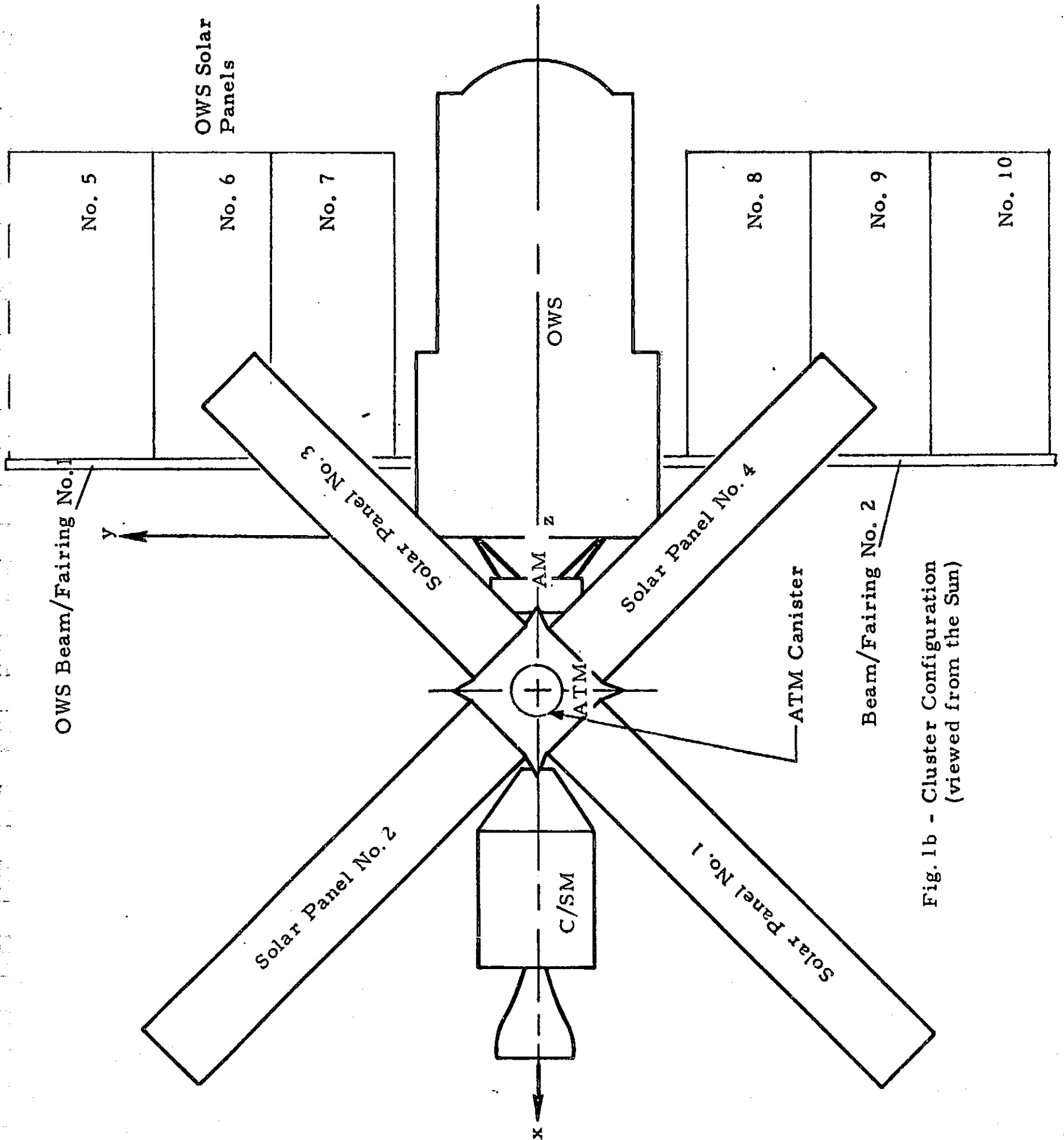
Fig. 1b - Cluster Configuration (viewed from the Sun)
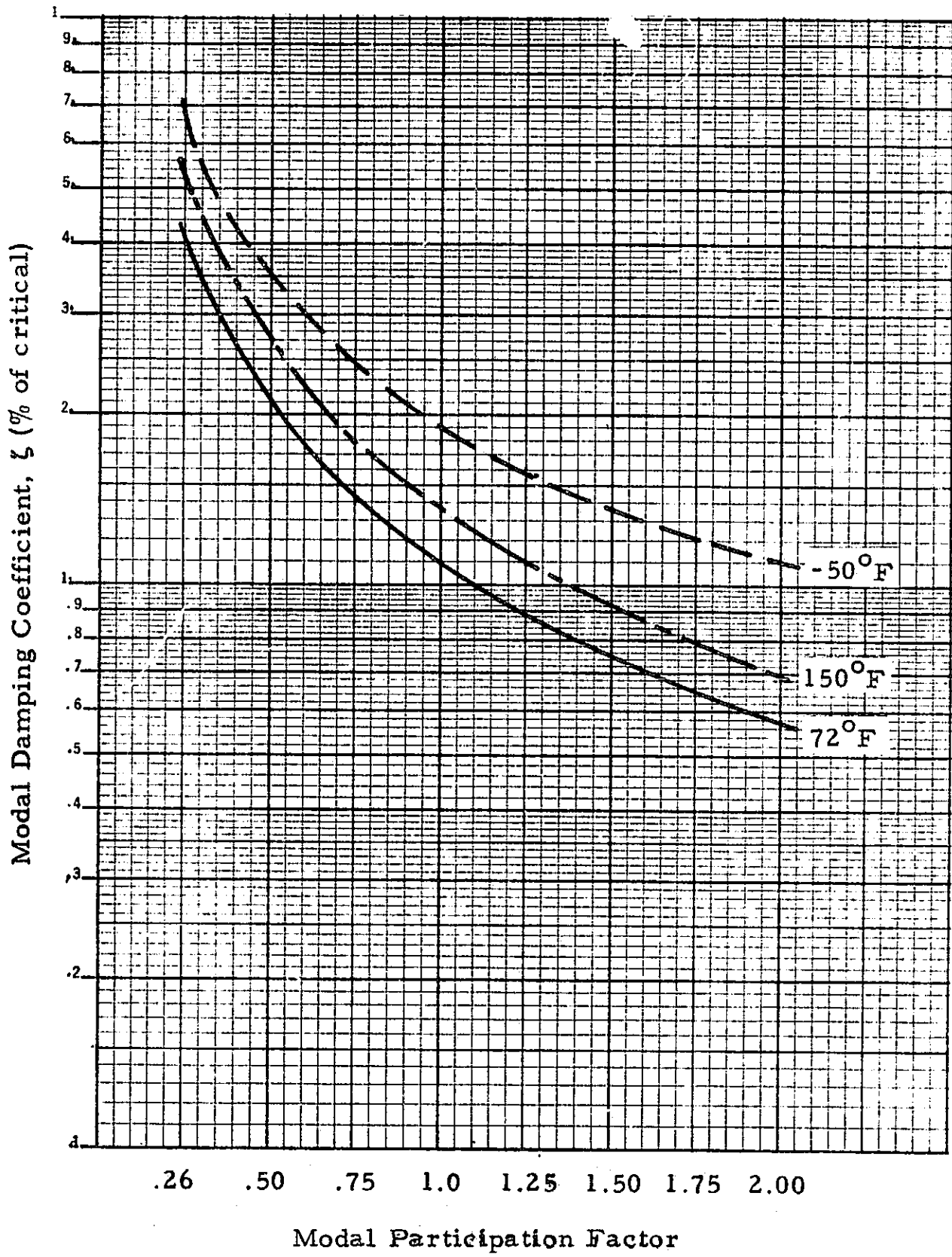
Fig. 2 - Modal Damping Coefficient, Mode 1
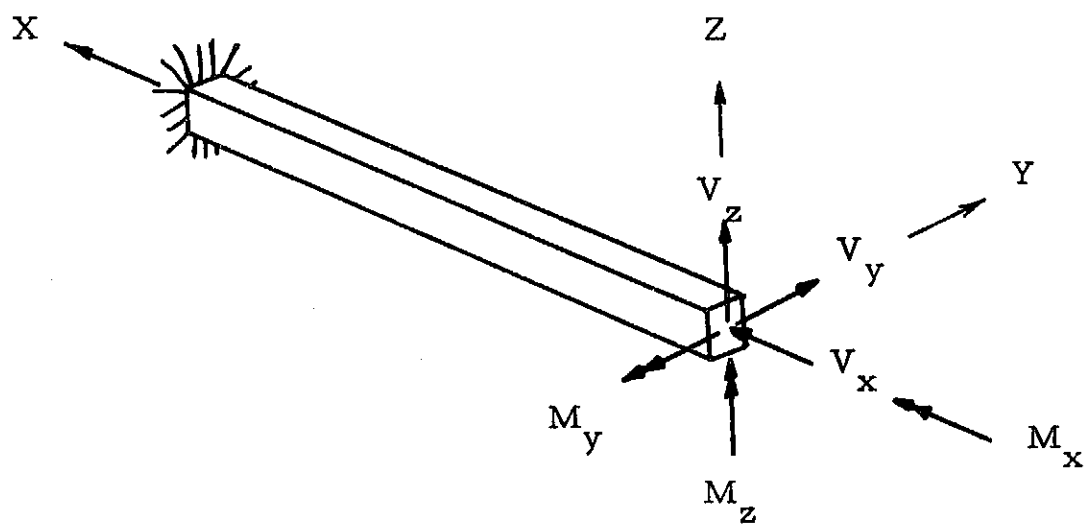
Figure 3 - Orientation of Member and Loads
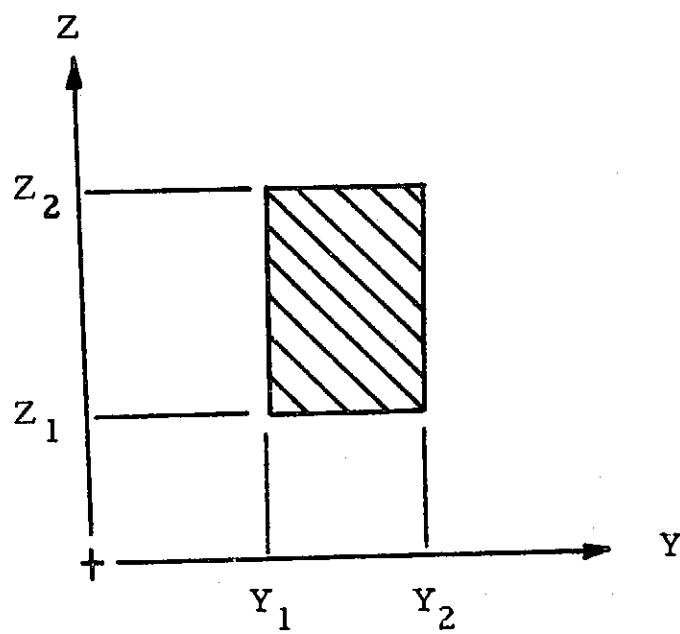
Figure 4 - Cross-Sectional Limits

102

N_x

1/4-in. bolts
torqued to
70 in-lb
(ABMA-STD-18)

1/4 in. x 2.0 in.

Nx

RTV 90 Sealant

Test Joint
Interface

Test Section
Tension Bolted Specimen
Ref. Dwg R72102SH1. (LMSC)

Nx

1/4-in. bolts torqued
to 40 in-lb.

0.2 in. x 3.0 in.

RTV 90 Sealant

Nx

4-deg Ramp

Test Joint
Interface

Test Section
Shear-Bolted Specimen
Ref. Dwg. R72102SH2. (LMSC)
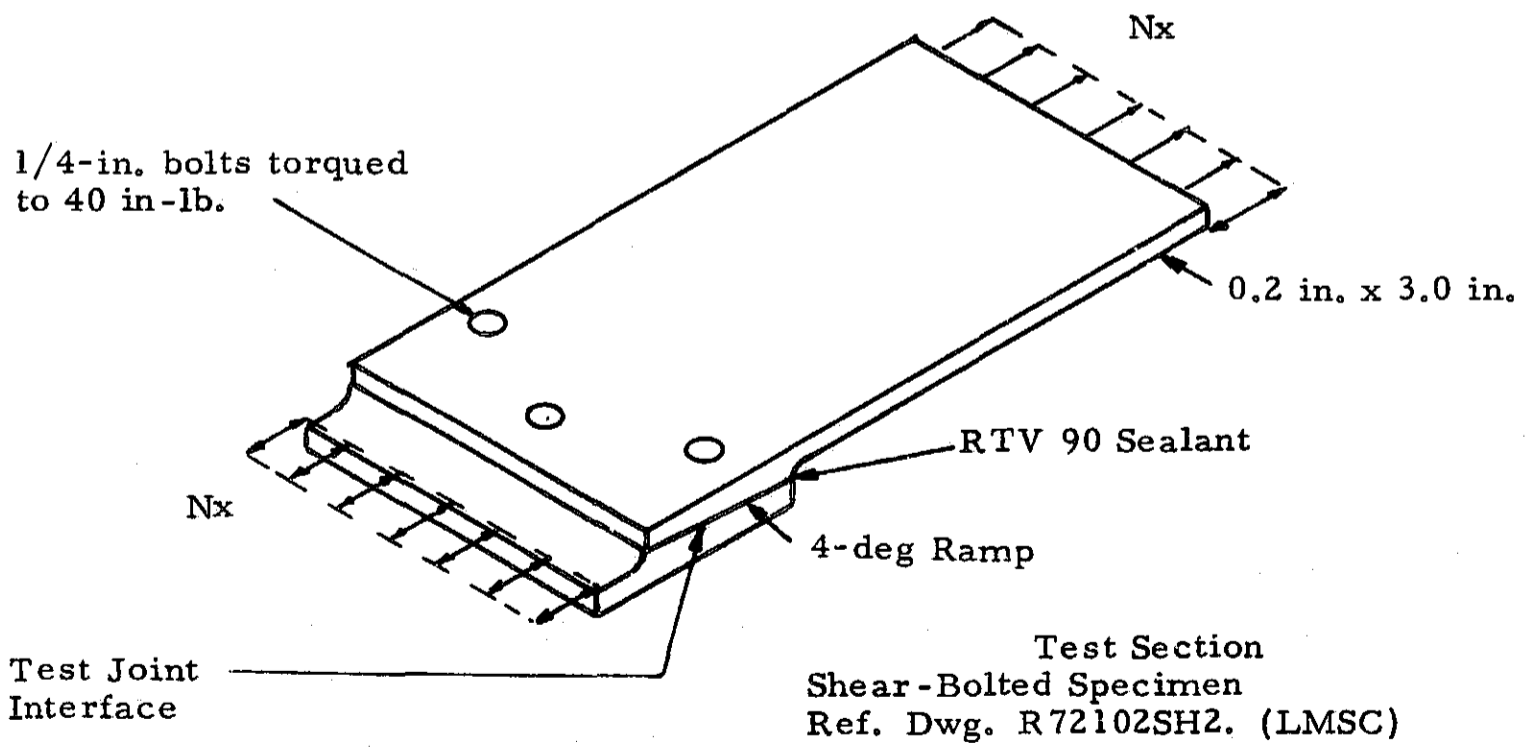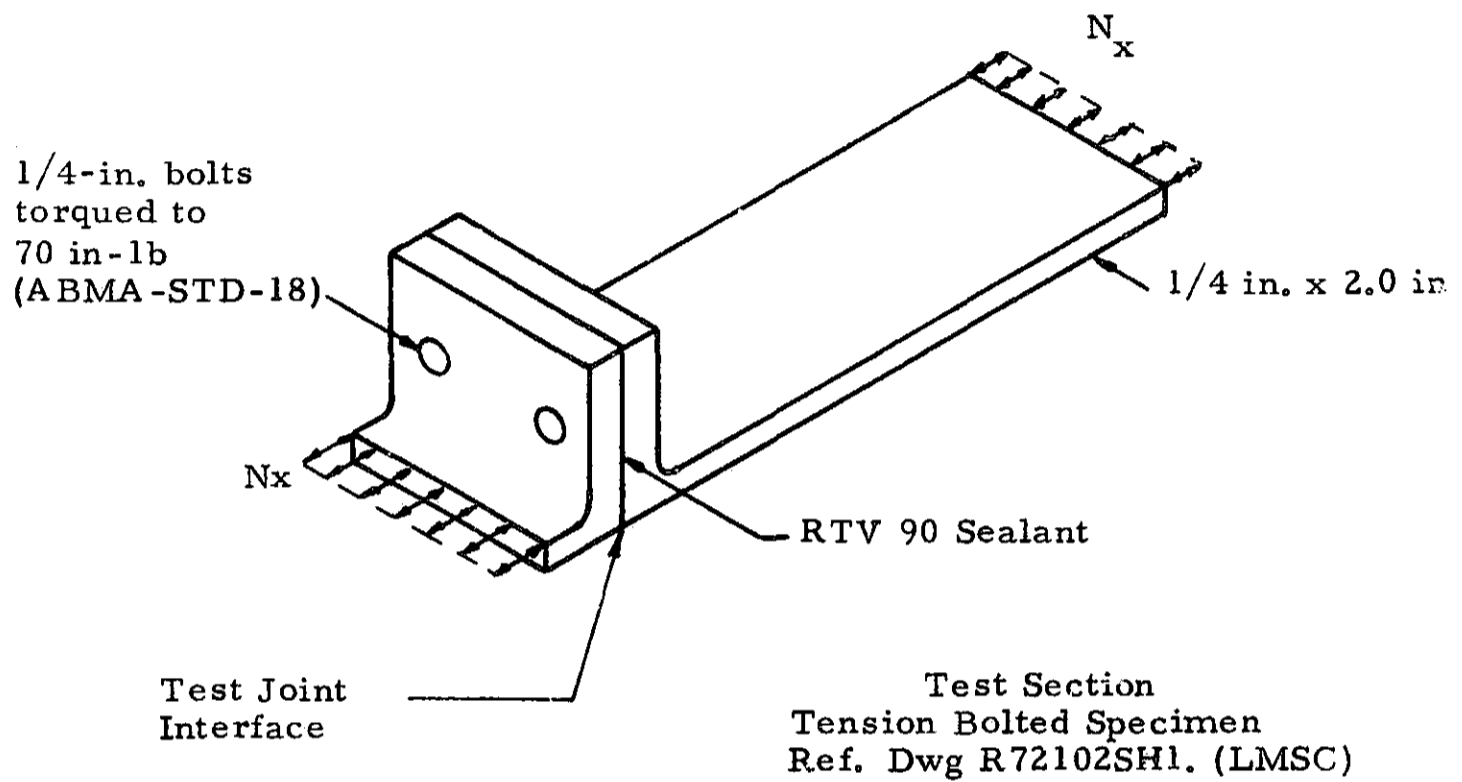
Fig. 5 - Test Specimens
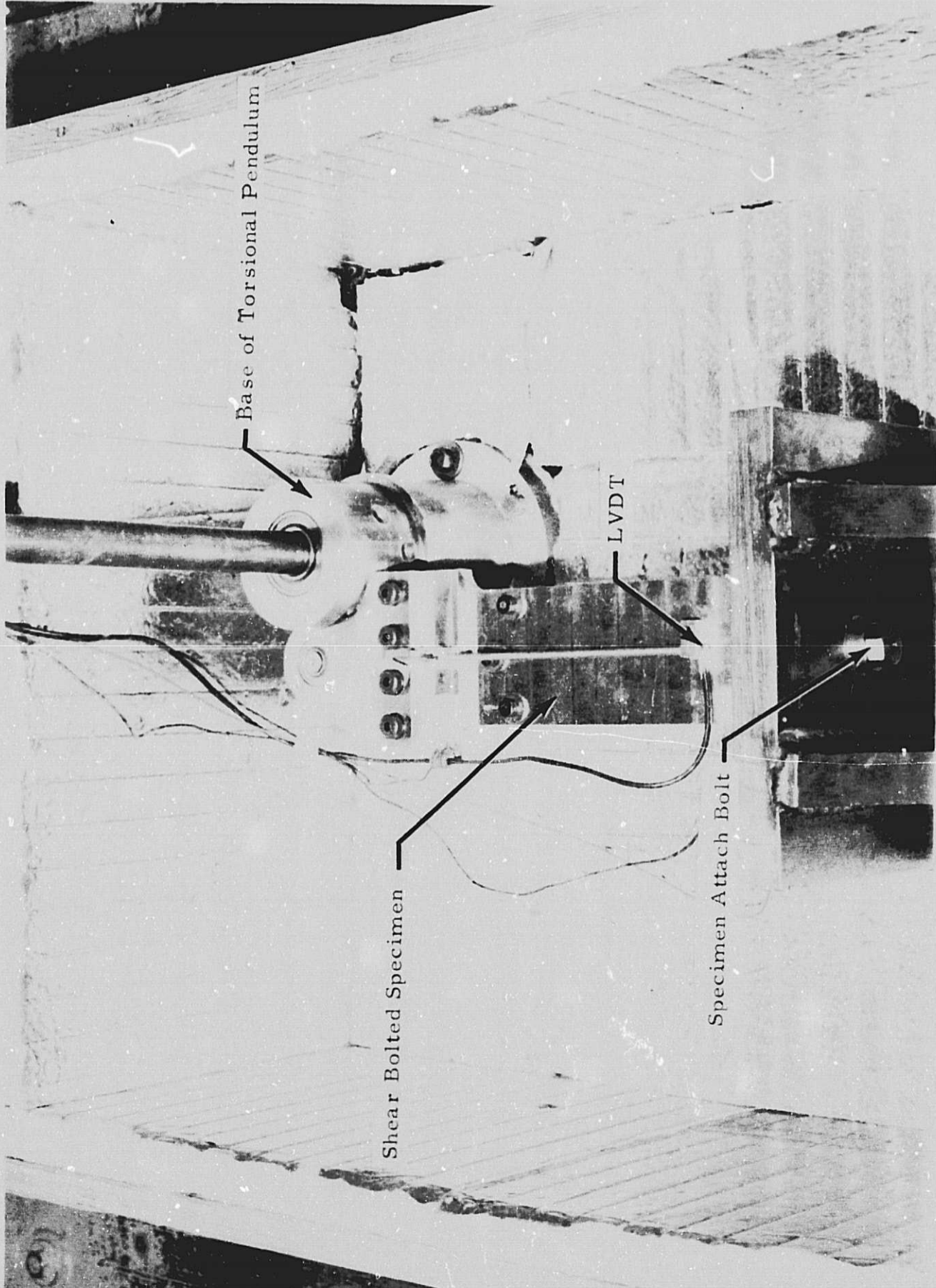
Fig. 6a - Specimen Mounting
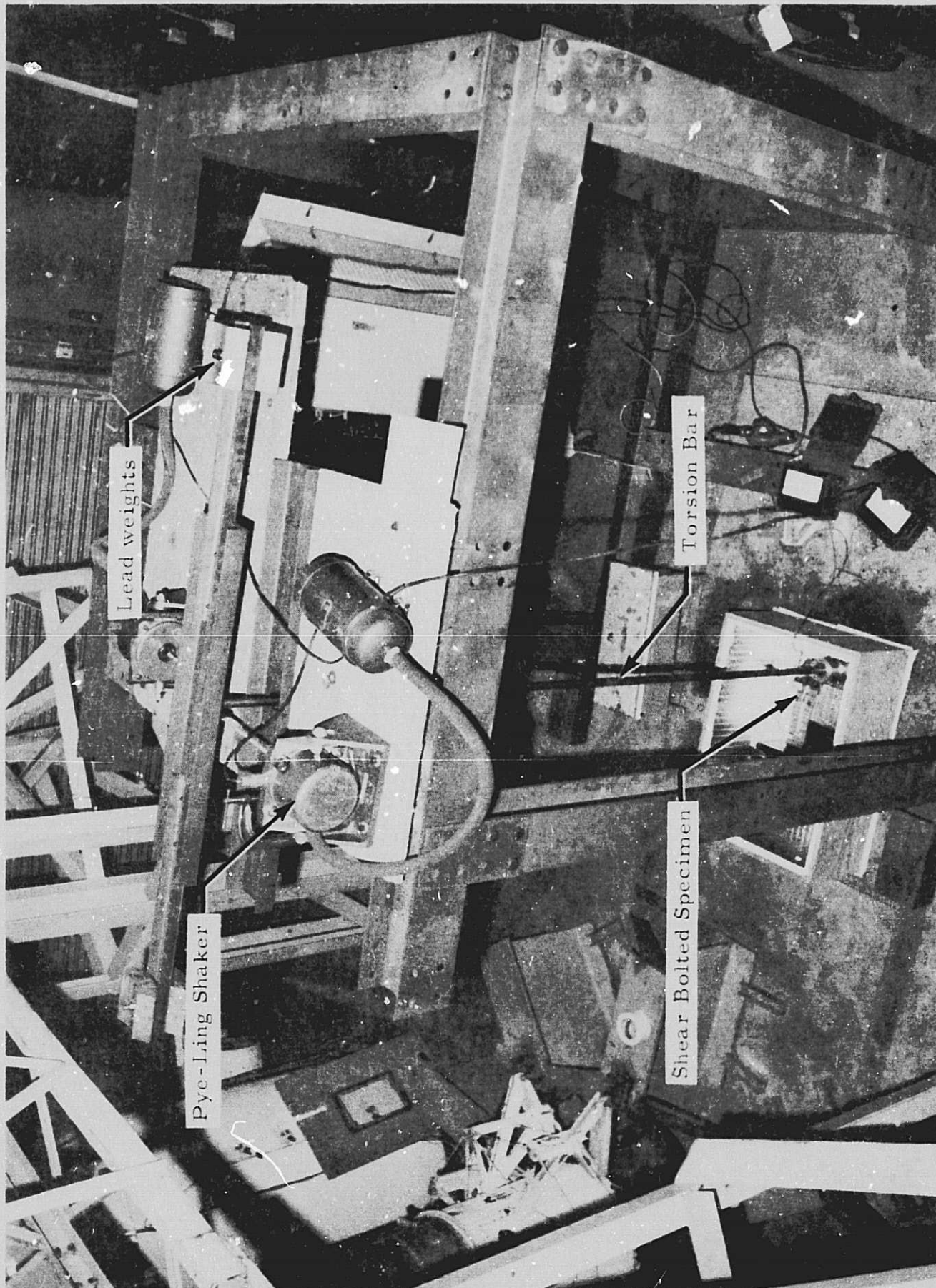
Fig. 6b - Torsional Pendulum
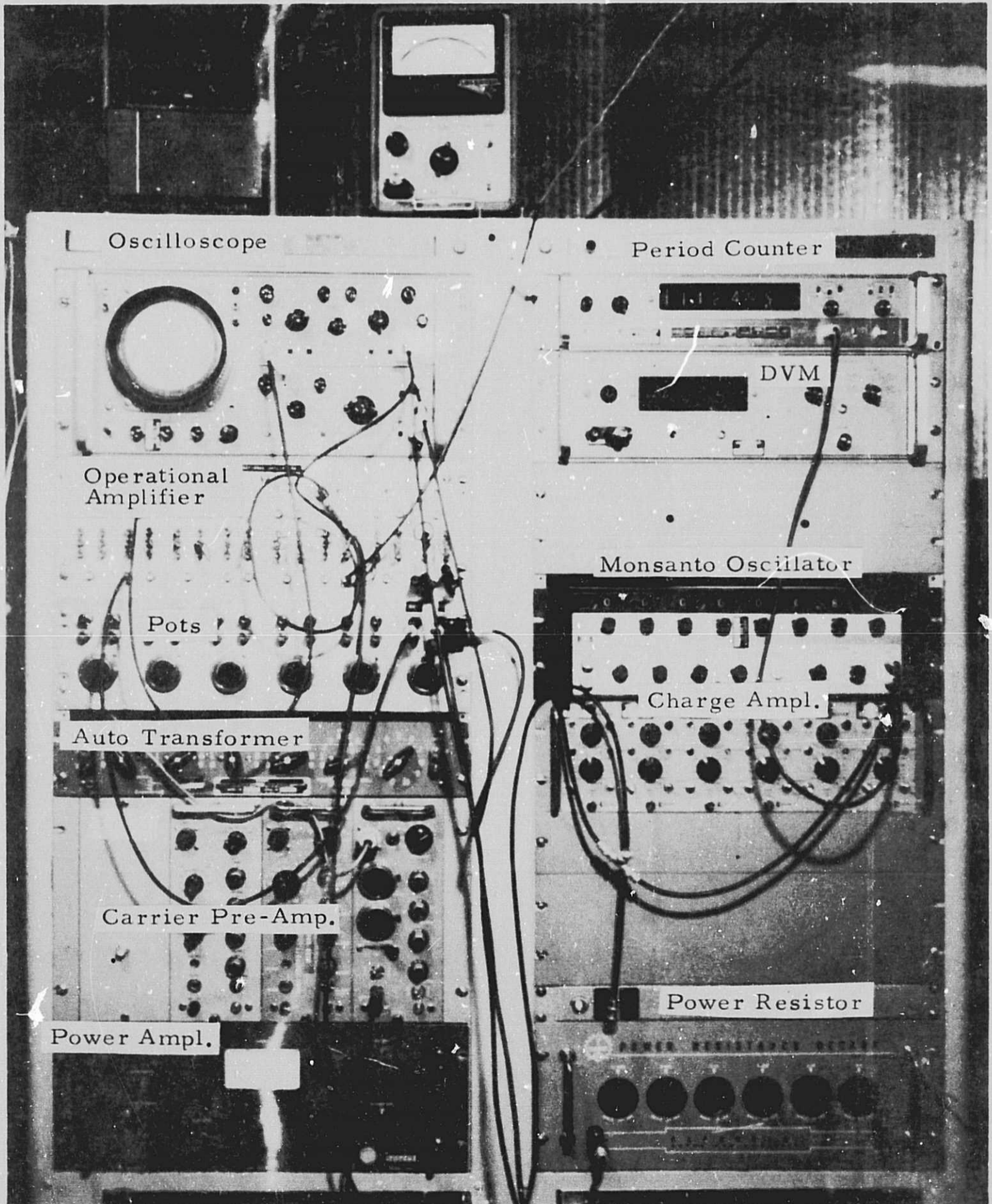
Fig. 6c - Instrument Rack
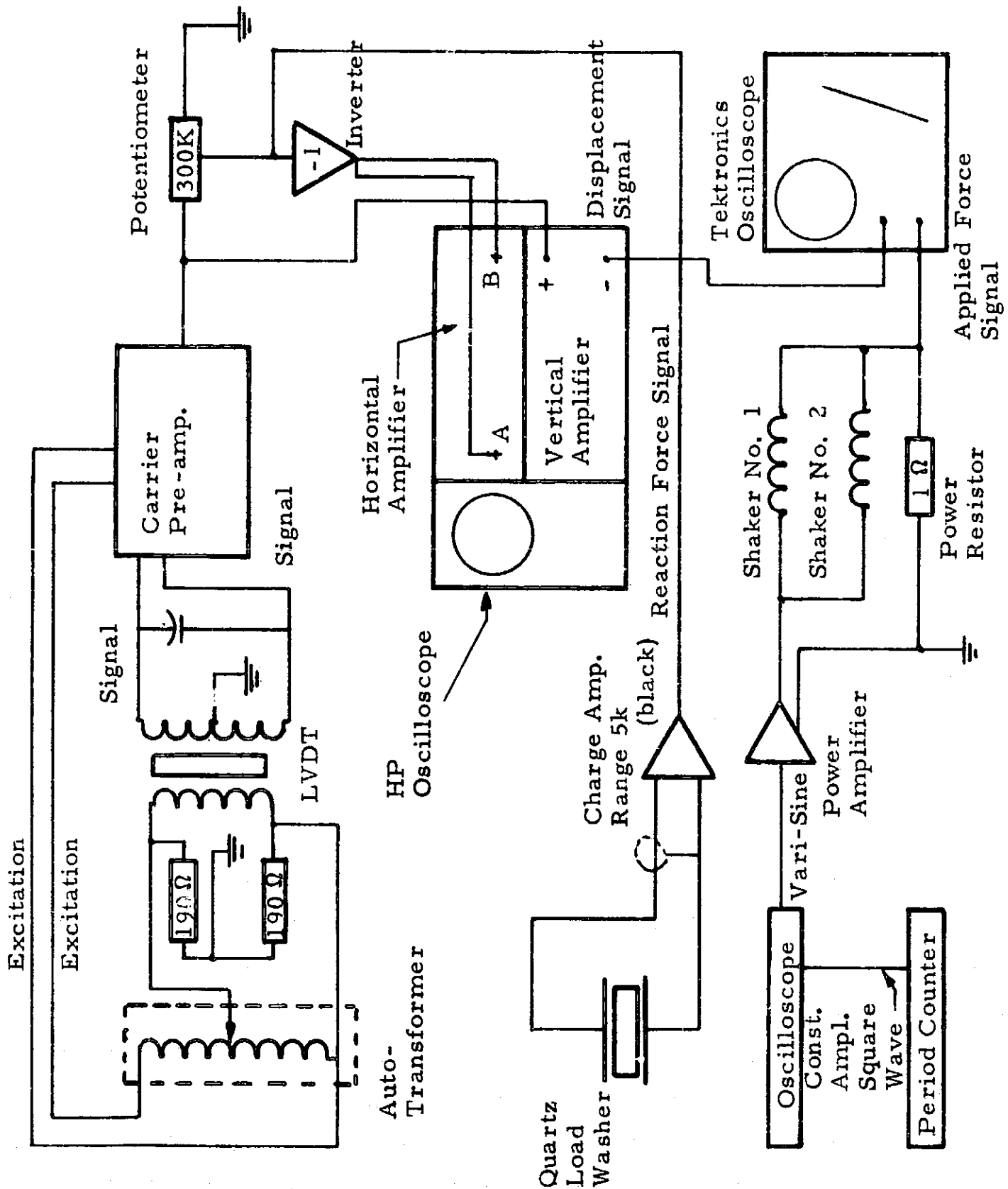
Fig. 7 - Instrumentation for Torsional Pendulum
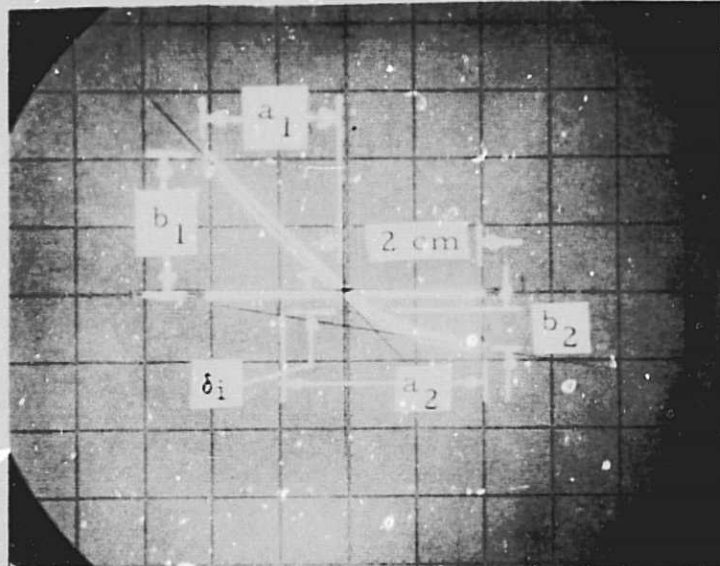
Test No. 12

Hysteriesis Loop

Horizontal (Force) Scale:
127.5 lb/cm

Vertical (Deflection) Scale:
0.001 in./cm
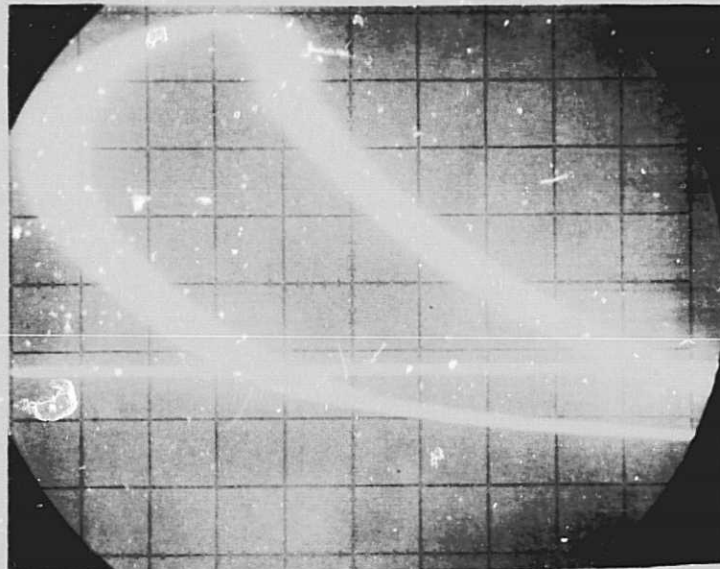
Positive Half of
Hysteresis Loop Expanded

Horizontal Scale: 5.1 lb/cm

Vertical Scale: 0.0004 in./cm

Enclosed Area: 21.52 cm^2 =
21.9 in.-lb/in.-width
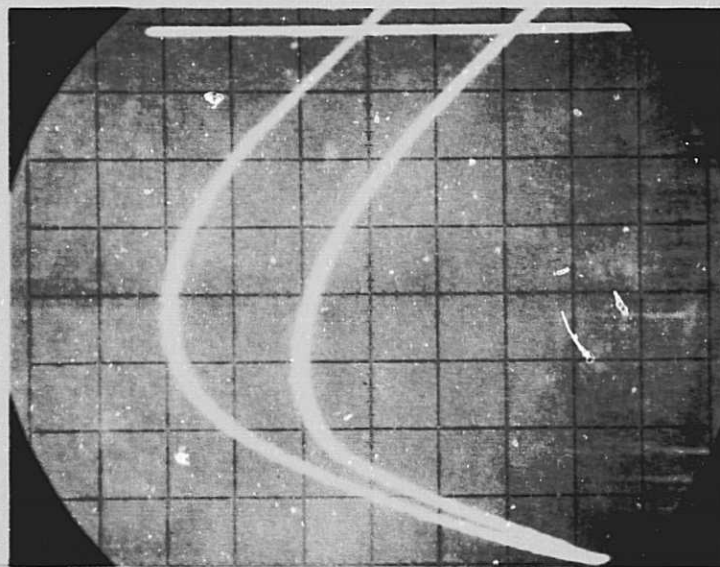
Negative Half of
Hysteresis Loop Expanded

Horizontal Scale: 12.75 lb/cm

Vertical Scale: 0.0001 in./cm

Enclosed Area: 13.52 cm^2 =
8.62 in.-lb/in.-width

Fig. 8 - Test Photographs — Tension-Bolted Specimen
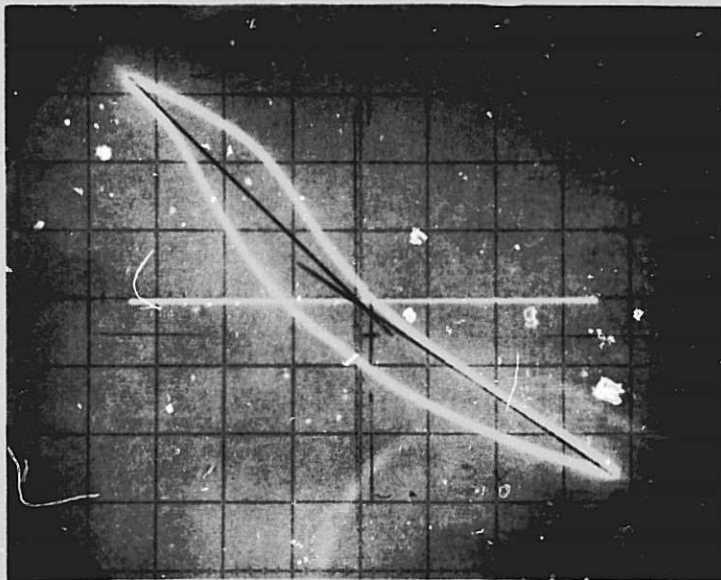
Test No. 32

Hysteresis Loop

Horizontal (Force) Scale:
127.5 lb/cm

Vertical (Deflection) Scale:
0.001 in./cm
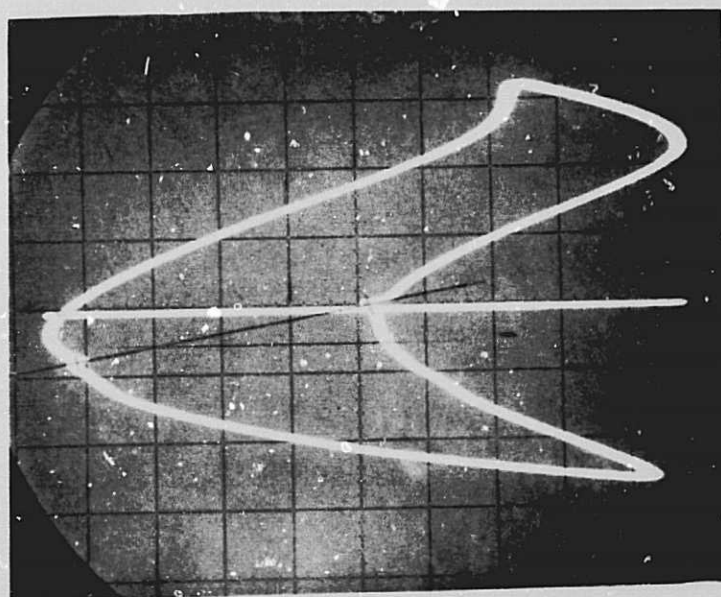
Expanded Hysteresis
Loop

Horizontal Scale: 25.5 lb/cm

Vertical: 0.001 in./cm

Enclosed Area = 22.6 cm^2 =
191.7 in.-lb/in.-width

Fig. 9 - Test Photographs — Shear-Bolted Specimen
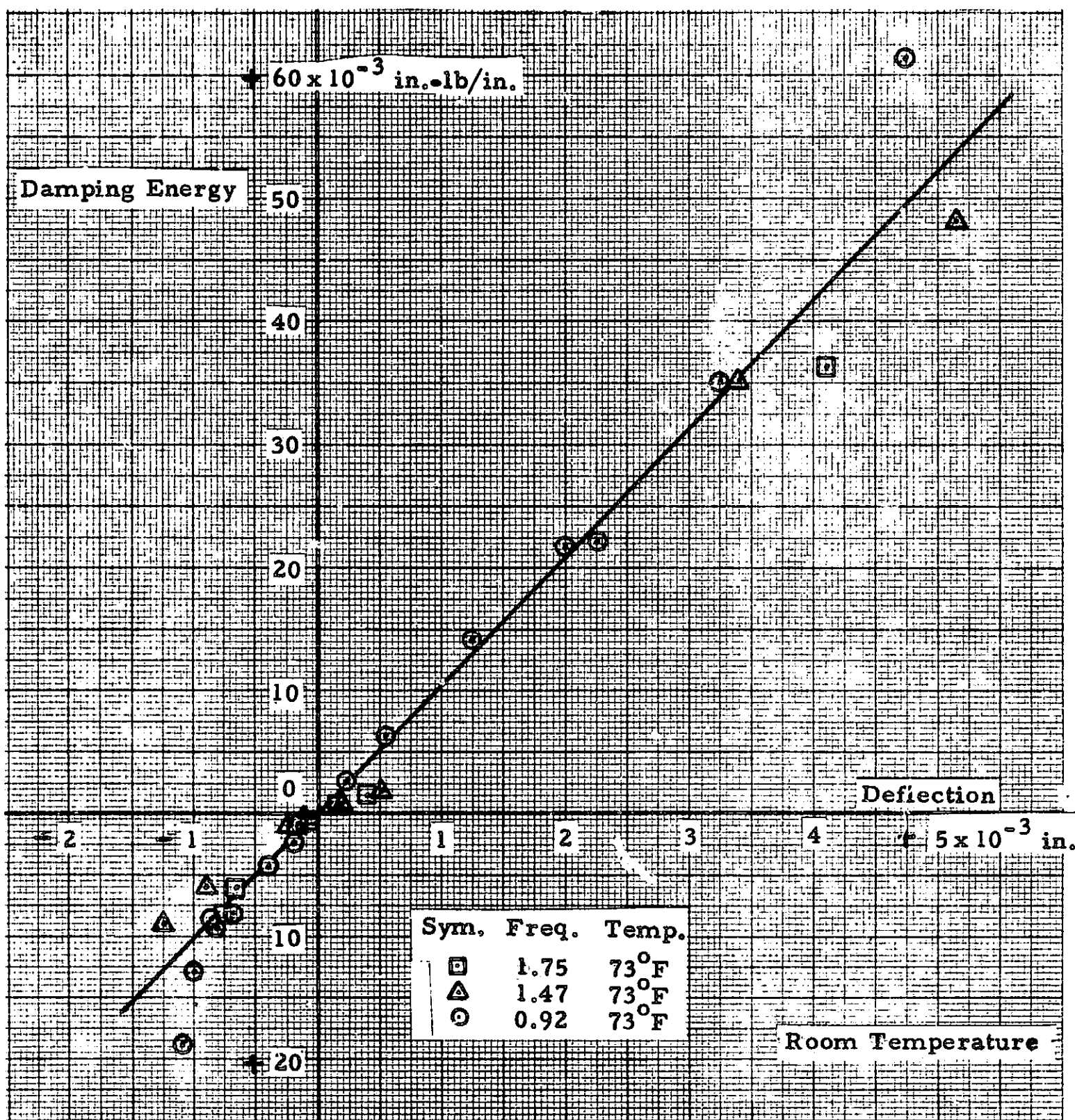
Fig. 10a - Damping Energy vs Deflection for Tension-Bolted Joint
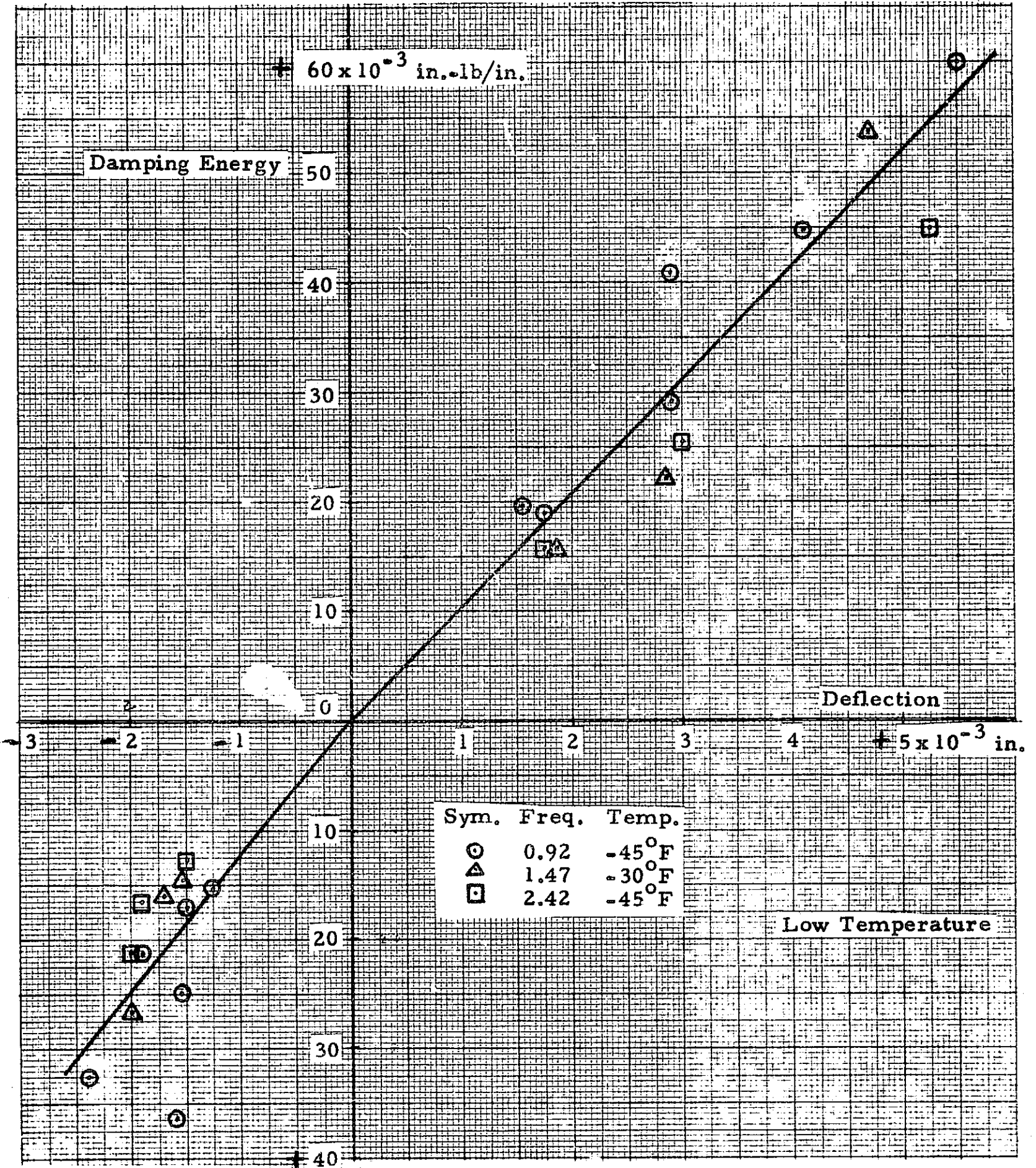
Fig. 10b - Damping Energy vs Deflection for Tension-Bolted Joint
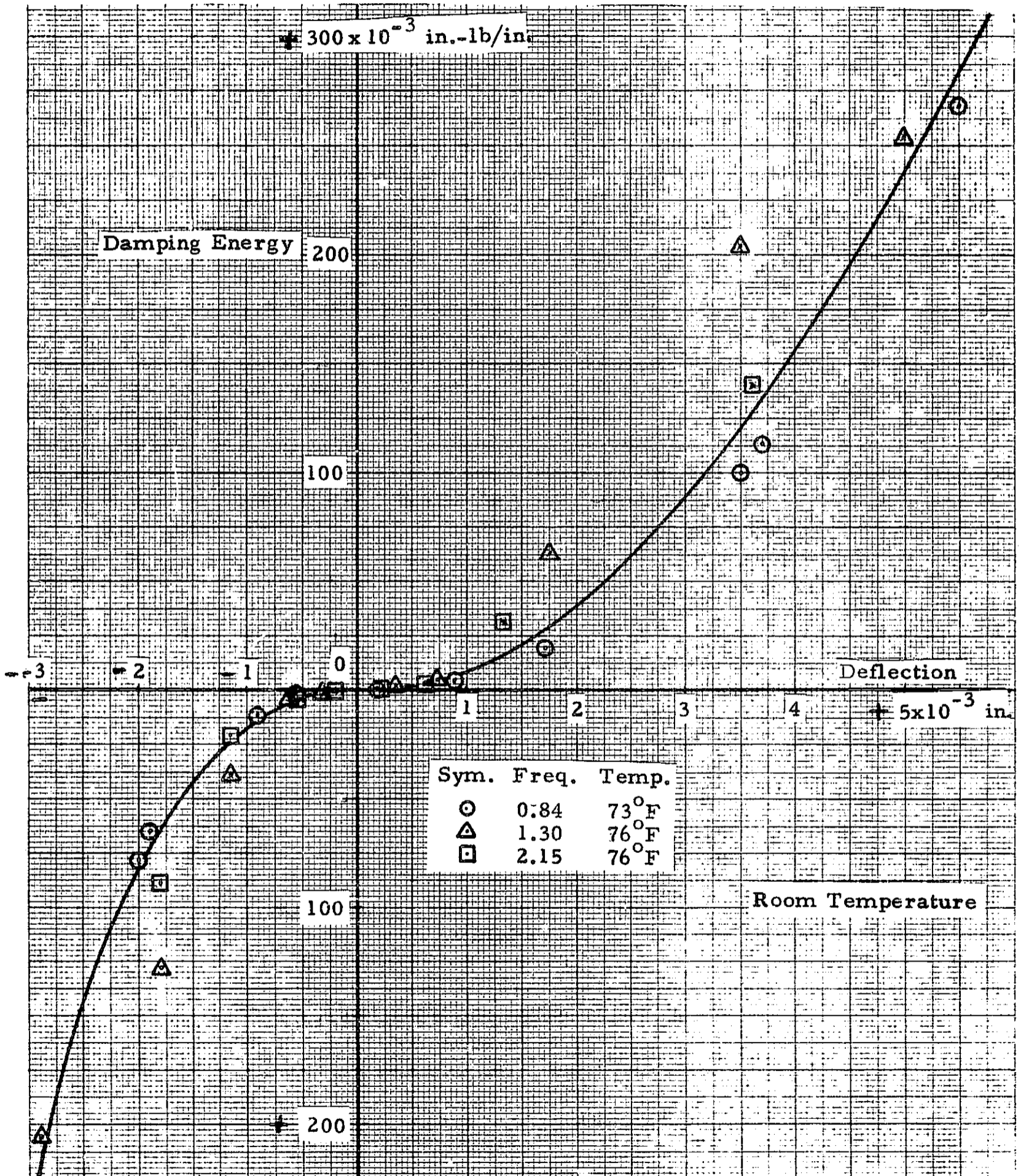
Fig. 11a - Damping Energy vs Deflection for Shear-Bolted Joint
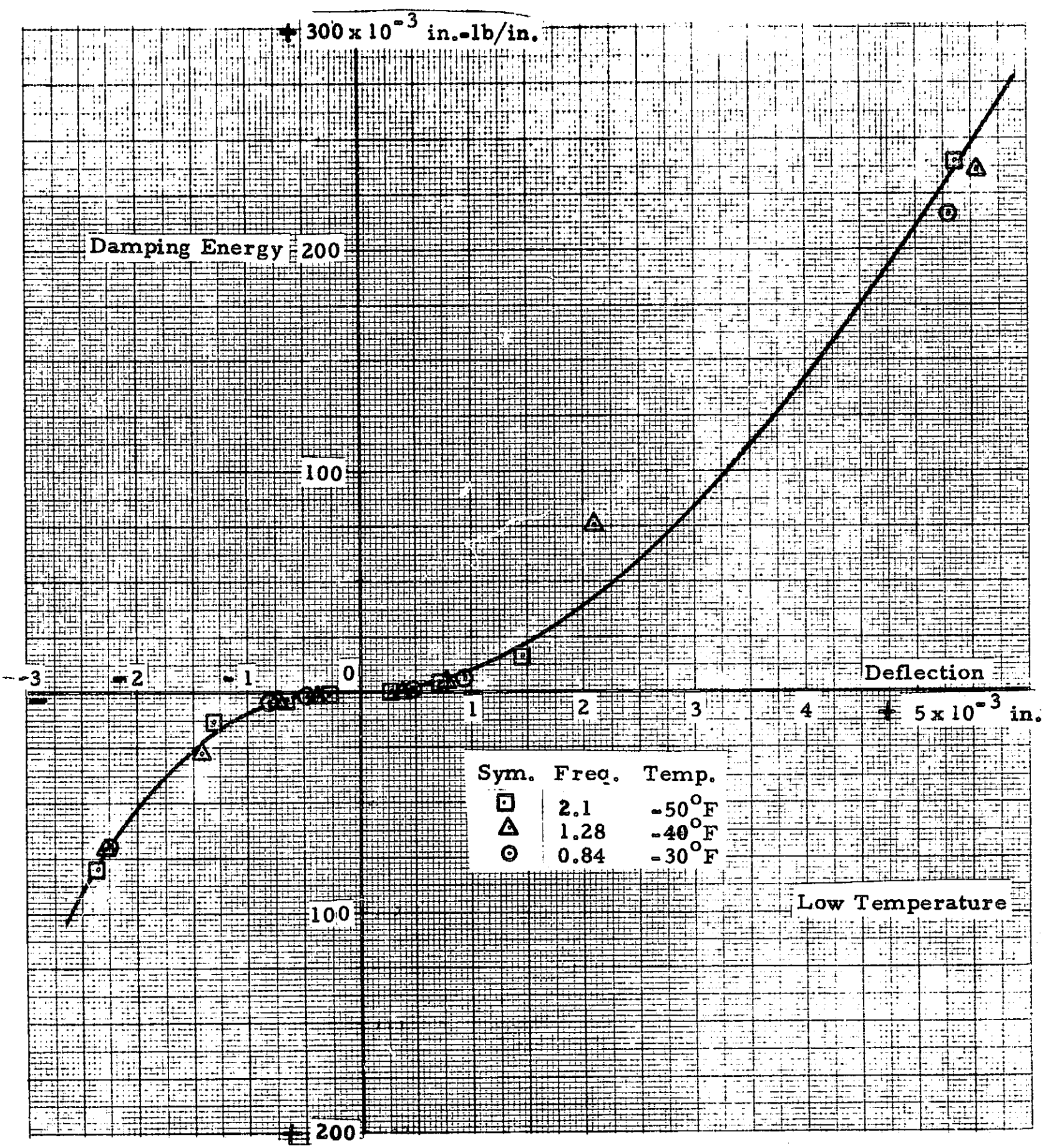
Fig. 11b - Damping Energy vs Deflection for Shear-Bolted Joint
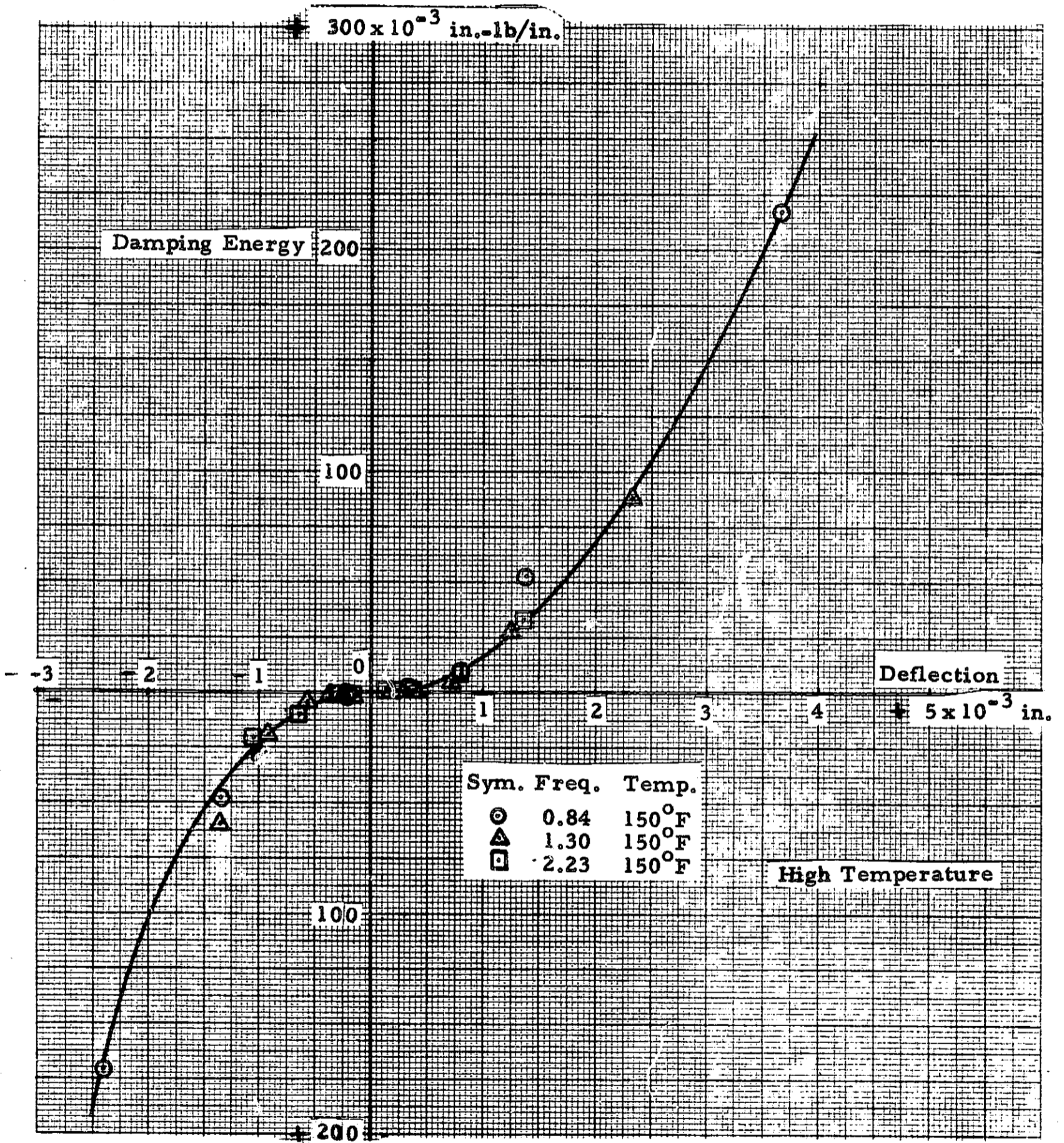
Fig. 11c - Damping Energy vs Deflection for Shear-Bolted Joint
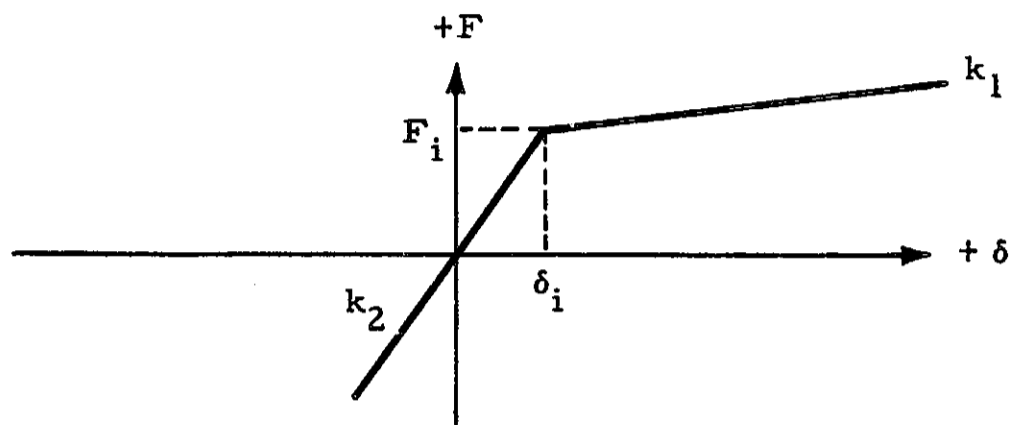
Fig. 12 - Joint Force-Displacement Relation
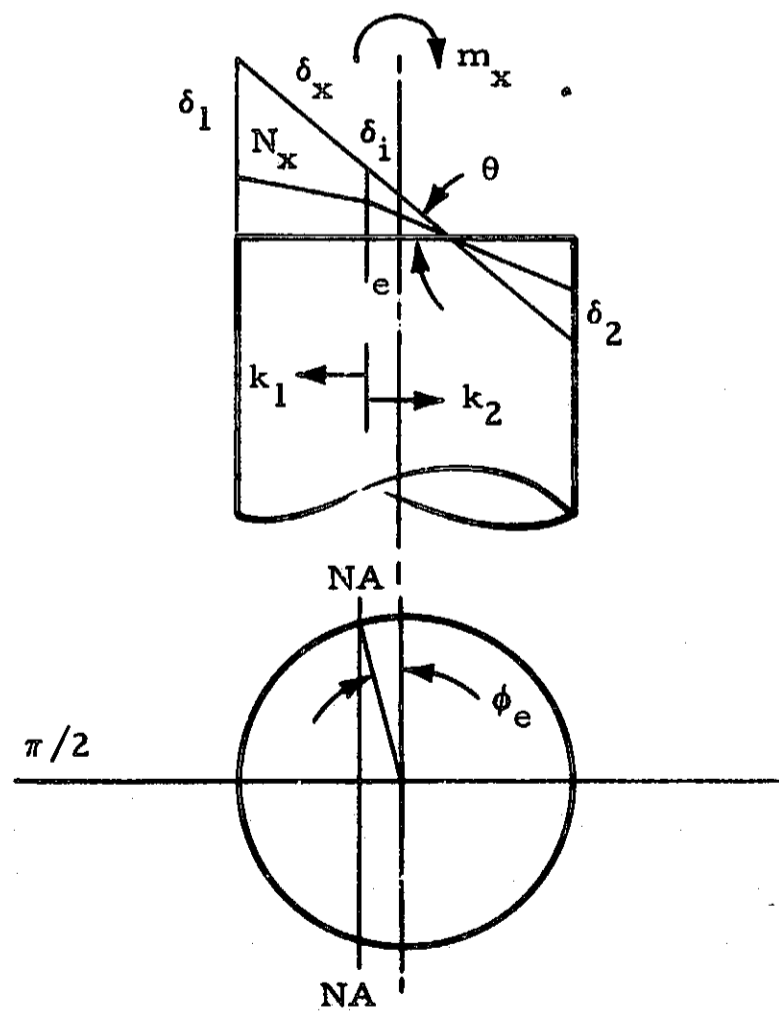
Fig. 13 - Docking Port Load-Deflection Distribution

115
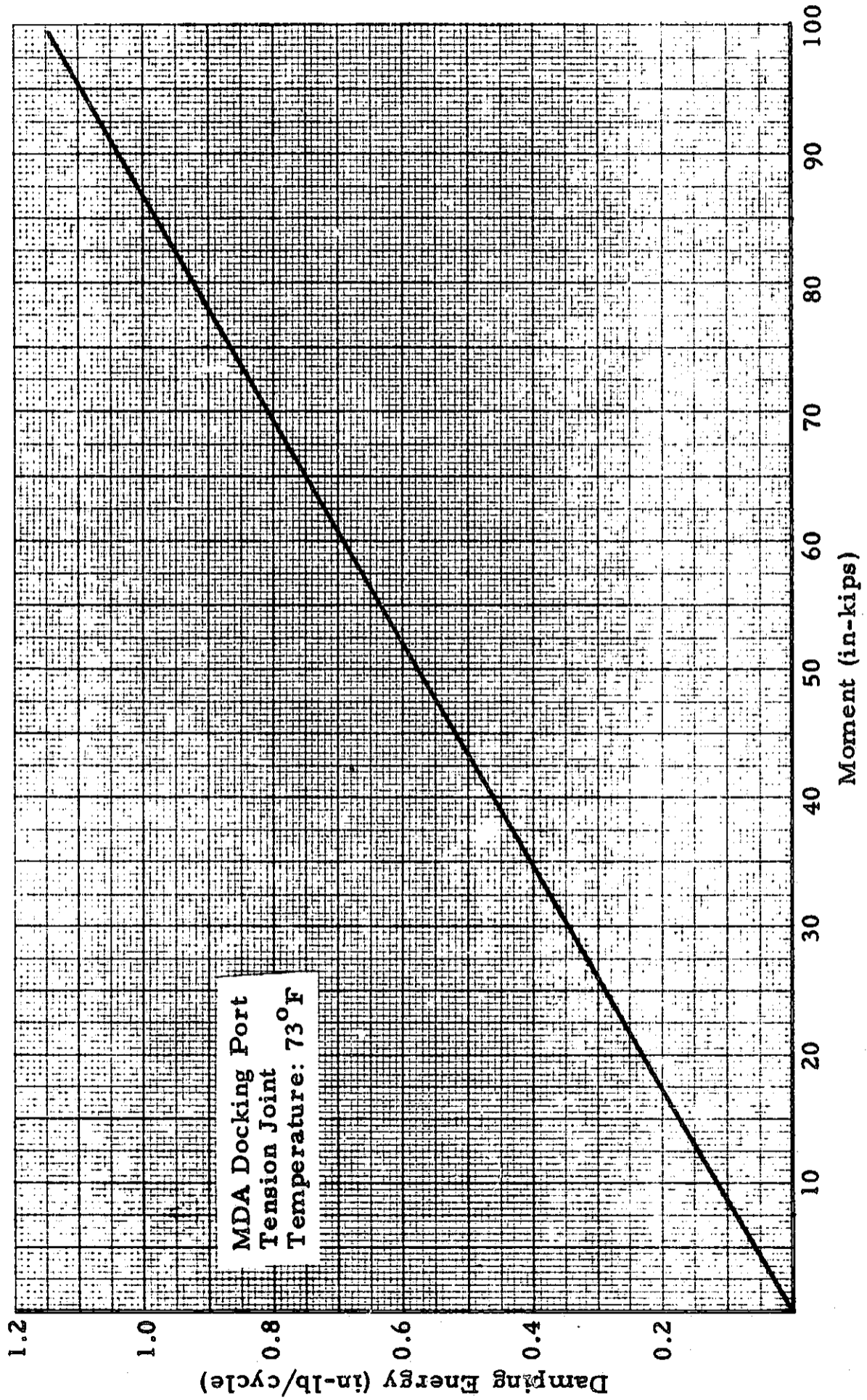
Fig. 14a – Docking Port Damping – Tension Joint, Room Temperature
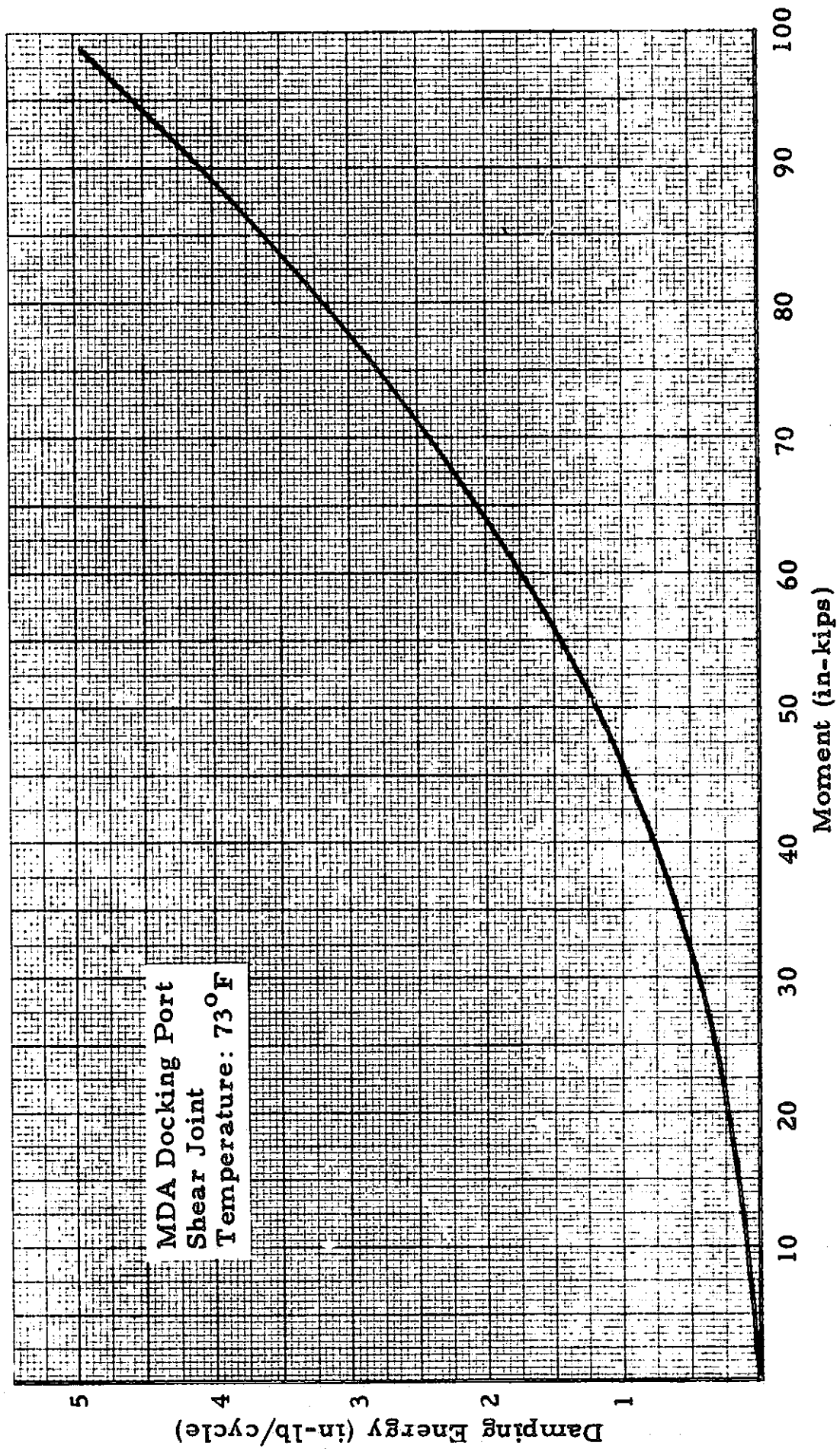
Fig. 14b – Docking Port Damping – Shear Joint, Room Temperature

117
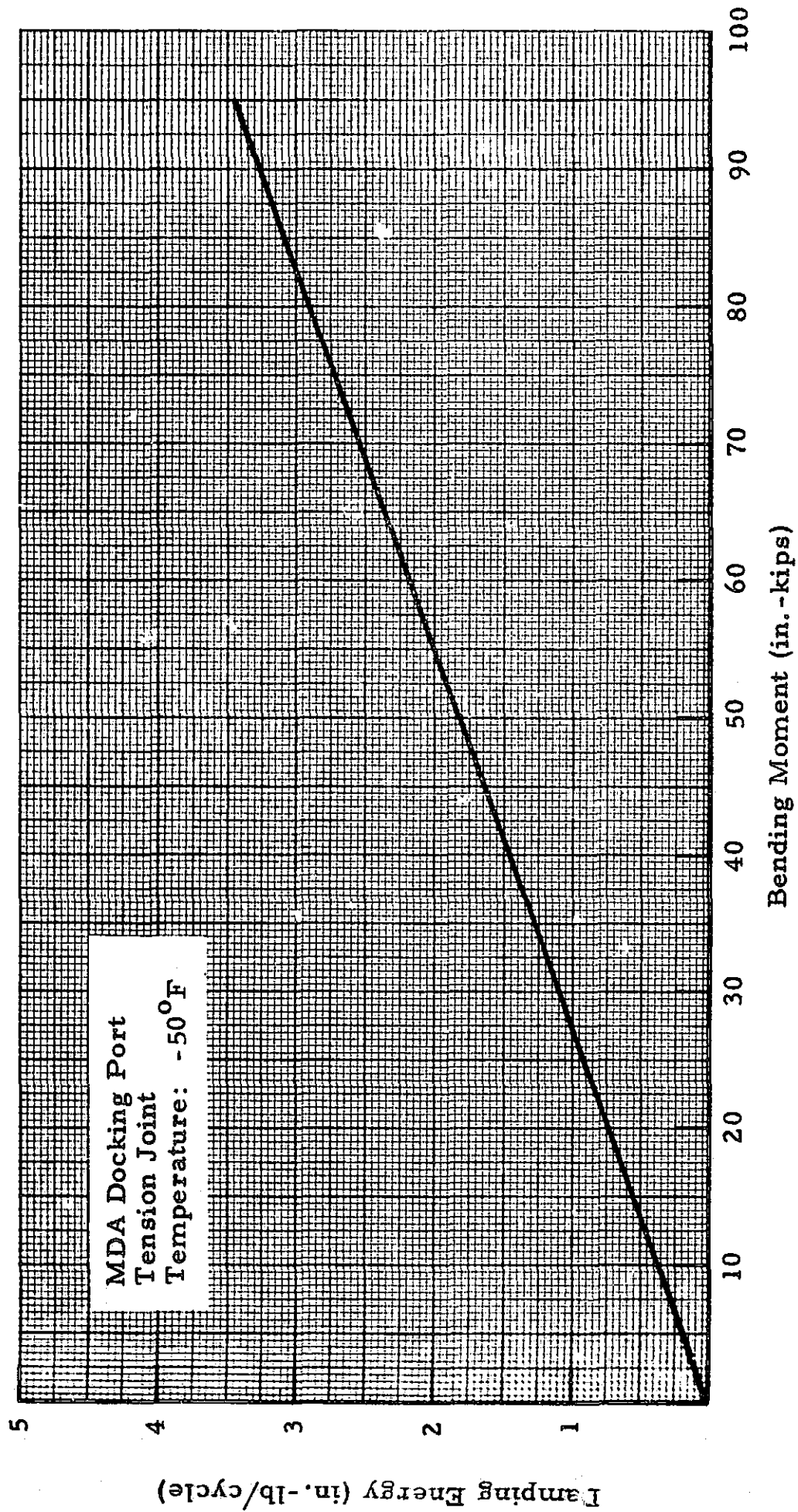
Fig. 15a – Docking Port Damping – Tension Joint, Low Temperature
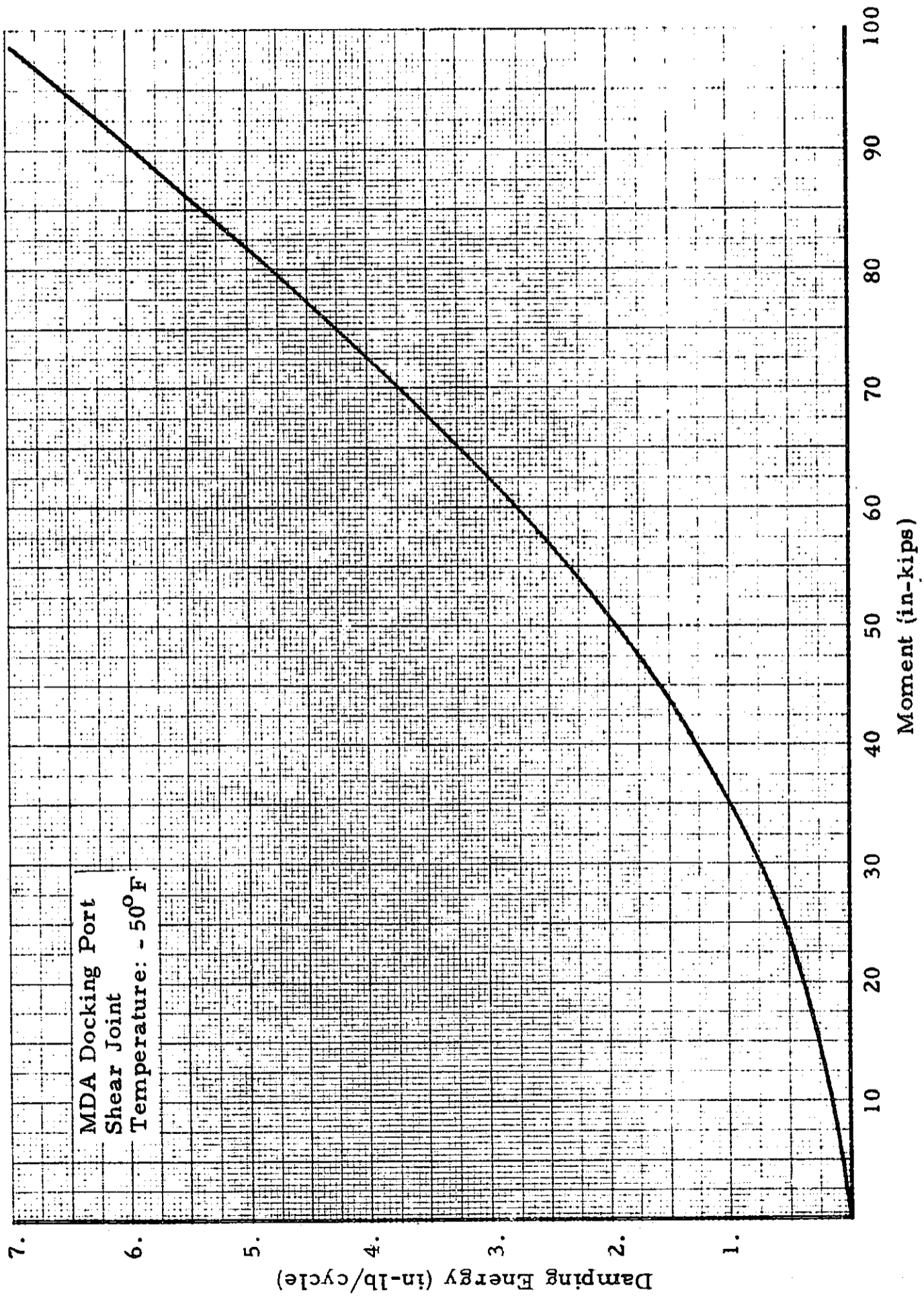
Fig. 15b – Docking Port Damping – Shear Joint, Low Temperature
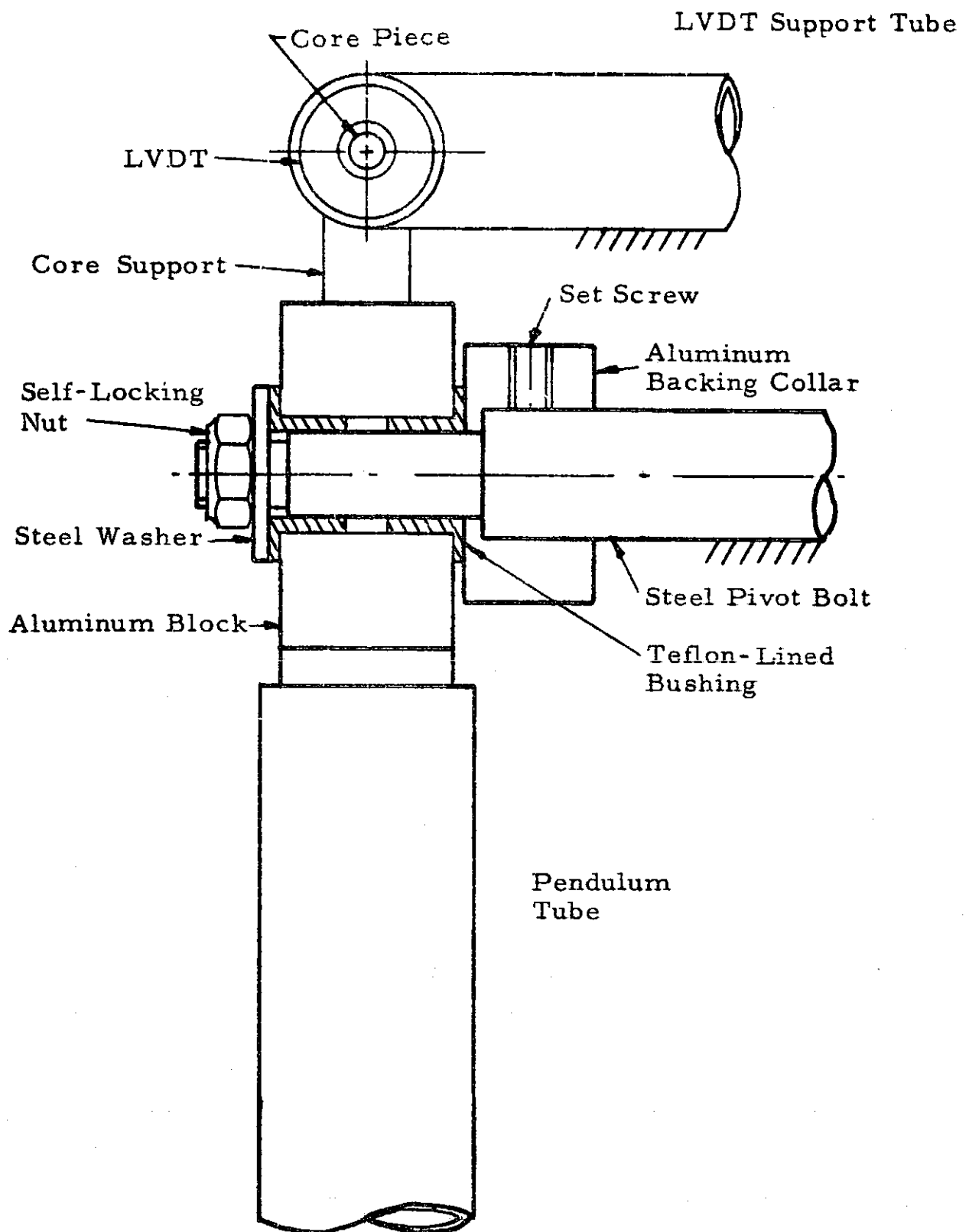
Fig. 16 - Test Specimen — Solar Panel Scissors Joint

Feed Rate: sec/in. 10   20

Frequency: Hz
         0.30   0.33

Decay: in./cycle
     0.475   0.11

Load: lb.
         9.5   98.5

50 50

0.34 0.34

0.09 0.07

143.5 254.5

Test Conditions
Date: 4-22-69 1:00 p.m.
Nut: Normal (finger tight)
Temp: 73° F
Weights: lower position
Starting Amplitude: 3.0 in.

3

2

1

0

-1

-2

-3
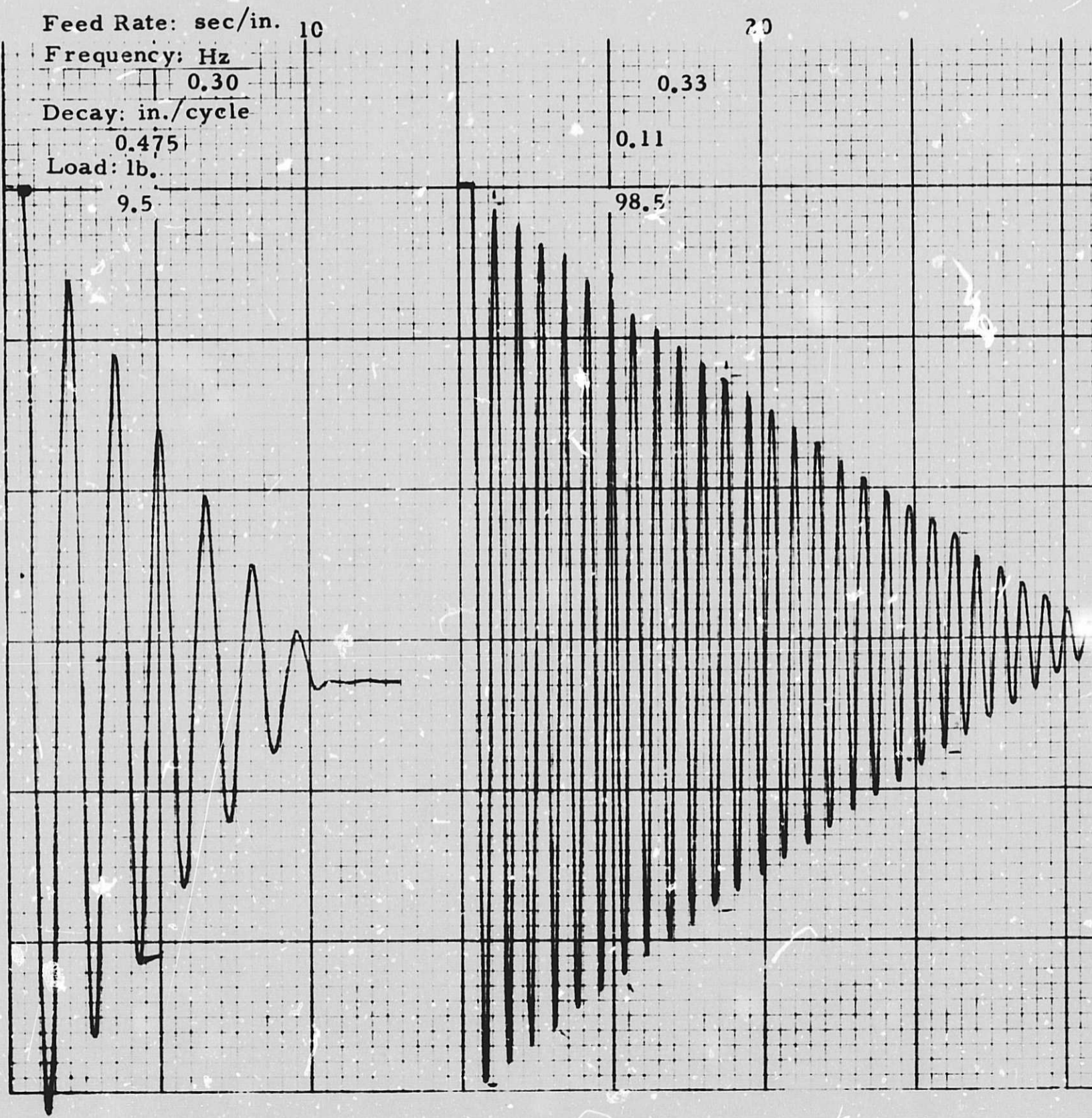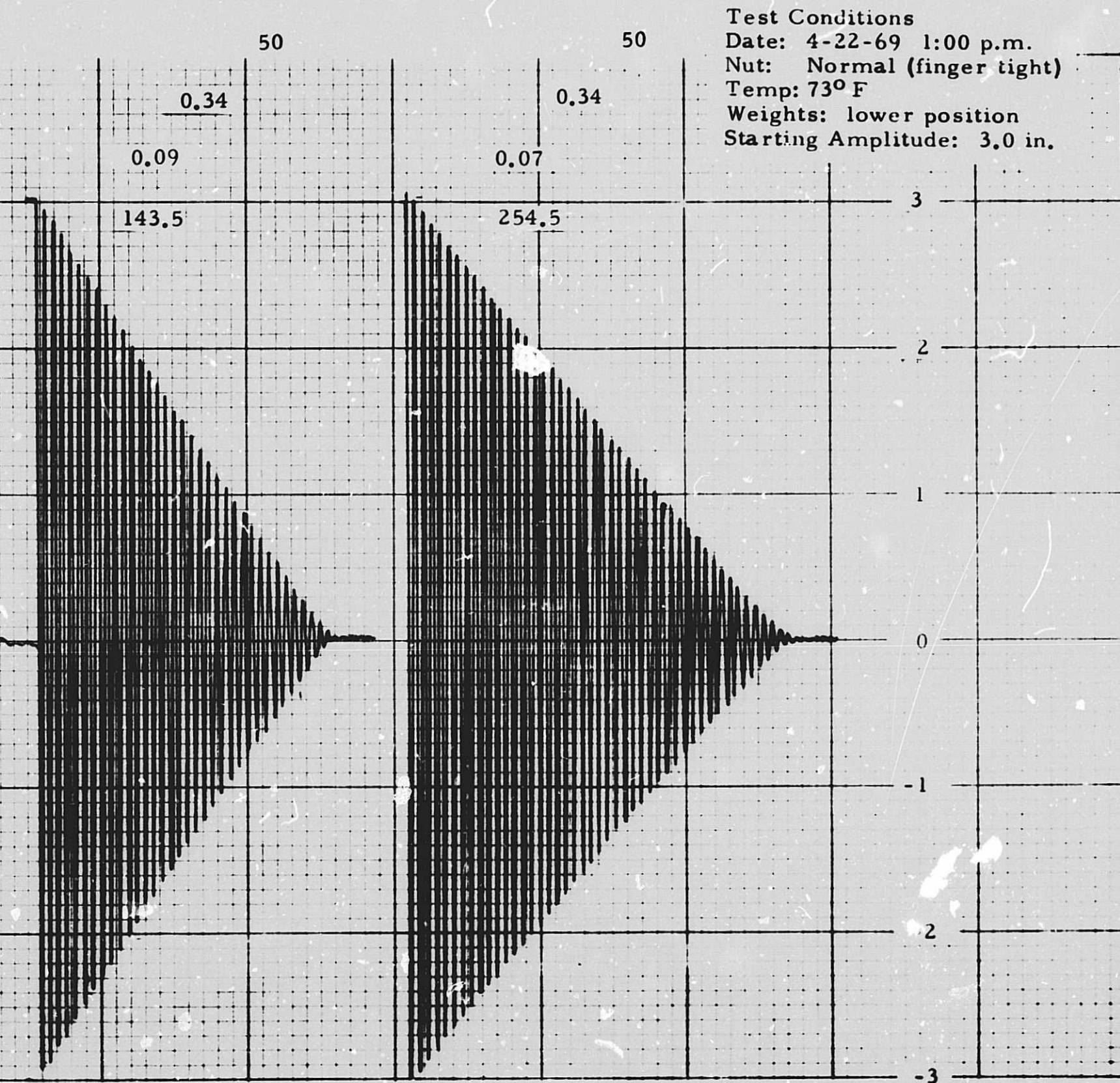
**Fig. 17 - Pendulum Decay Curves —
Solar Panel Joint**
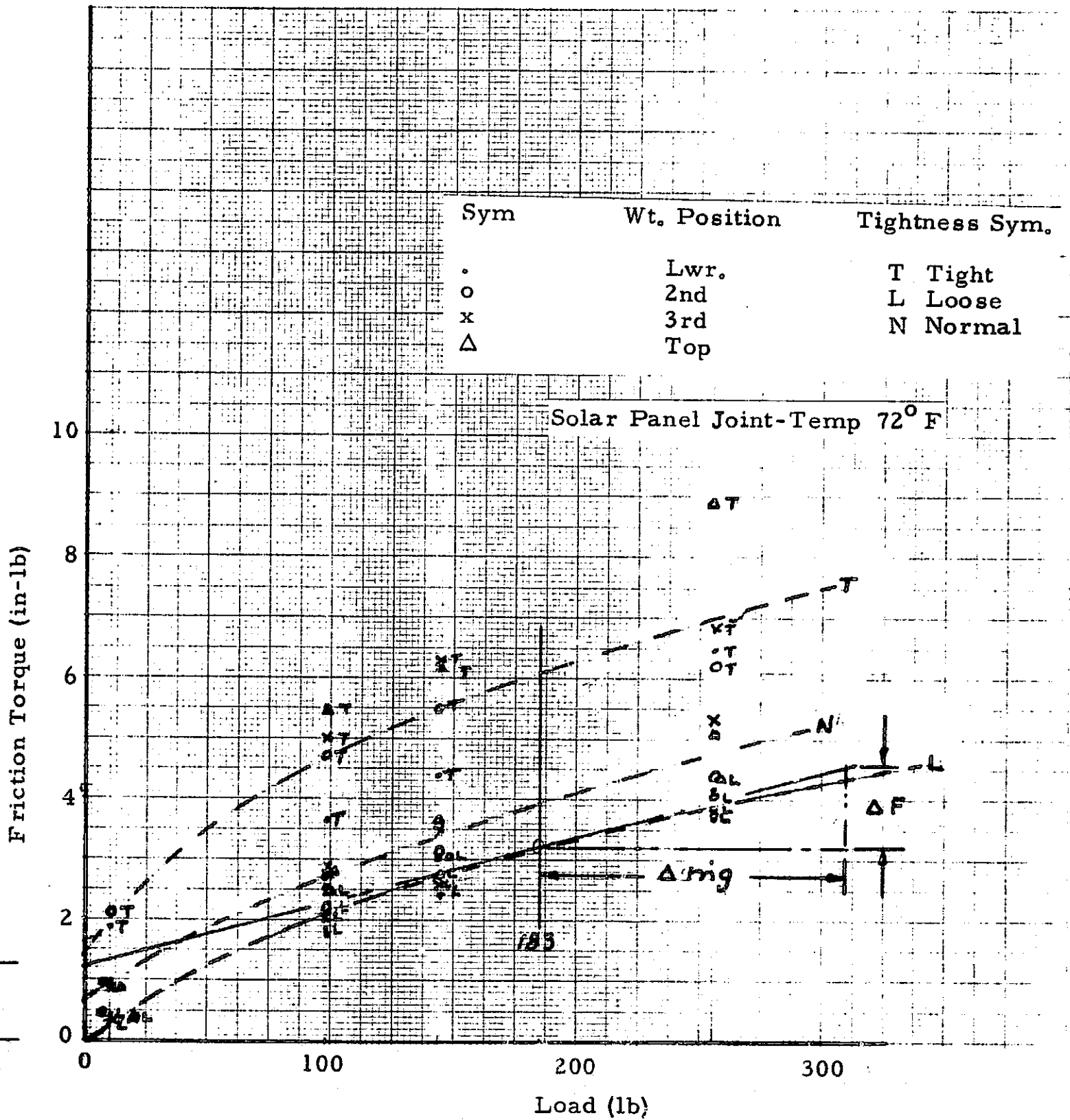
Fig. 18 - Friction Torque vs Load
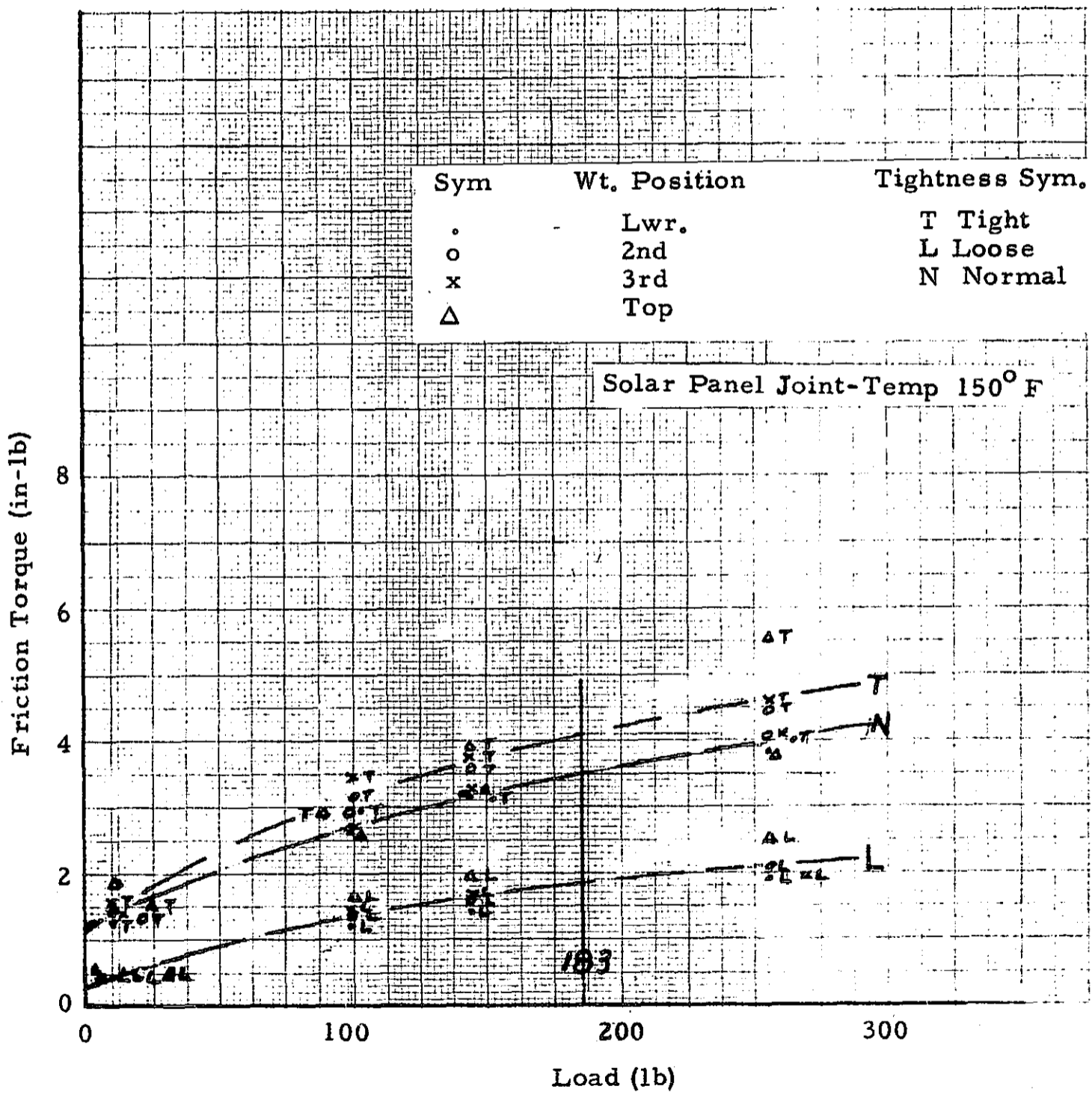
Fig. 19 - Friction Torque vs Load
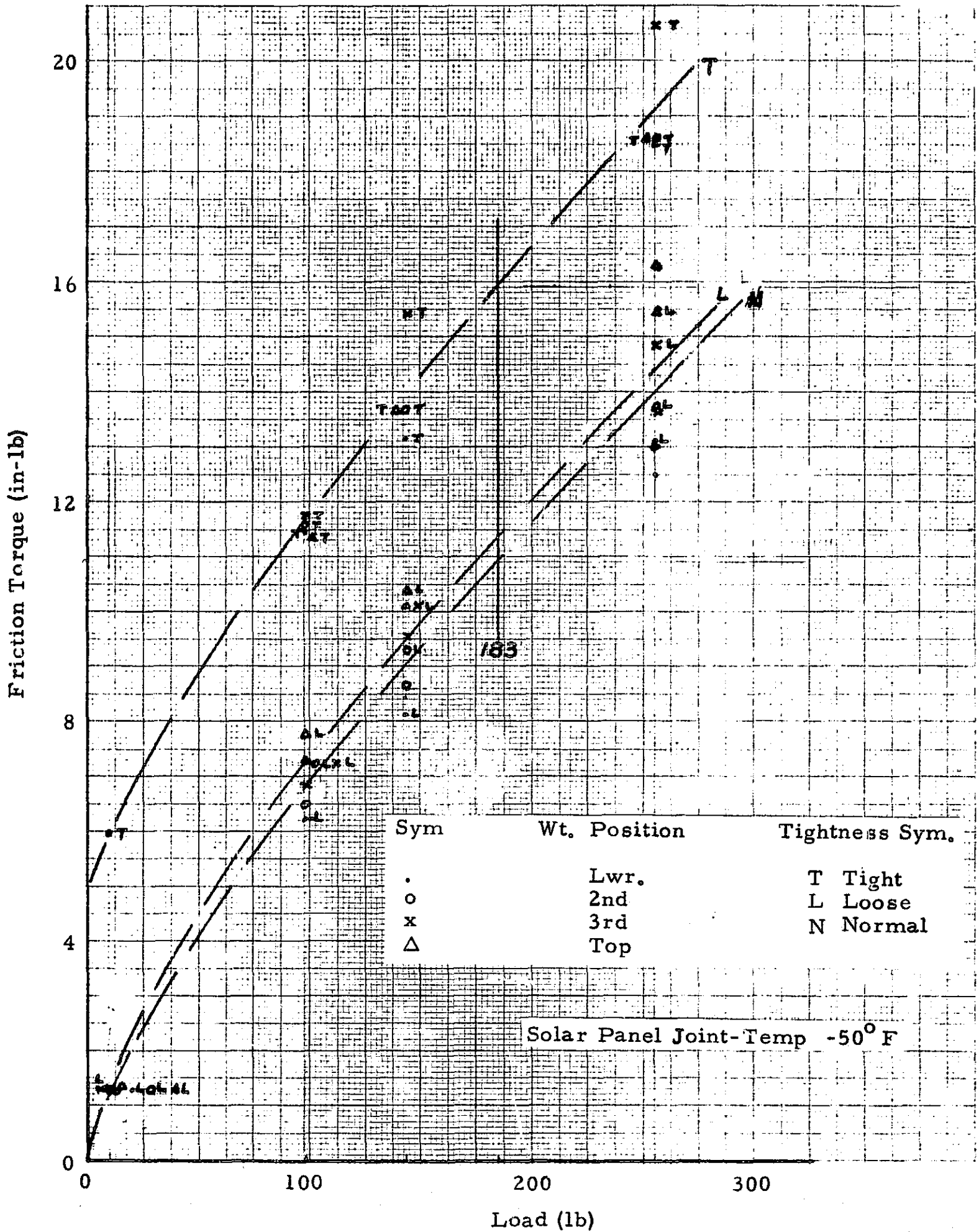
Fig. 20 - Friction Torque vs Load
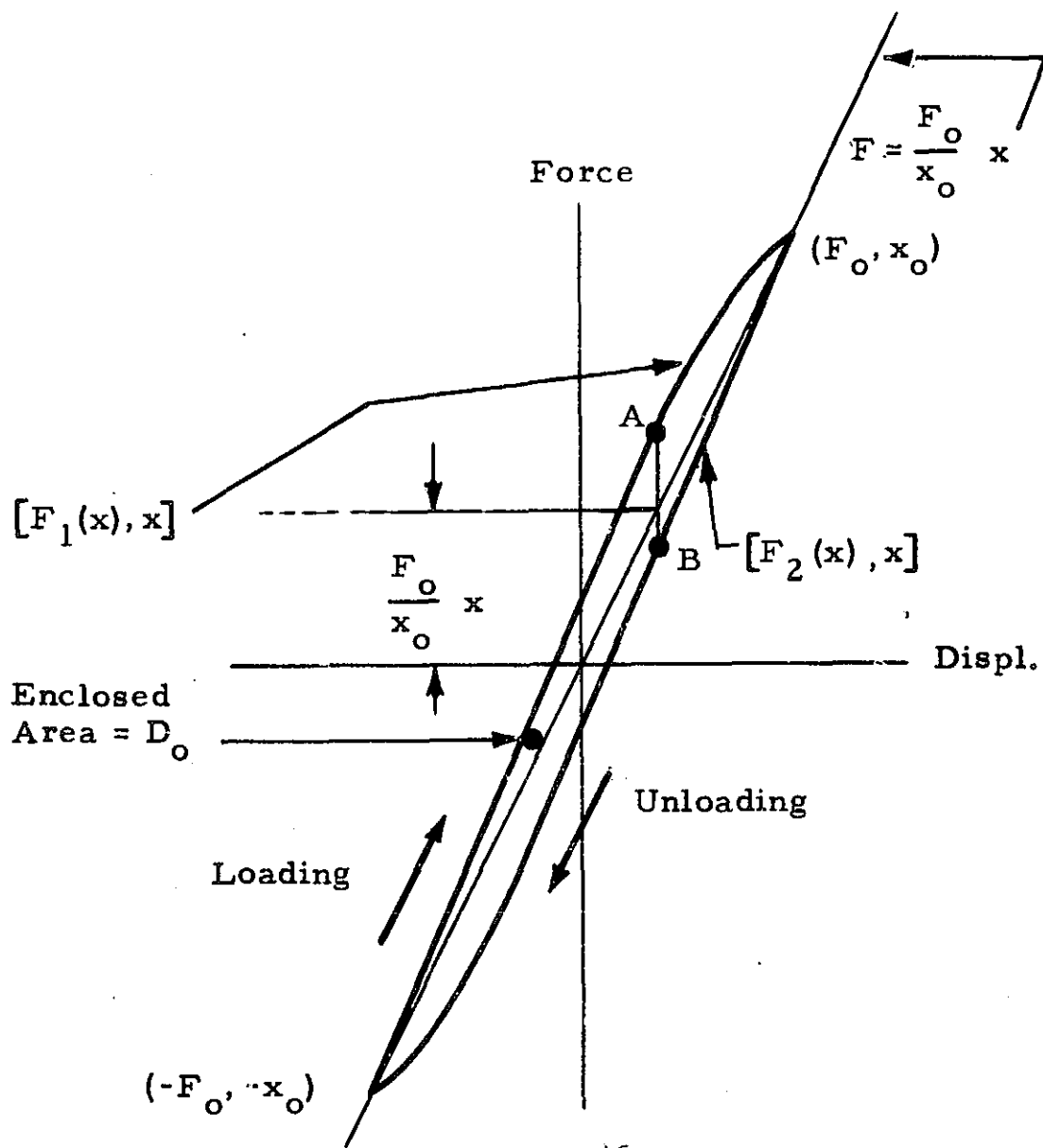
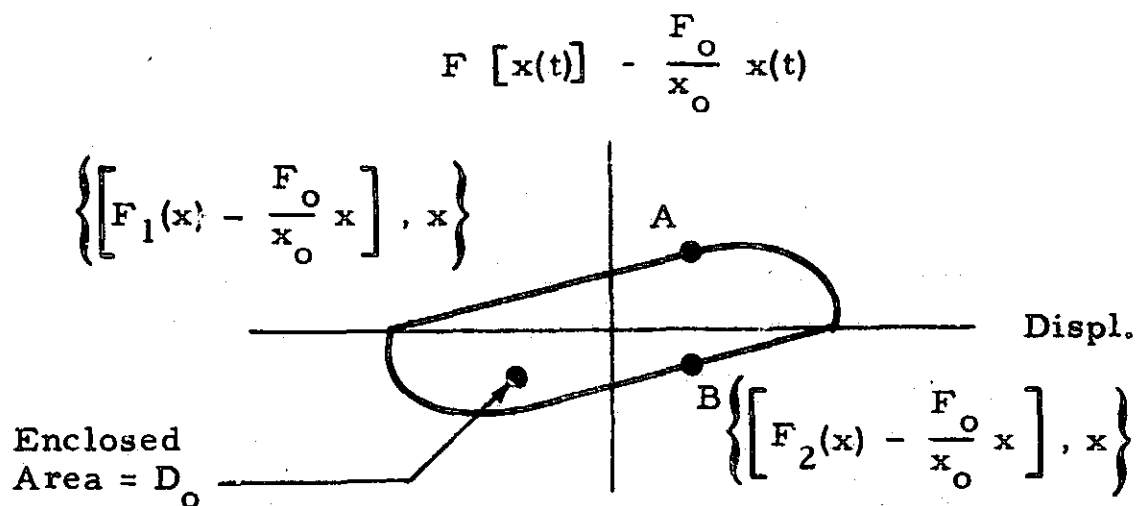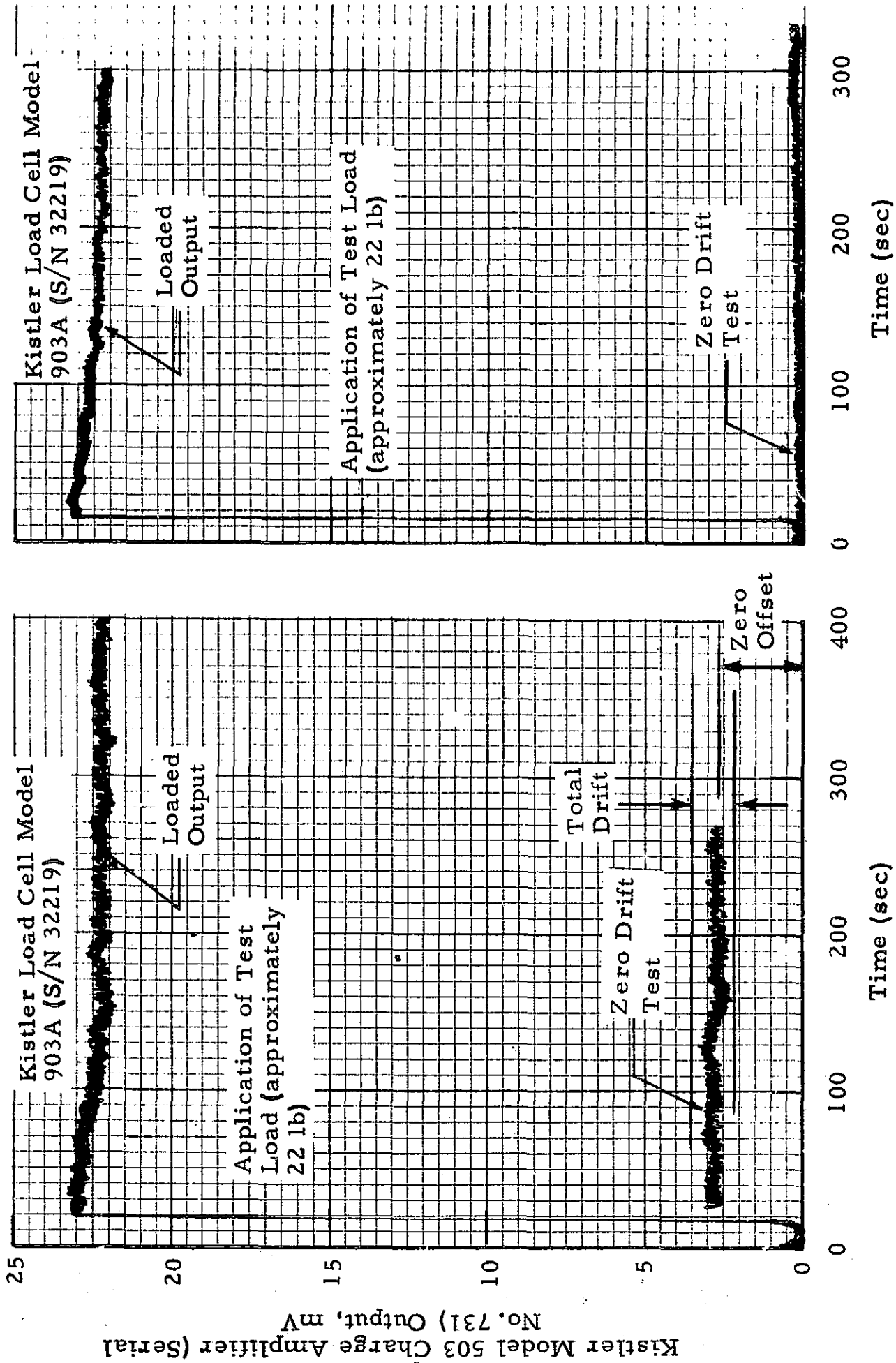Fig. 21 - Hypothetical Hysteresis Force-Deflection-Relationship

Fig. 22 - "Expanded Hysteresis Loop"

125

(a) Charge Amplified is "Long Time Constant" Mode; Range = 5k

(b) Charge Amplified in "Long Time Constant" Mode; Range = 2k

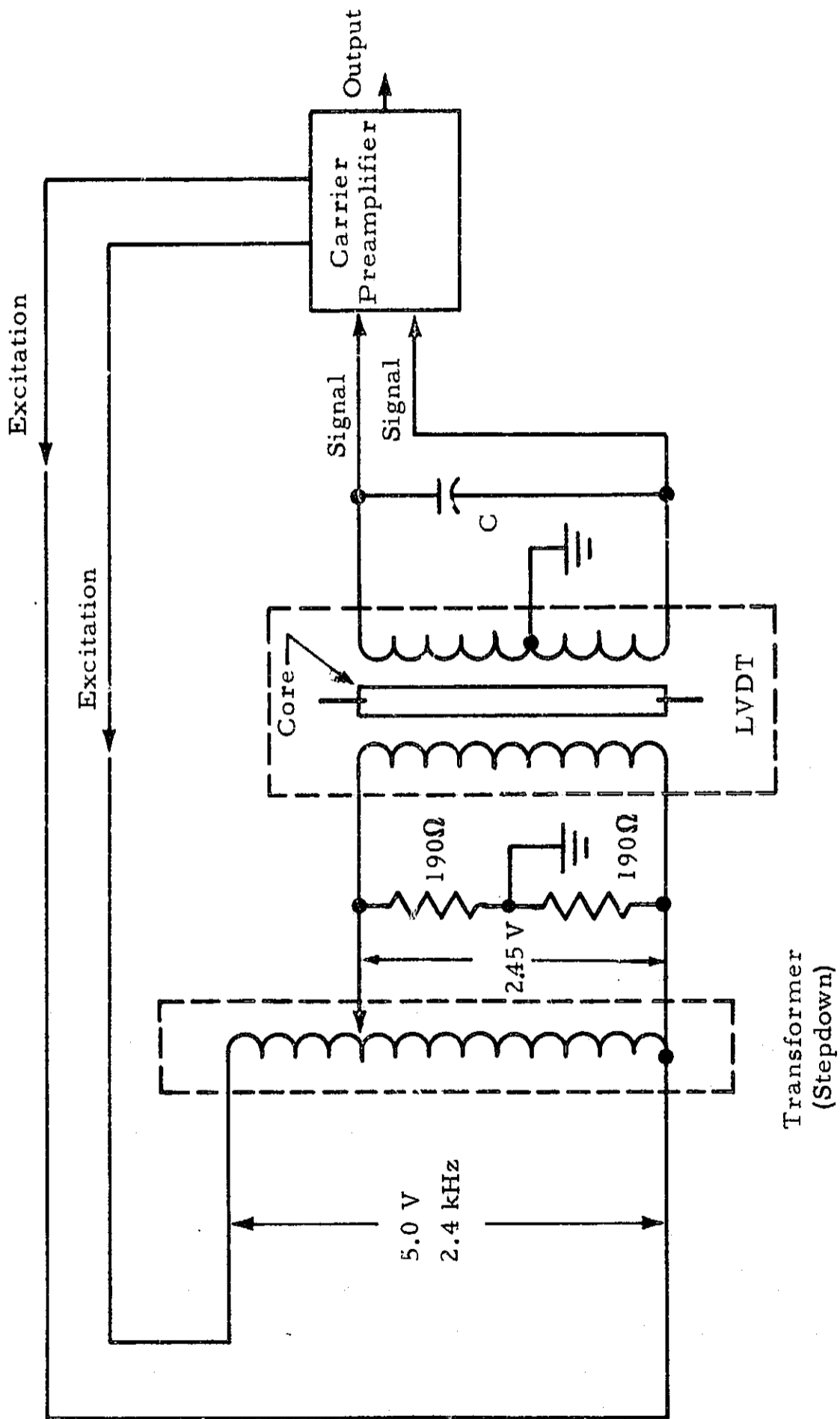Fig. 23 - Force-Measuring System — Zero Drift and Time Constant Check Tests
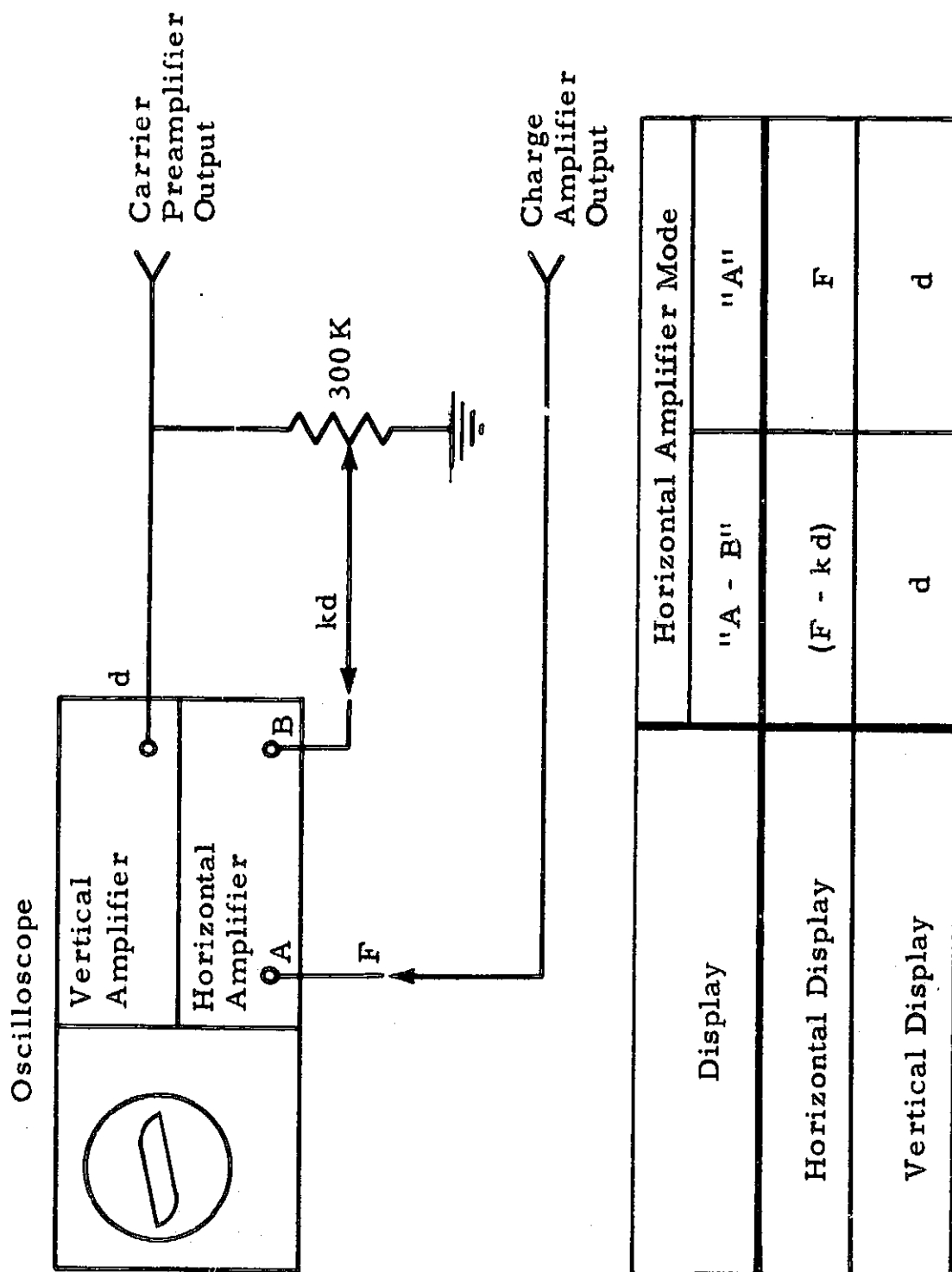
Fig. 24 - Displacement Sensing Instrumentation

Fig. 25 – Docking Port Joint Test – Data Recording Schematic

Horizontal Amplifier Mode		
Display	"A – B"	"A"
Horizontal Display	(F – kd)	F
Vertical Display	d	d